Birefringence of Polymer Solutions in Time Dependent Flows

Thesis by

Enrique Geffroy Aguilar

in Partial Fulfillment of the Requirements

for the Degree of

Doctor of Philosophy

California Institute of Technology

Pasadena, California

1990

(Submitted November 17, 1989)

A mi Tere bonita.

A nuestros queridos Viejos.

Acknowledgements

This thesis was made possible with the assistance of many people to whom I owe my deepest gratitude. To a good friend George Griffith who also provided 45 years of experience as the greatest instrument designer. To Chic Nakawatase; his patient and careful work made possible a great apparatus. To Helen Dewitt who always processed in a thoughful manner a never ending stream of paperwork in order to obtain all the necessary components for the laboratory work. To John Yehle and Tom Dunn whose electronic expertise allowed me to put together several devices that have yet to fail. To Evangelos Petroutsos, David Gillespie, and Rick Koshi for their numerous suggestions for the development of the computer programs used for the control and data acquisition of the experiments.

To our many friends who made the difficult times bearable and the good times unforgetable. Especially good, old Francísco Avila (I will not forget the chocolate repeatedly taken from my desk), the always tranquil Jaywant Arakeri, Pablo de Urquijo, Luca D'Agostino, Luciana Astiz, and Carlos Uzcategui. I enjoyed many discussions about science, and about "everything else" with Ardith El-Kareh (I have passed the official Leal's Group Mouse-Trap) Kathy Lewis, and Edward P. Ascoli. Some other members of the L. G. Leal research group also assisted me on many occasions: Chris Koh, Paul N. Dunlap, Ricky Ng, and Octavio Manero, and more recently Moshe Shapira. It was a pleasure working along with everyone!

The Universidad Nacional Autónoma de México generous support is greatly appreciated. Dr. George Rickards and Guillermo Aguilar whose sincere interest and encouragement made possible my departure to, and stay at Caltech. I also would like to thank Professors J. F. Brady, N. W. Tschoegl, Fred Shair, and David James (of the University of Toronto, Canada) for their valuable discussions and interest in this work. I am also grateful to all of my previous teachers who interested me in the fields of science; especially, Tete Hirales, Drs. Ricardo Tsumura and Hector Riveros, who thought me much more than the mere subject. I would like to thank

my advisor Prof. L. Gary Leal for his patience and support for so many years. His keen and critical intellect has been an important guide from which I have benefited the most.

Finally, to my wife Tere and my family who have been my source of strength, joy and love.

Abstract

This is a study of changes of conformation of macromolecules in polymeric solutions which are subjected to time-dependent extensional flows generated by a two-roll mill flow device. The flows produced by the two-roll mill are linear, and two-dimensional. It has a stagnation point at the center of the flow field where the magnitudes of the strain-rates are greater than the vorticity. This study of conformational changes is based on data around the vicinity of the stagnation point, I for steady state flows, and several transient flow histories such as start-up, cessation, and double-step flows. We also present an analytical solution for the creeping flow generated by an infinitely long two-roll mill embedded in an unbounded fluid. This solution is used as a benchmark to compare the behavior of the polymer solutions when subjected to flows with different values for the ratio of rate-of-strain to vorticity.

The conformational changes are determined experimentally using the Two-color Flow-Birefringence which provides an instantaneous and point-wise measure of the anisotropy of the fluid, together with the relative orientation of the anisotropy with respect to the principal axes of the flow field. Based on relaxation of the fluid anisotropy the characteristic time-scales of the polymer have been evaluated as a function of the flow field properties and the degree of conformational change of the macromolecules. Data for two polymeric solution is presented. The first polymer system is the so-called test-fluid M1. This polymeric solution is shown to degrade significantly, even for small values of the velocity gradient, as measured by the changes in the macroscopic relaxation time-scales. The second solution is a concentrated polystyrene solution that presents overshoots and undershoots of the polymer conformation dependent of the ratio of vorticity to rate-of-strain. When subjected to large deformations, this polystyrene solution shows not only the

possibility of a reduced number of entanglements, but also a significant deformation of the macromolecule segments associated to a shorter relaxation time-scale for the dynamics of concentrated solutions, which corresponds to that predicted by the intermediate relaxation time-scale of Doi-Edwards model.

Contents

Introduction

Understanding of the dynamics of polymeric fluids is of great importance for the processing of polymers with the objective of producing materials of extraordinary properties. One of the simplest methods for the characterization of polymeric liquid dynamics is a determination of the spectrum of relaxation times, when the fluid is subjected to a macroscopic deformation imposed by a flow field. The observed characteristic time-scales depends strongly on the type of deformation as well as on the deformation history. The type of deformations that tend to enhance most significantly those properties of interest for many polymeric materials are those that produce a strong alignment and stretch of the polymer chain along preferencial directions; that is, in most cases a high degree of anisotropy of the polymer microstructure produces the desired properties of the material.

The evaluation of relaxation time-scales when the polymer microstructure has been subjected to large deformations is in most cases difficult. As a consequence, the data published to date has been limited mostly to cases involving relatively small conformation changes, such as uniaxial extensional flows where the maximum total strain is rather small, or simple shear flows (*e.g.*, Couette flows), where it is impossible to attain large conformational changes of the polymer, because of the significant influence of vorticity for this type of flow. The primary sources of difficulty are the lack of flow fields where large deformations can be imposed on the polymers, and also the tight coupling that exists between flow effects and

conformational effects. That is, when large deformations are imposed upon the polymeric fluid, the same flow properties that cause the conformation of polymer molecules to change, are also affected by the changes of the polymer molecules. Consequently, in order to produce useful data for the characterization of polymeric materials it is desirable to measure, simultaneously, and in an independent manner, the properties of the flow field, and the polymer conformation.

In part I of this work we present an experimental apparatus as well as the methodologies required for evaluation of the relaxation time-scales for polymeric solutions when *large* deformations of the polymer conformation have been imposed. The flow device used in these studies is a co-rotating two-roll mill, and is presented in Chapter 1. The flow field of a two roll-mill has a *stagnation* point located at the center, along the line of centers between the rollers. It is possible to impose very large deformations (as well as large deformation-rates) to the molecules around this region, and thus, obtain large conformational changes of the polymer molecules. Furthermore, this flow device is capable of generating flows that have a wide range of ratios of vorticity to rate of strain from a very close approximation to that of simple shear flow, to those so-called "strong" flow fields in which the vorticity is less important and, the polymer conformation is dominated by the extensional character of the flow. In addition, in its current configuration, the two-roll mill can provide a wide range of deformation histories, including step changes in the velocity gradient such as cessation and inception of steady flow, double-step, etc. This provides the needed flexibility for evaluation of the characteristic time-scales of polymeric liquids for different flow types.

We present an analytical solution for the Stokes approximation of a Newtonian liquid in a two-roll mill with rollers of infinite length. The solution is given in terms of a Fourier series, and takes advantage of the symmetry characteristics of a two roll-mill for co-rotating rollers of equal radii. This solution is used to calculate the magnitude of the velocity gradient as well as the ratio of vorticity to strain rate given the geometry of the flow device and the rollers angular speed.

In order to characterize the relaxation time-scales of the polymer fluid, it is necessary to evaluate the characteristic times of the flow field and also the flow induced anisotropy of the polymer molecules. The optical techniques used for this purpose are described in Chapter 2. The experimental methodology to measure the degree of anisotropy of the polymer microstructure is the so-called Two-Color Birefringence method. This technique is capable of fast, point-wise measurements of the optical anisotropy of the fluid, with very good reproducibility. Indeed, our implementation of the TCB is capable of point-wise measurements even in non-homogeneous flow fields with a spatial resolution of approximately 50 μm. It is also capable of tracking the time-evolution of the fluid anisotropy for transient flows at a rate of 2×10^4 data points per second. The flow field properties are determined using the Homodyne Light Scattering technique (HLS) developed in this laboratory, and which provides the a real-time point-wise measurement of the velocity gradient of the flow.

In Chapter 3 the main features of the pseudo-code for the execution of all possible experiments with this apparatus is given. The complete apparatus and peripherial instrumentation are controlled by a computer. This computer makes extensive use of real-time computer techniques and algorithms for data acquisition and for displays of data on the screen in real-time. We also present the implementation of the most important portions of code for the real-time virtual machine.

In part II, we present results obtained—to date—with this apparatus, for the characterization of optical properties of two polymeric liquids. In Chapter 4 we present results for a semi-dilute solution of high molecular weight polyisobutene in a solvent made up of short chains of polybutylene and kerosene. This solution is now known in the literature as the test-fluid M1. It is a solution that is highly elastic, but we found that, it also degrades rather easily when subjected to large deformations. The observed degradation is shown to be due to scission of the high molecular weight tail of the polymer sample which not only decreases the fluid anisotropy but also produces a reduction of its characteristic relaxation time-

scale. Taking account of the degradation of the sample, we have shown that the characteristic relaxation time, for cessation of steady flow, decreases as the shear rate increases, but augments significantly if the flow field is not completely arrested but a small shear rate is maintained. The M1 solution also shows strong overshoots at the abrupt onset of steady flow for almost all values of the deformation rate; even for the lowest values accessible to this apparatus (0.5 sec.$^{-1}$) which are in general, smaller than those commonly reported in the literature for the same type of fluids. Furthermore, The anisotropy is limited to a slender region emanating from the stagnation point. The decrease in relaxation time with increase of shear rate, and the overshoot in inception of flow are characteristic of *concentrated* solutions. On the other hand, the increase in the relaxation time in the presence of a weak flow, and the localized polymer-flow interactions are consistent with models for dilute solutions that include a non-linear conformation dependent friction coefficient.

The second solution that we have studied is a concentrated solution of polystyrene (of narrow molecular weight distribution and average weight of 3.84×10^6) in a high viscosity solvent. The solvent is made up of low MW polystyrene and toluene. This solution also shows strong non-linear viscoelastic effects. For inception of steady flow, strong overshoots in the birefringence are found to exist, followed in some cases, by significant *undershoots.* These effects depend on the ratio of vorticity to strain-rate, the position within the flow field, and the shear rate. For this second fluid, we have also tested a wide range of ratios of vorticity to strain-rate in order to study the "transition" between the phenomena observed in simple shear flows (by others) and those observed in pure shear, especially those properties where the current literature shows marked qualitative differences. The observed variation of polymer anisotropy as a function of position in the flow field, is in strong contrast to that observed for the test-fluid M1. For this solution the anisotropy is no longer limited to the region around the stagnation point but covers the complete flow field accessible to the experimentalist. As a consequence of this global phenomena, the response of the polymeric liquid is not only affected by the local conditions

of the flow field, but also by the conditions of the far afield. This is especially important for transient flows for these effects provide information that is useful in discriminating temporal effects due to transient behavior of the *flow field* itself from those associated with the dynamics of the polymeric microstructure. Conversely, relaxation after cessation of flow, which is extrictly and uniquely the result of the dynamics of the fluid, also shows the capacity to generate global effects, such as rotation of the fluid during relaxation. Based on observed transient phenomena, it is also possible to evaluate changes in the microstructure of the polymer fluid, where the effects of different time-scales of the dynamics of the polymer microstructure can be studied by evaluating various time-scales of the observed anisotropy.

Part I

The Experimental Apparatus

Chapter 1

The Two-Roll Mill Flow Device

Enrique Geffroy*
California Institute of Technology
Department of Chemical Engineering

Edward P. Ascoli†

and

L. Gary Leal‡
University of California, Santa Barbara
Department of Chemical and Nuclear Engineering

October 24, 1989

*California Institute of Technology, Chemical Engineering, mail code 210-41, 1201 E. California Blvd., Pasadena, CA 91125, USA. (818) 356-4670.

†Rockwell International, Rocketdyne Division, M/S WC75, 6633 Canoga Park Ave., Canoga park, CA. 91303

‡To whom correspondence should be addressed: University of California, Chemical and Nuclear Engineering Dept., Santa Barbara, CA 93106, USA. Tel:(805)961-8510, Fax:(805)961-4731.

The Two-Roll Mill Flow Device

Abstract

Here we present an analytical solution for the flow field of a two-roll mill with co-rotating rollers of infinite length and immersed in an unbounded liquid. This solution corresponds to a steady two-dimensional flow, where the inertial terms are negligible. Furthermore, we take full advantage of the symmetry characteristics of a two-roll mill of identical rollers rotating with the same angular speed. The analytical solution is used to calculate the magnitude of the velocity gradient, the flow parameter that relates the ratio of vorticity of the flow to its strain-rate, as well as the angle of the bisector for the incoming and outgoing flow axis at the stagnation point. These parameters are of great importance as benchmarks for the study of polymeric liquids in two-roll mill flows. Subsequently, we present a flow cell constructed in our laboratories for studies of polymeric solutions. The flow cell is designed to take advantage of optical methods to determine the material, as well as the flow field properties. Finally, we discuss its most important mechanical and optical characteristics.

Chapter 1

The Two-Roll Mill Flow Device

In order to study the dynamics of polymers when subjected to large departures from an equilibrium configuration, it is necessary to have a well characterized flow field in which flow elements undergo both large strains and large strain-rates, at least locally. Such a flow can cause large conformational changes of the macromolecular structure. In the first part of this chapter we discuss the general characteristics for such a flow, and discuss some specific advantages of the two-roll mill over such flows as simple shear (*e.g.*, Couette flow) or pure extensional flow. Subsequently, an analytical solution is given for a two-roll mill in an *unbounded* fluid. This solution is given in bipolar coordinates, and corresponds to the Stokes approximation for two identical co-rotating rollers with equal angular speeds. It is given as a series expansion where all of the coefficients can be accurately calculated and are independent of the number of terms used to describe the stream function. It is used to calculate the relationship between the angular speed of the rollers and the magnitude of the velocity gradient as well as other parameters, based on the geometrical characteristics of the two-roll mill such as roller radii and roller gap. This is followed by the actual design and other considerations for the two-roll mill used with this apparatus in conjunction with the optical arrangement. Finally we give a brief explanation of the characteristics of those time *histories* of the flow field that are most interesting for the study of polymeric liquids.

1.1 A Flow Field Capable of Large Deformations

We are primarily concerned with the dynamics of macromolecular fluids for flows that are *linear, two-dimensional* and *strong* in the sense that the strain-rate exceeds the vorticity. The importance of this class of flows (and of strong flows in general) is that they have the potential to deform the structure of a polymeric liquid from a moderate state of quasi-equilibrium to almost its full contour length; conditions that are impossible to generate in weak flows, such as simple shear flow.[1] The class of 2-D strong flows can be generated locally (to a good degree of approximation) at the stagnation point of either a two-roll mill or a four-roll mill of the Taylor type [1]. A four-roll mill, illustrated in Figure 1.1(a), corresponds to two pairs of diagonally-opposed rollers which rotate at the same speed but in opposite directions. A stagnation point exists at the center of the device and different ratios of rate of strain to vorticity can be produced in the region between the rollers by using different combinations of direction and rotation rates for the diagonally-opposed roller pairs.

A streakline photograph is given by Fuller and Leal [8] which illustrates some of flows that can be obtained. The two-roll mill with co-rotating rollers, illustrated in figure 1.1(b), also generates a flow field with a stagnation point at the center, but being more suitable for producing strong flows with a smaller ratio of rate-of-strain to vorticity.

If the flows produced by the two-roll and four-roll mills are truly linear and two-dimensional (both assumptions being approximately true in the central region near the stagnation point, as shown experimentally by Lagnado and Leal [3], and Dunlap and Leal [4] for small Reynolds number), the complete class of flows obtained can be represented as a continuous one-parameter family, with a velocity gradient tensor

[1] Consequently, most of the literature that describes experimental work on shear flow of polymeric fluids only provides information about the quasi-equilibrium conformation, and this is its major disadvantage.

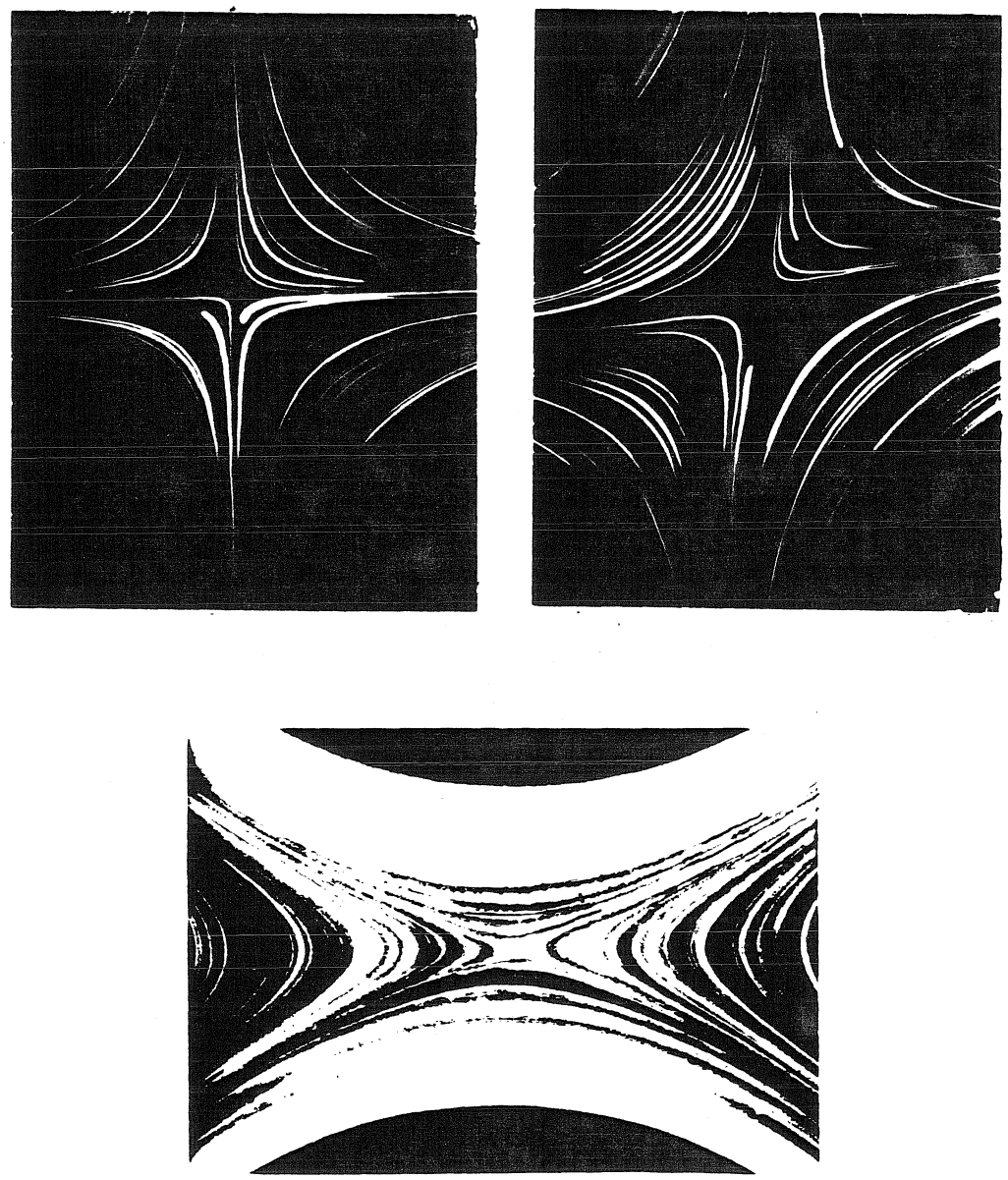

Figure 1.1: (a) The four-roll mill configuration for $\lambda = 1$ and $\lambda = 0.4$; different values for the flow parameter λ are obtained by setting different speeds on the opposing pairs of rollers. (b) The two-roll mill flow field, corresponding to a value of $\lambda = 0.1501$.

expressed by

$$\dot{\Gamma} = \frac{\dot{\gamma}}{2}\begin{bmatrix} (1+\lambda) & (1-\lambda) & 0 \\ -(1-\lambda) & -(1+\lambda) & 0 \\ 0 & 0 & 0 \end{bmatrix},$$

where $\dot{\gamma}$ is the *magnitude* of the velocity gradient, and is commonly called the shear rate, and λ is a "flow-type" parameter that determines the ratio of the strain-rate to the vorticity in the flow. The case of $\lambda = 1$ corresponds to a pure straining (hyperbolic) flow. However, *strong* flows (see for example [5, 17, 19, 5]) are generated whenever

$$0 < \lambda \leq 1,$$

and a weak flow (*e.g.*, simple shear flow) whenever $\lambda \leq 0$. Using the two-roll mill to generate flows with a range of values of the flow parameter λ requires variations of the ratio of the roller diameter to the gap width. In contrast, the geometry remains fixed in the four-roll mill, and various values of λ are generated by using different ratios of rotation speed and direction for the opposing pair of rollers. However, the four-roll mill is not the most appropriate flow device for flows with values of λ close to 0 (zero). Specifically, with a four-roll mill it is impossible to generate a flow field that approaches simple shear flow, and the minimum value of $|\lambda|$ accessible to this flow device is approximately 0.25 [17]. On the other hand, the two-roll mill is *best* suited for values of the flow parameter that are closer to zero than one, with the overall characteristics improving for λ values near zero (*e.g.*, the 2-D characteristics of the flow fields improve as the perturbation effects of the boundaries—due to the finite length of the rollers—decrease as $\lambda \rightarrow 0$). Furthermore, the principal advantage of the "two-roll mill" is that it generates flows of comparable (although, always smaller) vorticity to strain-rate, thus allowing a slower, more controlled deformation of the macromolecules, within the range of values of $\dot{\gamma}$ accessible to the two-roll mill. Flows characterized by λ values near unity induce mostly high degrees of polymer deformation, with different shear-rate values (even the smallest accessible to the flow device) having similar effects on the observed conformational changes.

A second advantage of the two-roll mill over the four-roll mill is the existence of an analytical solution of the *unbounded* two-dimensional creeping flow problem for this geometry and the potential for numerical solutions of the bounded problem.[2] This solution allow us to calculate the flow parameter λ, the angle defined by the inflow and outflow axis shown in Figure 1.2, as well as the magnitude of the velocity gradient, based on the two geometrical parameters of the two-roll mill (the roller radii, and the distance between the roller axes), and the angular velocity of the rollers. These calculated flow characteristics provide and initial basis to evaluate the degree of polymer deformation, and the degree of alignment of the stretched polymer along the principal direction of the velocity gradient tensor, as a function of flow type, and shear rate. These calculated characteristics can also be compared with experimentally determined velocity gradients as measured with the homodyne light scattering technique presented in section §2.4.

1.2 The Flow-Field of an Ideal Two-Roll Mill

The *general* form of the steady, two-dimensional flow, where the inertia terms are viewed as negligible for two cylinders of arbitrary radius, and separated by an arbitrary distance was given by Jeffery [10] in 1920. For the particular case of a cylinder rotating eccentrically inside a cylinder, the detailed Stokes flow solution was also given by Jeffery [11] two years later, while only partial solutions were obtained for the flow field exterior to two co-rotating cylinders. More recently, Dunlap and Leal [4] gave an analytical approximation of Jeffery's general solution for the case of two exterior rollers rotating with equal speed, which valid in the vicinity of the stagnation point. In addition, Kapur, Ascoli, Shapira and Leal [12] have obtained and analytical solution for both the co-rotating and counter-rotating cases, and also obtained a numerical solution for the bounded problem

[2]To our knowledge, there is not a solution available to date for the four-roll mill geometry. See for example Torza [9] for an empirical evaluation of the strain rate in a four-roll mill, and its dependence on geometry and angular speed. Torza observed differences of up to one third from "calculated" values, as the ratio of roller gap to roller radius varied from $0.21 \leq h/R \leq 3.3$.

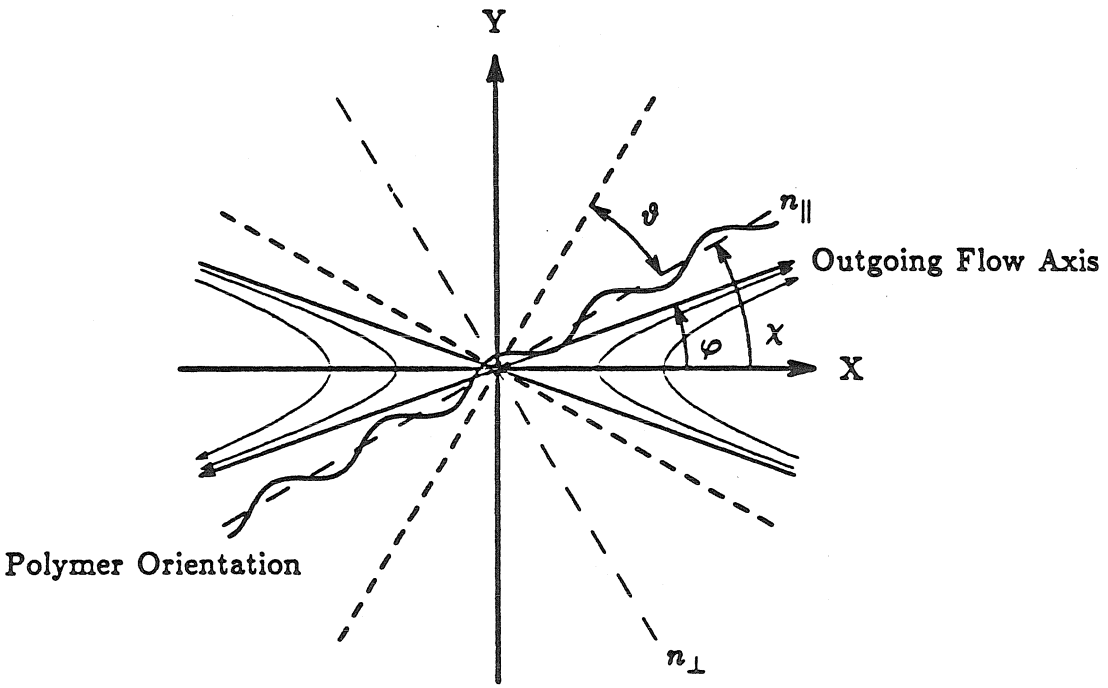

Figure 1.2: The flow field coordinate system of the two-roll mill and its relationship to the optical coordinate system defined by the incident blue beam polarization.

(two cylinders inside a box). An alternative analytical solution by Geffroy, Ascoli and Leal [13] of the unbounded co-rotating case is presented below, in a form that is better suited for our current needs. We have used the later solution to calculate the flow field characteristics based on the geometrical parameters of our flow device.

Jeffery's general solution of $\nabla^4\Psi = 0$, which describes two-dimensional creeping flows, is given in bipolar coordinates (α, β), which are related to the (x, y) plane by

$$(\alpha + i\beta) = \log\left(\frac{x + i(y+a)}{x + i(y-a)}\right) .$$

or also expressed as

$$x = \frac{a \sin\beta}{\cosh\alpha - \cos\beta} , \qquad y = \frac{a \sinh\alpha}{\cosh\alpha - \cos\beta} , \tag{1.1}$$

where a is a real positive length. Figure 1.3 shows curves of constant α and β, with the x and y axes coinciding with the curves for $\alpha = 0$ and $\beta = 0$ respectively. Curves of constant α are nonconcentric circles with limit points $\alpha = \pm\infty$ and the curves of constant β are orthogonal everywhere to the curves of constant α. The geometrical parameters of the flow device are expressed in bipolar coordinate parameters as

$$R = \frac{a}{\sinh\alpha_R} \quad \text{and} \quad \frac{g}{R} = \cosh\alpha_R - 1 , \tag{1.2}$$

where the rollers with radii R are curves of constant $\alpha = \pm\alpha_R$ and g is the gap between the rollers [14].

The general form for the stream function given by Jeffery [10] is:

$$\begin{aligned} h\Psi \;=\; & A_0 \cosh\alpha + B_0\,\alpha(\cosh\alpha - \cos\beta) + \\ & + C_0 \sinh\alpha + \; D_0\alpha\sinh\alpha + \\ & + K(\cosh\alpha - \cos\beta)\,\log(\cosh\alpha - \cos\beta) + \\ & + (A_1 \cosh 2\alpha + B_1 + C_1 \sinh 2\alpha)\cos\beta + \\ & + (A_1' \cosh 2\alpha + C_1' \sinh 2\alpha)\,\sin\beta + \\ & + \sum_{n=2}^{\infty} (\phi_n(\alpha)\cos n\beta + \phi_n'(\alpha)\sin n\beta) \end{aligned} \tag{1.3}$$

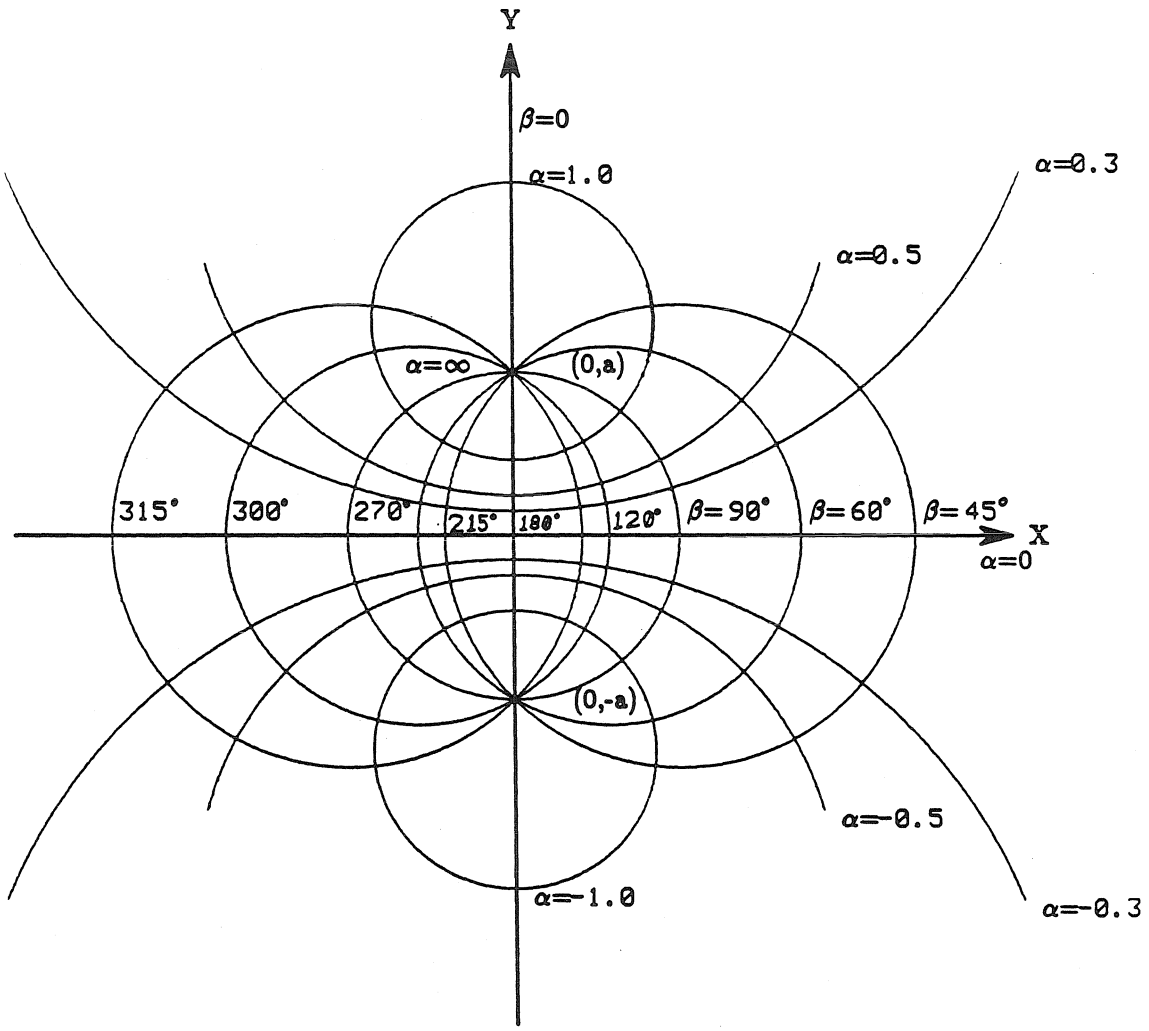

Figure 1.3: Bipolar cylindrical coordinates used in Stokes flow exterior to the two-roll mill. Curves of constant $\alpha = \pm\alpha_R$ correspond to the Roller position.

where $h = (\cosh\alpha - \cos\beta)/a$ is the metric factor, and ϕ_n and ϕ'_n are given by

$$\begin{aligned}\phi_n &= A_n \cosh(n+1)\alpha + \\ &\quad + B_n \cosh(n-1)\alpha + C_n \sinh(n+1)\alpha + D_n \sinh(n-1)\alpha, \qquad (1.4)\\ \phi'_n &= A'_n \cosh(n+1)\alpha + \\ &\quad + B'_n \cosh(n-1)\alpha + C'_n \sinh(n+1)\alpha + D'_n \sinh(n-1)\alpha. \qquad (1.5)\end{aligned}$$

The solution should be totally symmetric with respect to the x and y plane when the rollers have equal radii and rotate at equal speeds. These two symmetry conditions in bipolar coordinates are:

$$\begin{aligned}\Psi(\alpha,\beta) &= \Psi(-\alpha,\beta)\\ \Psi(\alpha,\beta) &= \Psi(\alpha,-\beta). \qquad (1.6)\end{aligned}$$

Using the symmetry equations 1.6 we find that $B_0,\ C_0,\ C_1,\ C'_1,\ A'_1 \equiv 0$, as well as *all* $C_n,\ D_n$, and $\phi'_n(\alpha) \equiv 0$. The general solution for a two-roll mill with equal co-rotating rollers and equal angular speed, is consequently expressed in its most general form by

$$\begin{aligned}h\Psi &= A_0 \cosh\alpha + D_0\alpha \sinh\alpha + \\ &\quad + K(\cosh\alpha - \cos\beta)\,\log(\cosh\alpha - \cos\beta) + \\ &\quad + \sum_{n=1}^{\infty} (A_n \cosh(n+1)\alpha + B_n cosh(n-1)\alpha)\cos\beta \qquad (1.7)\end{aligned}$$

The logarithmic term corresponds to two point sources of vorticity at $\alpha = \pm\infty$ (see for example Currie [15])

In addition to the symmetry conditions expressed by equations 1.6, the solution must satisfy the no-slip boundary condition at the roller surfaces ($\alpha = \pm\alpha_R$). If we denote the angular speed of the rollers as ω, this condition is:

$$-h\,\frac{\partial\Psi}{\partial\alpha}\bigg|_{\alpha_R} = -u_\beta(\alpha_R) = \omega R\,. \qquad (1.8)$$

The kinematic condition which guarantees no-flow through roller surfaces is

$$h\,\frac{\partial\Psi}{\partial\beta}\bigg|_{\alpha_R} = u_\alpha(\alpha_R) = 0\,. \qquad (1.9)$$

Also, the flow field is required to vanish at infinity. This boundary condition is expressed by

$$\mathbf{u}(\alpha = 0, \beta = 0) = 0 \ . \tag{1.10}$$

Now, in terms of the components of the velocity field we have

$$u_\alpha \equiv h\frac{\partial \Psi}{\partial \beta} = \frac{\partial (h\Psi)}{\partial \beta} - h\Psi\left(\frac{1}{h}\frac{\partial h}{\partial \beta}\right) \ , \tag{1.11}$$

$$u_\beta \equiv -\frac{h\partial \Psi}{\partial \alpha} = -\frac{\partial (h\Psi)}{\partial \alpha} + h\Psi\left(\frac{1}{h}\frac{\partial h}{\partial \alpha}\right) \ . \tag{1.12}$$

It is clear, upon substitution of the general solution 1.7, that the first terms of the right hand side of equations 1.11 and 1.12 go to zero at infinity for arbitrary choice of the constants. However, the second terms are undetermined, and consequently, in order to satisfy equation 1.10 it is necessary for $h\Psi$ to vanish at infinity, *i.e.*, $h\Psi(\alpha = 0,\ \beta = 0) = 0$. Hence, as a result we have that

$$A_0 = \sum_{n=1}^{\infty} (A_n + B_n) \ , \tag{1.13}$$

and, this is the first condition to be satisfied by the coefficients in equation 1.7 To proceed further, it is best to find an expression for the logarithmic terms appearing in the general solution (eq. 1.7) in terms of a Fourier series. Using equation 1.514 of Gradshteyn and Rizhik [16],

$$\ln(1 + 2x\cos\phi + x^2) = -2\sum_{n=1}^{\infty} \frac{\cos n\phi}{n} x^n \ ,$$

where

$$\ln(x + \sqrt{1 + x^2}) = \arcsin x; \quad x^2 \leq 1 \quad \text{and} \quad x\cos\phi \neq 1 \ ,$$

together with the change of variables

$$\phi = \beta, \quad \text{and} \quad \frac{1 - x^2}{2x} = \cosh\alpha_R \ ,$$

we can express

$$\ln(\cosh\alpha - \cos\beta) \ = \ a_0 + \sum_{n=1}^{\infty} a_n \cos n\beta \ , \tag{1.14}$$

$$\cos\beta \ln(\cosh\alpha - \cos\beta) = \frac{a_1}{2} + \left[a_0 + \frac{a_2}{2}\right]\cos\beta + \frac{1}{2}\sum_{k=2}^{\infty}(a_{n+1} + a_{n-1})\cos n\beta \ , \tag{1.15}$$

where $a_0 = \alpha - \ln 2$, and $a_n = -2e^{-n\alpha}/n$ for all $n \geq 1$. Also,

$$\begin{aligned}(\cosh\alpha \ - \ \cos\beta)\ln(\cosh\alpha - \cos\beta) &= \\ &= \left[a_0\cosh\alpha - \frac{a_1}{2}\right] + \left[a_1\cosh\alpha - a_0 - \frac{a_2}{2}\right]\cos\beta + \\ &+ \sum_{n=2}^{\infty}[a_n\cosh\alpha - a_{n+1} - a_{n-1}]\cos n\beta \\ &\equiv b_0 + b_1\cos\beta + \sum_{n=2}^{\infty} b_n\cos n\beta \ . \end{aligned} \tag{1.16}$$

Now applying the kinematic condition at the rollers surface (no flow through the roller) we have $\Psi(\alpha_R, \ \beta) = M$ for all β. Collecting terms according to the order of the $\cos n\beta$ function, we obtain a second set of equalities to be used for the determination of the coefficients for the stream function,

$$(A_0 - M)\cosh\alpha_R + D_0\alpha_R\sinh\alpha_R + Kb_0 = 0 \ , \tag{1.17}$$

$$M + A_1\cosh 2\alpha_R + B_1 + Kb_1 = 0 \ , \tag{1.18}$$

$$\text{for } n \geq 2 \quad A_n\cosh(n+1)\alpha_R + B_n\cosh(n+1)\alpha_R + Kb_n = 0 \ . \tag{1.19}$$

Now applying the no-slip boundary conditions at the roller surface we have

$$\begin{aligned} u_\beta(\alpha_R) &= R\omega \\ u_\beta &= -\frac{h\partial\Psi}{\partial\alpha} = -\frac{\partial h\Psi}{\partial\alpha} + h\Psi\left(\frac{1}{h}\frac{\partial h}{\partial\alpha}\right)\Big|_{\alpha_R} \end{aligned} \tag{1.20}$$

and consequently, when the expansions for the logarithmic terms given by equations 1.14-1.16 are used, we obtain a third set of equalities

$$[A_0 + D_0 + K(1 + a_0) - M - R\omega]\sinh\alpha_R + D_0\alpha_R\cosh\alpha_R = 0 \ , \tag{1.21}$$

$$2A_1\sinh(2\alpha_R) + Ka_1\cosh\alpha_R = 0 \ , \tag{1.22}$$

$$(n+1)A_n\sinh(n+1)\alpha_R + (n-1)B_n\sinh(n-1)\alpha_R + Ka_n\sinh\alpha_R = 0 \ , \tag{1.23}$$

where equation 1.23 is valid for all $n \geq 2$. From equations 1.13 and 1.18-1.23 we have A_0, D_0, M, K, A_1, B_1, A_n and B_n as unknowns with only $2n+5$ equations. However, we know that M is the value of Ψ at the rollers surface. If we set $M = 0$ then we have the same number of equations as the number of unknowns. Now let us solve for the system of equations involving all A_n and B_n for $n \geq 2$. Thus, using equations 1.19 and 1.23 we obtain

$$\frac{A_n}{K} = \frac{(n+1) - e^{-2n\alpha_R} - ne^{-2\alpha_R}}{n(n+1)\left[\sinh 2n\alpha_R + n \sinh 2\alpha_R\right]}, \tag{1.24}$$

$$\frac{B_n}{K} = -\frac{(1-n) - e^{-2n\alpha_R} + e^{2\alpha_R}}{n(n-1)\left[\sinh 2n\alpha_R + n \sinh 2\alpha_R\right]} . \tag{1.25}$$

It is important to note that these two equalities do not depend on any other parameter besides α_R (apart, of course, from n). Furthermore, it is possible to calculate the sum of these two terms to the necessary accuracy without regard of the other coefficients. That is, using equations 1.13, 1.25 and 1.25 we have

$$\begin{aligned} -A_0 + A_1 + B_1 &= -\sum_{n=2}^{\infty}(A_n + B_n) \\ &= -K\sum_{n=2}^{\infty}\left(\frac{A_n}{K} + \frac{B_n}{K}\right) = -KS , \end{aligned} \tag{1.26}$$

where the *partial* sum $S^{(n)}$ can easily be calculated to the necessary accuracy and only depends on the geometrical parameters of the two-roll mill through α_R. With the remaining equations 1.18-1.23 we can now solve for the other coefficients. The accuracy in computing the remaining coefficients K, A_0, D_0, A_1, and B_1 mainly depends on the accuracy initially required for $S^{(n)}$. From equations 1.18-1.23 plus some tedious algebra, we have

$$K = R\omega(T - W)^{-1} \tag{1.27}$$

where T and W are functions of α_R,

$$T = \left((1 + a_0)\sinh\alpha_R - b_0\frac{\alpha_R \cosh\alpha_R - \sinh\alpha_R}{\alpha_R \sinh\alpha_R}\right) , \tag{1.28}$$

$$W = \left(\frac{a_0 \sinh\alpha_R}{2\sinh 2\alpha_R} + b_1 - \frac{a_1 \sinh\alpha_r \cosh 2\alpha_R}{2\sinh\alpha_R} - S\right)\left(\frac{1}{\sinh\alpha_R} + \frac{\cosh\alpha_R}{\alpha_R}\right) . \tag{1.29}$$

The remaining coefficients are

$$A_0 = K\left[\frac{a_1 \sinh\alpha_R}{2\sinh 2\alpha_R} + b_1 - \frac{a_1 \sinh\alpha_R \cosh 2\alpha_R}{2\sinh 2\alpha_R} - S\right] , \tag{1.30}$$

$$D_0 = -\frac{A_0 \cosh\alpha_R + Kb_0}{\alpha_R \sinh\alpha_R} , \tag{1.31}$$

$$B_1 = -Kb_1 + \frac{Ka_1 \sinh\alpha_R \cosh 2\alpha_R}{2\sinh 2\alpha_R} , \tag{1.32}$$

$$A_1 = -\frac{Ka_1 \sinh\alpha_R}{2\sinh 2\alpha_R} . \tag{1.33}$$

These equalities complete the solution for the stream function for the Stokes approximation for the co-rotating two-roll mill.

We are now interested in calculating the characteristics of the flow field in the vicinity of the stagnation point. Applying equations 1.11 and 1.12 to the stream function (equation 1.7 with coefficients 1.25-1.33) we have

$$\begin{aligned} u_\alpha &= K[\sin\beta \ln(\cosh\alpha - \cos\beta) - \frac{\sin\beta}{\cosh\alpha - \cos\beta}[h\Psi] - \\ &\quad - \sum_{n=1}^{\infty} n(A_n \cosh(n+1)\alpha + B_n \cosh(n-1)\alpha)\sin n\beta , \end{aligned} \tag{1.34}$$

and

$$\begin{aligned} u_\beta &= A_0 \sinh\alpha + D_0(\alpha\sinh\alpha + \sinh\alpha) + \\ &+ K\sinh\alpha \ln(\cosh\alpha - \cos\beta) + \sinh\alpha - [h\Psi]\frac{\sinh\alpha}{h} + \\ &+ \sum_{n=1}^{\infty}[(n+1)A_n \sinh(n+1)\alpha + (n-1)B_n \sinh(n-1)\alpha)]\cos n\beta . \end{aligned} \tag{1.35}$$

Then, replacing all transcendental functions by their Taylor's series expansions (up to second order terms) around $\alpha = 0$, $\beta = \pi$, with $y = \alpha/2$, and $x = (\pi - \beta)/2$, we obtain

$$u_y = u_\alpha = x\frac{R\omega}{T-W}\left[2 + Q + \sum_{n=1}^{\infty}(2n^2 + i^{2n})\left(\frac{A_n}{K} + \frac{B_n}{K}\right)\right] , \tag{1.36}$$

$$\begin{aligned} -u_x = u_\beta &= y\frac{-R\omega}{T-W}[2 + Q + 4P + \\ &+ \sum_{n=1}^{\infty} i^{2n}\left(\frac{A_n}{K} + \frac{B_n}{K} - 2(n+1)^2\frac{A_n}{K} - 2(n-1)^2\frac{B_n}{K}\right)] , \end{aligned} \tag{1.37}$$

where Q and P are the coefficients A_0 and D_0 normalized by K. Given the linear character of the Stokes approximation, it is then possible to express the velocity field as $\mathbf{u} = \dot{\Gamma} \cdot \mathbf{r}$. That is,

$$\begin{bmatrix} u_x \\ u_y \end{bmatrix} = \dot{\gamma} \begin{bmatrix} 0 & 1 \\ \lambda & 0 \end{bmatrix} \begin{bmatrix} x \\ y \end{bmatrix} , \tag{1.38}$$

where it is now clear that the *magnitude* of the velocity gradient is

$$\dot{\gamma} = \frac{-R\omega}{T-W} \quad [2 + Q + 4P + \\ + \sum_{n=1}^{\infty} i^{2n} \left(\frac{A_n}{K} + \frac{B_n}{K} - 2(n+1)^2 \frac{A_n}{K} - 2(n-1)^2 \frac{B_n}{K} \right)] \ , \tag{1.39}$$

and the flow type parameter λ is given by

$$\lambda = \frac{2 + Q + \sum_{n=1}^{\infty} (2n^2 + i^{2n}) \left(\frac{A_n}{K} + \frac{B_n}{K} \right)}{2 + Q + 4P + \sum_{n=1}^{\infty} i^{2n} \left(\frac{A_n}{K} + \frac{B_n}{K} - 2(n+1)^2 \frac{A_n}{K} - 2(n-1)^2 \frac{B_n}{K} \right)} \tag{1.40}$$

The acute angle of crossing for the center streamlines, 2θ, defined as half the angle between the in-flow and out-flow axes depends on the flow type parameter in the form

$$\theta = \tan^{-1}(\lambda^{1/2}) \ . \tag{1.41}$$

The orientation *theta* corresponds to the orientation of the principal eigenvector, and is also the most likely orientation of a deformable body in the flow field [17, 18]. The equations 1.39, 1.40, and 1.41 are used in the next section for calculation of the most relevant parameters for a flow cell of the two-roll mill type that is the basis for the studies of polymeric solutions under strong flow deformations that are reported in Part II of this thesis.

1.3 The Flow Device

The two-roll mill designed and built in our laboratory is shown in Figure 1.4. There are three special features of this particular two-roll mill: (a) we can monitor and control the fluid temperature; an essential feature for most polymeric solutions

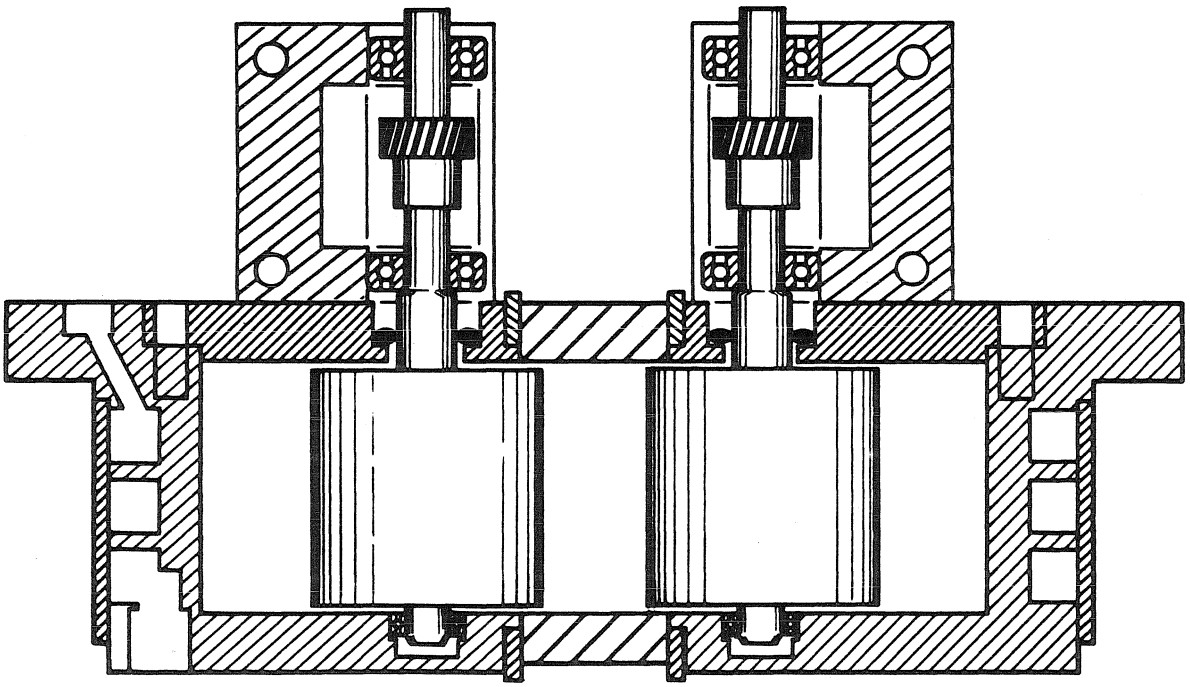

Figure 1.4: The two-roll mill flow device. The rollers are driven by a single stepping motor coupled to them via identical worm-and-gear assemblies. The rollers are supported by three sets of bearings to guarantee colinearity of the axis of rotation and to minimize excentric wobbling of the rollers.

where small temperature changes can have a very significant effect on material parameters, such as the shear viscosity; (b) the glass windows are mounted onto the flow cell in a way that minimizes possible degradation of the optical characteristics of the incident beam, that is used for birefringence and light scattering measurements (this, and other related ideas, will be discussed in the following section); and (c) the mechanical design assures the highest degree of parallelism between the rollers axes, with the least eccentricity about each roller axis in order to reduce possible asymmetries of the flow field. A high degree of parallelism among the roller axes is needed to assure two-dimensional flow fields, while a minimal degree of eccentricity guarantees that the position of the stagnation point remains fixed in space, with a constant value for the flow parameter λ. These characteristics become important requirements whenever the flow or the fluid properties vary strongly as a function of position, or whenever non-homogeneous effects are to be studied.

The flow cell maintains the roller axes at a fixed distance and the two-roll mill actually corresponds to a pair (chosen from a set of eight pairs) of rollers that can is installed inside the flow cell. The complete flow device is made of stainless steel and has been surface-treated with black chrome. The maximum volume capacity of the flow cell is 115 ml. (which corresponds to the flow cell with the smallest rollers) and it has an optical path length (in vacuum) of 2.54 cm. (*i.e.*, the length parallel to the cylinder axes). Stainless steel provides the chemical inertness (of the container) necessary for the typical polymer/solvent combinations. The blackened surface treatment on the flow device is desirable for optical measurements in order to reduce background scattered light. The glass windows are glued to a mount that can be rotated about its center, and have holding screws that are also used to adjust the stress at three points on the rim of the window mount in order to minimize the residual stress of the glass windows; these ideas are discussed later in the section describing the optical part of the apparatus. These windows are made of optical flats of high quality and have an antireflective coating on the external surface for maximum transmission at 500 nm. They are approximately 1.5 cm. in diameter,

and the clear aperture is approximately 1.2 cm. with the area "reduction" due mainly to the observed high stresses along the perimeter of the supporting mount.

The flow device has a cooling loop around the cylindrical portion of the flow cell body designed to maintain the fluid at a constant temperature. The cooling circuit includes a variable flow rate pump immersed in a constant temperature bath, with the flow rate of the cooling liquid controlled by a Leeds & Northop PID controller. The cooling liquid in the constant temperature bath has a temperature that is 0.5 degrees below the set-point for most operating conditions. The control loop is based on temperature readings obtained within the flow device by means of a calibrated thermistor (12900 Ω at 20 degrees Celsius) on one arm of a Wheatstone resistance bridge. The observed variations of the temperature at the thermistor point never exceed 0.2° Celsius; the average fluctuation for an experimental run is of the order of 0.04° Celsius for the range of conditions accessible to this apparatus.

The requirements for a stable, symmetric, two-dimensional, and highly reproducible and accurate flow field imply that the design criteria for the roller assembly should guarantee: (a) the same physical characteristics (such as radius and eccentricity) for both rollers since geometrical parameters define the position of the stagnation point as well as the value of the flow parameter λ; and (b) a truly synchronous rotation of both rollers, so that the temporal evolution of the speed of the rollers is identical at all times. The need for synchronization between the rollers is best resolved by using only one motor to drive both rollers, with a worm-and-gear couplings used to connect the motor and rollers. The rollers for our flow device are driven by a set of identical worm-and-gear assemblies and connected by a single shaft to a stepping motor (Superior Electric motor Slo-Syn M062-FD09 driven by a MODULINX programmable microstep indexer IMD128). It is also important to minimize the play between worm and gear assemblies to avoid small phase differences between the two rollers. This requirement was achieved by maintaining a fixed position for the axes of the worms and gears, together with a tight coupling, regardless of the load, angular position or speed of the motor.

The worm positions are fixed by using thrust bearings along the shaft at both ends of the worms (for axial loading) together with angular contact bearings (for radial loading). To keep the roller shaft position fixed, and in order to maintain the least excentricity for the rollers within the flow cell, each of the rollers runs on three bearings, while allowing a "frictionless" rotation. Within the flow device, the rollers rotate with the shaft held at both ends, so that the wobbling is minimized and should be no more than the possible play within the bearings. The wobbling of the shaft section near the gears is reduced by pre-loading the upper roller bearings.

It is only after the relative position of the motor and the roller shafts are maintained constant (without excessive friction and little play) that a minimal perturbation of the idealized flow field is possible; excessive play in the gear assemblies can cause changes in the *relative* speed of rotation of the rollers, and the effects of eccentric rollers can displace the stagnation point away from and around the geometric center of the flow device. The flow device has two possible sets of worm-gear assemblies with reduction ratios of 5:1 and 20:1. These gear sets are very useful in expanding the number of programmable motor speeds accessible to the experiment, and yield a minimum angular speed for the rollers of $\pi/200$ radians per second, and a top speed of 10π radians per second.

Our flow device has eight *pairs* of rollers of different diameters. In this design the distance between the rollers' axes is kept fixed (see Figure 1.5). Thus, as the diameter of the roller pairs is increased, the gap decreases and, as it tends to 0, the flow approaches the simple shear flow limit in the vicinity of the stagnation point. It is, in fact, possible to cover a *range* of flow-types corresponding to $0.01 \leq \lambda \leq 0.25$ with the available range of roller diameters. Table 1.1 contains the various values of the flow type parameter λ for each pair of rollers as a function of the geometrical parameters for the rollers[3] (radii) and the flow cell, such as gap size,

[3]The four smaller rollers are made of stainless steel with a black chrome coating. The remaining rollers have a stainless steel core and an annular part made of aluminum. The advantage of the later design is that the angular inertia is significantly smaller than if the cylinders are made of solid steel. These larger rollers have been black anodized.

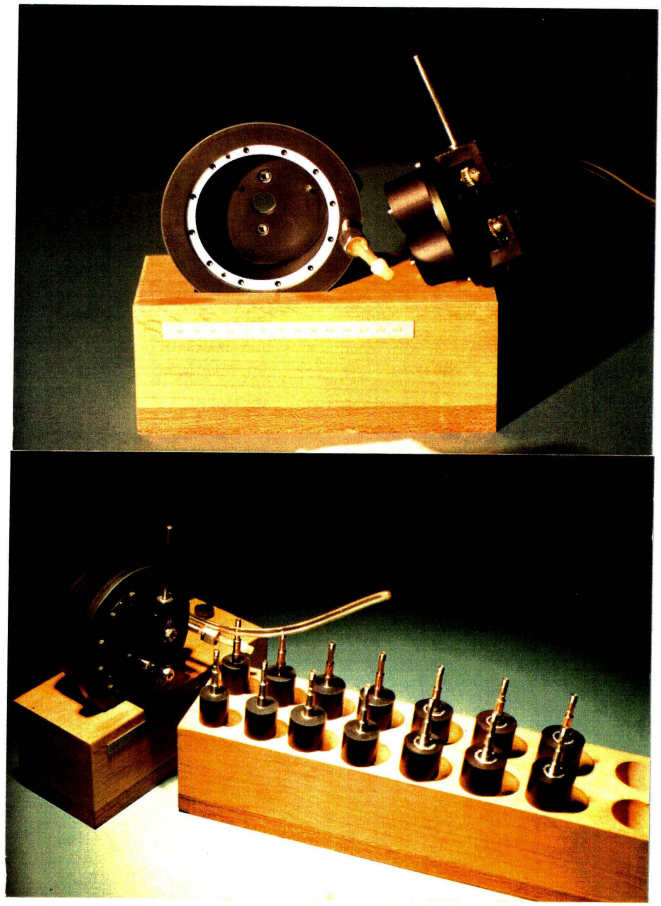

Figure 1.5: The two-roll mill flow device. The set of rollers cover a range of flow parameter values of $0.01 \leq \lambda \leq 0.25$ corresponding to the largest radius rollers (attached to the cover of the flow device) and the remaining sequence of rollers shown next to the flow cell.

Roller ID.	radius (cm)	gap (cm)	height: gap ratio	λ
A	1.665	0.070	36:1	0.0104
B	1.635	0.130	20:1	0.0196
C	1.570	0.260	9.8:1	0.0403
D	1.510	0.380	6.7:1	0.0605
E	1.400	0.600	4.2:1	0.100
F	1.278	0.844	3.1:1	0.150
G	1.169	1.062	2.4:1	0.201
H	1.075	1.250	2.0:1	0.250

Table 1.1: Geometrical characteristics of the two-roll mill. The flow field parameter has being calculated using equation 1.40.

the ratio of gap size to roller radius, and the ratio of roller length to gap size. In addition, Table 1.2 shows the angle made by the flow axes, the maximum values for the shear rate $\dot{\gamma}$, based upon roller rotation rates that are attainablein our system, and the eigenvalue $\dot{\gamma}\sqrt{\lambda}$ that can be obtained with each set of rollers. The roller length to gap size ratio is an important parameter because it is an indicator of the magnitude—for different flow geometries—of the largest possible shear rate that can be achieved before the effect of the end boundaries becomes significant. Lagnado and Leal [3] have studied the onset of three-dimensionality in the flow field with a four-roll mill by using streakline photography on planes perpendicular to the streamlines. Their purpose was to investigate the effects due to the end boundaries, *i.e.*, the effects caused by the finite size of the flow device along the axis parallel to the axis of the rollers. They concluded for the case of Newtonian fluids, that as long as the corresponding value of the Reynolds number Re for the four-roll mill does not exceed a value of 5, the two-dimensionality of these *finitely* bounded flows is acceptable in the sense that a large portion of the flow remains strictly two-dimensional. Furthermore, theoretical work on the stability of a general two-dimensional linear *unbounded* flow by Lagnado *et al.* [19] suggests that the onset of critical conditions should depend on the flow type parameter λ in

the form $\sqrt{\lambda}\dot{\gamma}$. Dunlap and Leal [4] found from flow visualization experiments in a

Roller ID.	λ	χ (degrees)	$\sqrt{\lambda}\dot{\gamma}_{max}$ (sec^{-1})	$\dot{\gamma}_{max}$ (sec^{-1})
A	0.0104	5.82	151.9	1490
B	0.0196	7.97	109.3	780.6
C	0.0403	11.35	74.2	369.4
D	0.0605	13.82	58.8	239.1
E	0.100	17.55	43.3	136.9
F	0.150	21.17	32.9	84.6
G	0.201	24.15	26.2	58.4
H	0.250	26.51	21.8	43.7

Table 1.2: Calculated parameter of the two-roll mill based on equations for creeping flow; equations 1.39 - 1.41.

two-roll mill that if the criteria for onset of "three-dimensional effects" is expressed as $Re\sqrt{\lambda} \sim 5$ the complete range of accessible flow fields can be covered under this generalized criteria. This condition is easily met by most of the polymeric solutions that we have used, because the solvent viscosity is quite high and the zero-shear-rate viscosity of our solutions is even higher.

Furthermore, by driving the rollers with a motor that is capable of varying speed as a function of time in a controlled, reproducible manner, the two-roll mill can generate a large variety of transient flows. The stepping motor used to drive this flow device is controlled by a computer program in a way such that different flow histories can easily be executed.[4] In this case, the range of possible flows not only includes variations in the shear rate $\dot{\gamma}$, and changes in the flow type parameter λ, but also variations in the temporal history. By using transient flows, we have been able to explore more readily the relaxation dynamics of polymeric solutions when subjected to large deformations. It is an alternative technique to the use

[4]This computer program also performs the data acquisition simultaneously for all of these flows. Consequently, no matter how complicated or fast the flow conditions are, our apparatus can produce an accurate and reliable set of data. A detailed explanation of the real-time software for these experiments is given later on in this appendix.

of oscillatory flows where it is only possible to impose small deformations on the fluid sample. Among the different flows that can be attained with our apparatus are steady state flows, plus some of the simplest transient flows such as start-up, relaxation after cessation of steady flow, or double-steps flows.

1.4 Time Dependent Flow Histories

The advantage of a computer controlling the flow field is the immense number of possibilities as to the time evolution of the boundary conditions for any flow device. It is important to emphasize that the experimentalist is only in a position to prescribe the boundary motions, for the flow fields ultimate response at different points depends on the local properties of the fluid, which in the case of polymeric liquids can change drastically over short distances. For the evaluation of the dynamic properties of polymeric fluids, a few simple time-dependent flow histories suffice to provide enough, and interesting information. On the other hand, the response of the fluid to steady state flow can also provide important information, since data represents degrees of changes on the polymer conformation for a given magnitude of the velocity gradient.

1.4.1 Steady State Flow.

Steady flows are generated with a constant angular speed of the rollers. The computer software allows an automated sweep through a series of steady flows with different values of $\dot{\gamma}$. Besides the importance *per se* of measurements of polymeric flow characteristics under steady state flow conditions, these experiments can also provide information regarding the characteristic *time-scales* of these liquids, which in turn, are a direct consequence of the dominant polymer dynamics within the prescribed environment imposed by the flow. We can consider that the inverse of the shear rate for steady flow is an external time-scale imposed by the experimentalist upon the fluid. The response of the polymeric fluid to this external "forcing"

depends upon the relationship between the externally imposed time-scale and the internal relaxation time-scales of the fluid. The observable features of these fluids subjected to steady two-roll mill flows, such as the optical anisotropy of the polymer microstructure and its orientation as a function of shear rate—or any other parameter characterizing the flow field—thus contain important clues to the fluid time-scales. Changes of the flow parameter λ for steady flows can be used to study the possible relationships that exist between the characteristic time-scales (that is, dominant relaxation mechanisms) and the degree of deformation of the polymer microstructure as it varies as a function of λ while the shear rate is maintained constant.

1.4.2 Start-up and Cessation of Flow.

Cessation of steady flows corresponds to a "instantaneous" step-change[5] from a steady flow condition to a state of no-flow. Start-up of flow describes the exact opposite scenario. Cessation and start-up of flow are two of the simplest transient flows that can provide direct insight into the microscopic time-scales of the fluid. The relaxation of birefringence and orientation angle after cessation of flow has long been considered as a direct measure of the time-scale for the internal dynamics of the fluid. This relaxation time-scale depends only on the initial polymeric conformation as caused by the previous flow stage. Thus, it depends on the imposed shear rate as well as the duration of flow, and also on the flow type parameter.

Start-up of flow, on the other hand, has only more recently been recognized as another valuable technique to study the time-scales for evaluation of the microstructure of the fluid. For onset of flow, there are several characteristic time-scales that can be defined depending on the features of the observed behavior, such as the time

[5]Actually, all flow conditions are achieved via an acceleration ramp for the rollers angular velocity that although quite high, is still finite. The motor always requires less than a 1/20th of a second to reach any prescribed angular speed; mean values for the ramp-time are less than 2/100 of a second. The fastest macroscopic time-scales observed for the particular fluid sample were at least an order of magnitude longer. The acceleration ramp is one of the various parameters that the experimentalist has control of through the computer. The observed behavior was always checked for possible dependency of the time-ramp.

necessary to reach the maximum for any overshoots, the time for the overshoot to decay, etc. These time-scales also provide important information about the dynamics of the microstructure, specifically about the *initial* and *final* conformation of the microstructure. That is, the previous history of the fluid conformation before the onset of the flow is as important as the final conformational state that is reached. Consequently, those parameters which most likely affect the observed behavior for start-up flows are the acceleration under which the steady state is reached, the steady state shear rate, the flow type, and the amount of time the fluid stays at rest before the flow field is initiated. All of these parameters can be varied with the two-roll mill for start-up and cessation of flow.

1.4.3 Double-Step Type of Flows.

Double-step flows are similar to the abrupt start-up and cessation of flow, but play an important role in studying the polymer dynamics when the initial and final states are *not* states of final equilibrium. These flows impose on the fluid a continuous shear rate and alternate from a state of high shear rate to a state of low but nonzero shear rate (or *vice versa*). In these cases the time-scales of the underlying polymer dynamics can have several manifestations, such as the presence of overshoots, undershoots, etc. The pre-conditioning flow stage is used to set the initial conformation of the polymer microstructure and, hence, these flows provide information about the effects of the "initial conformational status" of the polymer molecule on the relaxation dynamics of the fluid. The time that the flow remains at a given shear rate, although obviously important, is always assumed to be long enough that the fluid has reached a state of quasi-equilibrium with the flow field that is easily reproducible. The main objective of long times is limiting the accessible polymer dynamics to those that occur with time-scales faster that those imposed by the flow field. Thus, the changes of the observed phenomena as a function of the low and high shear rate are the simplest and most useful information that can be obtained with this type of transient flows, although under particular circumstances

the length of the time at high and/or low shear may also be an important parameter to vary in these flows. This apparatus is capable of varying all of these parameters.

Bibliography

[1] G. I. Taylor; *Proc. Royal Society. (London)*, **146**,501-523(1934).

[2] G. G. Fuller and L. G. Leal; *J. Polym. Sci.: Polym. Phys. Ed.*, **19**,557-587(1981).

[3] R. L. Lagnado; *Ph. D. Thesis*, California Institute of Technology, Pasadena, Ca. (1985).

[4] P. N. Dunlap and L. G. Leal; *J. Non-Newtonian Fluid Mech.*, **23**,5-48(1987).

[5] R. I. Tanner; *Engineering Rheology*, Oxford Press, Oxford, 1988.

[6] G. G. Fuller, J. M. Rallison, R. L. Schimdt and L. G. Leal; *J. Fluid Mechanics*, **100**(3)555-575(1980).

[7] B. J. Bentley and L. G. Leal; *J. Fluid Mechanics*, **167**,219-240(1986).

[8] G. Astarita; *J. Non-Newtonian Fluid Mech.*, **6**,69-76(1979).

[9] S. Torza; *J. Polym. Sci.: Polym. Phys. Ed.*, **13**,43-57(1975).

[10] G. B. Jeffery; *Phyl. Trans. Royal Soc.*, A**221**,265-293(1920).

[11] G. B. Jeffery; *Proc. Royal Society (London)*, A**101**,169-174(1922).

[12] T. Kapur, E. P. Ascoli M. Shapira and L. G. Leal; in preparation 1990.

[13] E. Geffroy, E. P. Ascoli and L. G. Leal; in preparation 1990.

[14] J. M. Broadbent, D. C. Pountney, and K. Walters; *J. Non-Newtonian Fluid Mech.*, **3**,359-378(1978).

[15] I. G. Currie; *Fundamental Mechanics of Fluids*, McGraw-Hill Book Co., NewYork, 1974.

[16] I. S. Gradshteyn and I. M. Ryzhik; *Table of Integral Series, and Products.* Academic Press, New York, 1965.

[17] H. Giesekus; *Rheologica Acta*, *2*(2)112-122(1962).

[18] L. G. Leal; *Advances in Rheology*, Ed. B. Mena *et al.*, Vol. 1 pp. 191(1984).

[19] R. L. Lagnado, N. Phan-Thien and L. G. Leal; *Phys. Fluids*, **27**,(1984).

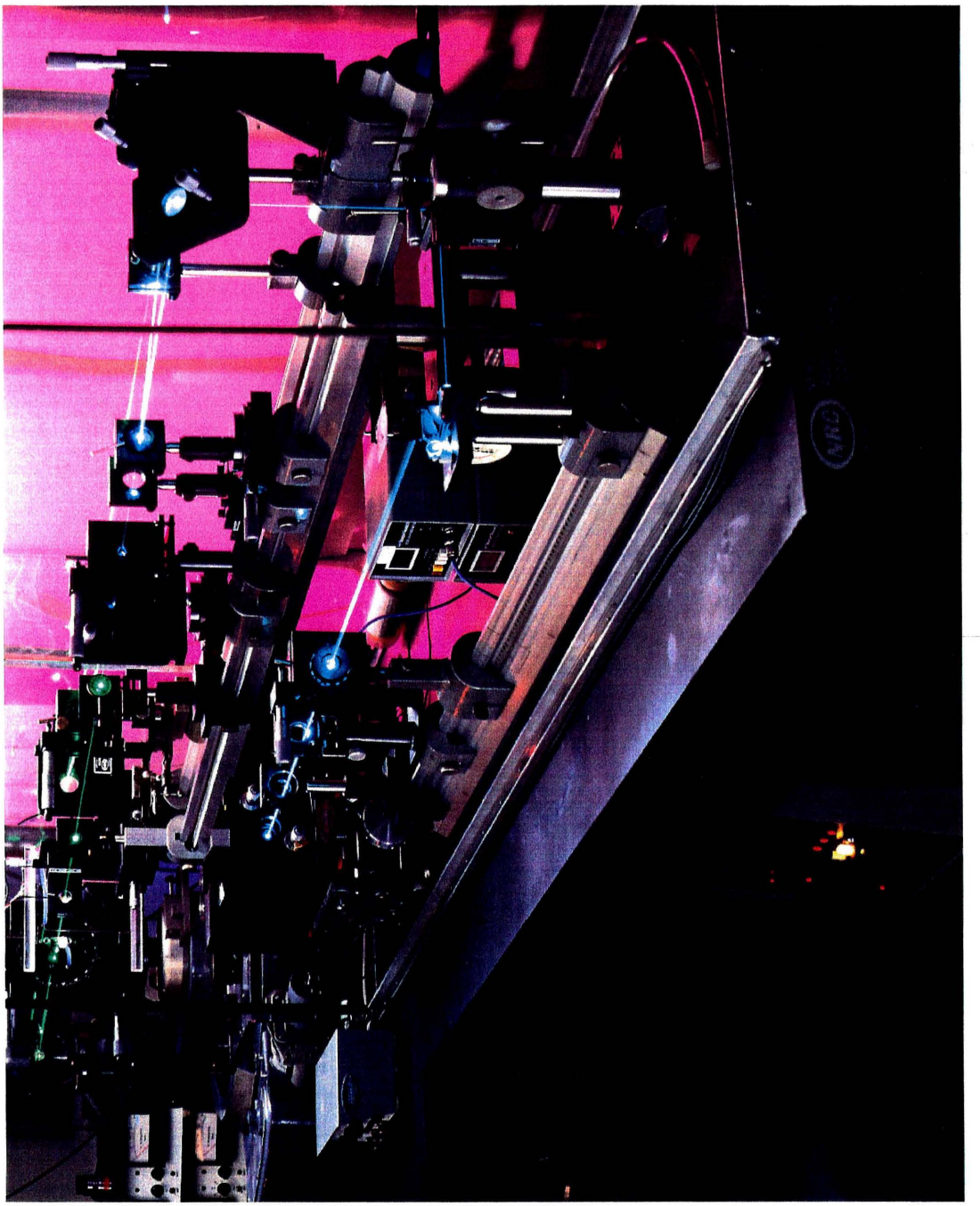

Chapter 2
The Experimental Optical Techniques

Chapter 2

The Experimental Optical Techniques

This chapter describes the two optical techniques used in this laboratory for characterizing the macromolecular conformation and the flow field of polymeric liquids. The experimental methodologies under consideration are the Two Color Flow Birefringence (TCFB) and the Homodyne Light Scattering (HLS). The first allows a simultaneous determination of the flow-induced optical anisotropy, and the orientation of this anisotropy with respect to the principal optical axis of the apparatus. The second technique provides a direct measure of the rate of deformation imposed by the flow fields upon the polymeric structure. In the following sections the principal characteristics of the flow-induced birefringence are presented first, along with a discussion of the limitations, sensitivities, and manipulation of the experimental data in order to enhance the quality of the measurements. This is followed by a description of the actual laboratory implementation of the TCFB technique. Finally, we present the HLS technique used for the evaluation of the principal components of the velocity gradient. Both techniques are sufficiently fast to allow measurements that are "instantaneous," relative to the most important characteristic time-scales for large deformations of the polymeric fluids.

2.1 Optical Characterization of Polymeric Liquids

First, we describe an experimental technique which evaluates the conformational changes suffered by the polymer due to the deformation history imposed by the flow field. For this purpose there exists a variety of different physical measurements that could be made in order to evaluate the dependence of polymer conformation on the characteristics of the flow. However, the experimental parameters that are usually reported for rheological measurements correspond to macroscopic averages evaluated at the boundaries of the flow devices. For example, this is true of the torque measured at the top surface of the cone-and-plate rheogoniometer, the shear rate as evaluated from the mean flow rate in a capillary tube, or the stress as measured by pressure transducers in a convergent flow, etc. On the other hand, the experimental techniques used here are of an optical nature, and in the past have been used extensively to "correlate" optical data with the deviatoric part of the stress tensor via the stress-optical law. Optical methods are specially advantageous when a *very fast* response of the system is needed, and all provide an indication of flow or material behavior that is *local* on the scale of the flow. A fast response and the capability to evaluate properties of interest in a "point wise" manner are two of the most important characteristics that are needed for studies of polymer solutions in a two-roll mill. However, it should be emphasized that optical techniques can provide important information about the structure of the liquid that is not otherwise accessible while using standard mechanical rheological tools. For example, optical techniques are usually more sensitive to the presence of additives, where the effects of dilute amounts of the material of interest can be studied easily by minimizing the optical effects of the solvent, than the standard techniques where the solvent effects are the dominant contribution. Furthermore, optical methods can effectively separate the individual contributions of different constituents of the liquid as well as different dynamic effects. We will discuss some of these ideas shortly.

2.1.1 Flow Induced Optical Anisotropy

The microstructure of polymeric liquids is highly anisotropic, that is, the polymer structure is such that the refractive index along the backbone of the molecule is slightly different from the refractive index along a direction perpendicular to the backbone. When these systems are at rest, the effect of thermal motions is to randomize the polymeric microstructure and thus produce a totally isotropic medium. On the other hand, whenever there is an average orientation of the different elements of the polymeric liquid, these fluids in general, show a high degree of optical anisotropy. This optical anisotropy is defined as a refractive index of a tensorial form with complex elements with different principal values. The real part of the tensor elements correspond to a measure of the speed of propagation of the electromagnetic wave in the medium, and when the principal values are different, the material is said to be optically birefringent. The imaginary part of each element is a measure of attenuation of these waves by scattering and absorption as they propagate through the medium, and when these principal values are different, the material is said to be dichroic. Using polarized light, it is then possible to measure the difference of the principal values of the real and the imaginary parts of the refractive index in the plane of the electric vector of the propagating wave.

There exists a great diversity of liquid systems for which the optical anisotropy is only limited to only one type of physical effect, *e.g.*, suspensions of non-spherical particles tend to be highly dichroic because the nonisotropic scattering is very strong for particles larger than the wavelength of the propagation wave, while polymeric solutions tend to be highly birefringent, with a much smaller contribution of dichroism.[1]

However, dichroism is an absorption effect and consequently, there may exist a

[1]Years ago, W. Heller [1] pointed out, that although dichroism is frequently an insignificant component of optical anisotropy for polymeric solutions, nevertheless, it is always necessary to be aware of the possible effects when analyzing experimental data of flow birefringence. This conditions of high dichroism are rarely encounter in reality because of the rather poor precision of most experiments. In the following sections we present some consequences of dichroism in polymer solutions an possible ways to reduce its effects of the experimental data.

region (or regions) of the spectrum in which the propagating wave is also highly attenuated, and therefore, where dichroism is equally important, even for polymer solutions! In the following subsection we will review the mathematical formalisms used in the evaluation of optical anisotropy.

There exist a number of optical techniques which can be used to evaluate the optical anisotropy of a sample, all of them extensively documented under the broad field called ellipsometry and polarimetry, in which polarized light is used to evaluate the optical anisotropy of the test sample (see for example Azzam and Bashara [2] for several possible variations of these techniques). Within the rheology of polymer solutions, most of the published works to date—where optical anisotropy is measured—are only concerned with the birefringence contributions. When the optical anisotropy is induced by a flow field then, the technique is known as flow-birefringence. This well known technique has been reviewed among others by Tsvetkov *et al.*, [3], Peterlin [4], Wales [5], and more recently by Janezschitz-Kriegl [6]. Flow birefringence is a noninvasive technique which yields both the *degree* of optical anisotropy, and the *orientation* of the principal axes of the refractive index tensor, with respect to the principal axes of the flow field. This technique has been used in the past for steady flows generated by two- and four-roll mills by Cressely *et al.*, [7, 8] in France and by Mackley, Keller and co-workers, [9, 10, 11, 12] in Britain. This technique has also been used extensively by the research group headed by Prof. L. G. Leal at Caltech to evaluate material properties of dilute and concentrated solutions. The main results appeared in the Ph.D. theses of Fuller [18], Dunlap [14] and R. Ng [15].

2.1.2 Transient Flow Anisotropy

In order to capture the transient behavior of the macroscopic properties of the polymeric liquid (subjected to transient flows with a two-roll mill) a very fast flow-birefringence technique must be used, since both the degree of birefringence and the orientation of the principal axes of the refractive index tensor are unknown

and vary with time. There are primarily two techniques available in the literature. These are the two-color flow birefringence (TCFB) proposed by Chow and Fuller [16] and used by them in conjunction with a Couette device, and variations of an automated-null ellipsometer proposed some time ago [2] and more recently reintroduced by Shindo *et al.*, [17, 18] and Frattini & Fuller [19] (specifically phase-modulated flow-birefringence, FMFB) for the study of polymeric systems under shear flow conditions. Both techniques are equally fast and reliable. However, the TCFB technique requires a more complex optical arrangement, but simpler optical elements, and very simple electronic instrumentation. The basic idea of TCFB is to evaluate the "instantaneous" birefringence and corresponding orientation by taking two measurements simultaneously, using two beams of polarized light of *different* color.

Our experimental arrangement is of the TCFB type and is specifically designed to perform measurements in *real* time for fluids that show a strong spatial variation of the flow-induced anisotropy. In particular, since the velocity gradient remains spatially uniform in a simple shear flow device (*i.e.*, all of the previously studied flow fields), as compared with the two-roll mill where it is a function of position, then using the TCFB technique with this flow device requires extra precaution. Thus, besides the requirements for the two-color flow birefringence as proposed by Chow and Fuller, the optical arrangement must also satisfy two supplementary criteria. First, the measurements must be done on precisely the same element of material volume at all times. Consequently, it is also required that the optical properties of the two colored beams, as they pass through the fluid, must be identical so that the measurements correspond to the *same* element of fluid volume. The second criterion requires that the cross section of the element of fluid perpendicular to the optical axis, to be very small compared to the flow field length scale, if the measurement is to be representative of the fluid properties with a "unique" flow history.

However, if it is properly configured, the TCFB technique can provide a measure

of the material behavior in a *point wise* manner on the scale of the flow (though, it is averaged over the length of the flow cell in the third direction and includes the effect of top and bottom boundaries). The current optical arrangement, together with the associated electronics, is capable of performing real time (10 kHz bandwidth) TCFB measurements within a sampling area across the flow field of approximately 75 microns in diameter. This experimental set-up also has the capability of translating the flow cell with respect to the optical system in order to evaluate the birefringence at all possible locations in the neighborhood of the stagnation point in the flow plane (within a radius of 0.75 cm.). The optical arrangement, together with the two-roll mill and a computer—for automated data acquisition and control—form the present experimental system.

2.2 Evaluation of Optical Anisotropy

The complete experimental study of the optical anisotropy of polymeric solutions requires a knowledge of both the *real* and *imaginary* parts of the refractive index tensor. This is a consequence of birefringence being related to the real part of the refractive index tensor—the difference, along perpendicular directions, of the two principal components—and dichroism corresponding to the difference of the principal components of the imaginary part. Experimentally however, both effects cause the same change on the parameters being evaluated. Therefore, the analysis of experimental data needs to take into account the possibility that, in most cases, the two physical phenomena will be present simultaneously. According to Onuki and Masao [24], the microscopic effects that give rise to fluid birefringence may have two contributions: one known as form birefringence and the other as intrinsic birefringence. Associated with form and intrinsic birefringence are two distinct physical phenomena. The former phenomenon is related to the orientation of the polymer segments, and the latter is due mainly to the anisotropy of the segment density correlation function. The same criteria applies for dichroism. For polymeric

solutions, however, its intrinsic dichroism is negligible.

2.2.1 Evaluation of Birefringence with the TCFB technique

The TCFB technique is essentially equivalent to a double null ellipsometer designed to provide information on the anisotropy of the medium, including the orientation of the principal axes of the refractive index tensor. That is, each measurement provides sufficient information to determine both the medium birefringence and the orientation of its anisotropy. This is the reason why two measurements are needed simultaneously, and the use of a beam of two colors—with one ellipsometer assigned to each color beam—allows determination of both parameters instantaneously.

The equations that describe electromagnetic propagation of elliptically polarized light, with a transverse electric field are

$$\begin{aligned} \mathbf{E}(\mathbf{r},\ t) &= [\mathrm{E}'\cos(\omega t - \mathbf{k}\cdot\mathbf{r} + \delta']\mathbf{u}' + \\ &+ [\mathrm{E}''\cos(\omega t - \mathbf{k}\cdot\mathbf{r} + \delta'']\mathbf{u}'' \end{aligned}$$

Here, $\mathbf{k}$ represents the direction of propagation of the electromagnetic wave, E′, E″ represent the amplitudes of the electric vector along the orthonormal directions $\mathbf{u}'$, $\mathbf{u}''$ respectively, and δ', δ'' are the phases of the electric vector relative to a fixed laboratory frame. The above equation is most useful for ellipsometric applications when the temporal description of the wave is dropped and $\mathbf{E}$ is written as

$$\mathbf{E} = (E_x \mathrm{e}^{i\delta_x z},\ E_y \mathrm{e}^{i\delta_y z})$$

where the phase factor $\delta_i = 2\pi n_i/\lambda$, and both, the amplitude of the electric field E_i and n_i are complex quantities; with n_i being the refractive index. The above equation contains all the information for the complete characterization of polarized light.

In order to determine the effects on polarized light as it traverses an anisotropic

media we make use of the Muller matrix calculus[2] for optical systems. The basis of the Muller calculus, is the fact that the polarization properties of light can be expressed by only four parameters. These are the so-called Stokes parameters of polarization. The Muller calculus, provides a formalism by which the interaction of light and matter is prescribed as 4×4 operators acting upon the Stokes parameters (for references see for example [25]). In this case the operator describing a polarizer $P(\alpha)$ with azimuthal orientation α based on the Ox axis, and with angles defined in the standard mathematical sense, is given by

$$P(\alpha) = \begin{vmatrix} 1 & \cos 2\alpha & \sin 2\alpha & 0 \\ \cos 2\alpha & \cos^2 2\alpha & \sin 2\alpha \cos 2\alpha & 0 \\ \sin 2\alpha & \sin 2\alpha \cos 2\alpha & \sin^2 2\alpha & 0 \\ 0 & 0 & 0 & 0 \end{vmatrix} . \tag{2.1}$$

For a birefringent medium $B(\beta, \delta)$, with retardation δ and orientation β relative to the Ox axis its Muller operator is

$$B(\beta,\ \delta) = \\ = \begin{vmatrix} 1 & 0 & 0 & 0 \\ 0 & \cos^2 2\beta + \sin^2 2\beta \cos\delta & \cos 2\beta \sin 2\beta(1 - \cos\delta) & \sin 2\beta \sin\delta \\ 0 & \cos 2\beta \sin 2\beta(1 - \cos\delta) & \sin^2 2\beta + \cos^2 2\beta \cos\delta & -\cos 2\beta \sin\delta \\ 0 & -\sin 2\beta \sin\delta & \cos 2\beta \sin\delta & \cos\delta \end{vmatrix} . \tag{2.2}$$

Therefore, for a null ellipsometer composed of a polarizer, a birefringent medium, and an analyzer, the polarization characteristics of the light past the analyzer, are given by the Stokes parameters $S^o = A(\alpha_A)B(\beta,\ \delta)P(\alpha_P)S^i$ where S^i and S^o represent the Stokes parameters of the incident and output light respectively. The first element of the Stokes parameter is the intensity of the light source. Hence, when an isotropic light detector is used after the analyzer, the first parameter is always measured. Furthermore, the incident light is usually a laser source and consequently, we can consider that it is already linearly polarized.

[2]There are several well established matrix calculus for the computation of polarization properties of light, such as the Jones or Muller's calculus. However, the Muller calculus has the advantage of being able to model some of the simpler optical elements that produce anisotropic *attenuation* of light. These are physical conditions that are, at the best, very difficult to manipulate with some of the other, more common methodologies. Therefore, in order to maintain the broadest capabilities for a system in which anisotropic attenuation, *i.e.*, dichroism is a weak, nonetheless measurable possibility for polymeric fluids we have followed here this line of computation.

For a two-color system it is best if the initial orientation of the light is along the bisector for the two polarizer directions. In this manner the light intensity attenuation by the polarizers is approximately equal for both incident beams. Thus, taking the laser output with a vertical polarization, polarizers with orientations that are $\pi/8$ away from the vertical line (that is symmetric with respect to the Oy axis), and their respective analyzers rotated by $\pi/2$ radians, we have a system of two null-ellipsometers with the capacity to measure the properties of interest. For the first ellipsometer, and from now on called the blue beam, $S^o = A(-\pi/8)B(\beta,\ \delta)P(3\pi/8)S^i$ with $S^i = \{{E_{y,B}}^2,\ -{E_{y,B}}^2,\ 0,\ 0\}$. The light intensity reaching a detector located after the analyzer is

$$\hat{I}_B = \frac{E_{y,B}^2}{2\sin^2\alpha_P}[1 - 2\cos 2\beta \sin 2\beta(1 - \cos\delta)] \ . \tag{2.3}$$

Equation 2.3 is based upon the orientation angle of the medium β with respect to the Ox axis (see Figure 1.2). Experimentally however, it is most desirable to measure angles with respect to the principal orientations as defined by the polarizers themselves. In this case, is best to redefine $\beta = \alpha_P - \chi$—where we have taken the standard mathematical convention for the angles—so that equation 2.3 becomes

$$\hat{I}_B = E_{y,B}^2 \sin^2(\delta_B/2)\sin^2(2\chi) \ . \tag{2.4}$$

This equation tell us that the system is totally symmetric for inversions of the direction of propagation of the electromagnetic wave. That is, the orientation angle cannot be distinguished from a series of equivalent orientations located $\pm n\pi/4$ radians relative to χ.

For the green beam the polarizer orientation is rotated $\pi/4$ radians relative to the blue polarizer direction. Let's say $\alpha = 5\pi/8$. In this case, the light intensity for the green beam reaching the green detector is also prescribed by equation 2.3. If the orientation of the blue polarizer is also used (instead of the laboratory frame of reference) to describe the light intensity reaching the green detector, then the blue polarizer becomes the preferential orientation, for both null-ellipsometers, and

$$\hat{I}_G = E_{y,G}^2 \sin^2(\delta_G/2)\cos^2(2\chi) \ . \tag{2.5}$$

Equations 2.4 and 2.5 provide the necessary information to calculate the orientation of the refractive index of the medium χ, and its retardance δ. Experimentally, it is only necessary to have relative orientations for the blue and green ellipsometers of $\pi/4$ radians, and to know the relative values of the incident radiations. That is, this specific angular separation is intrinsically included in the above equations. The relative values of the incident radiation can be incorporated by normalizing $\hat{I}_i$ by the corresponding $E_{y,i}^2$, where the latter quantity represents the maximum possible light intensity through the polarizer and analyzer but in this case with parallel orientations, and in the absence of the birefringent medium. In this way, the experimentally determined values are related to equations 2.4 and 2.5 by

$$i_B = \frac{\hat{I}_B}{{E_{y,B}}^2} = \frac{\hat{I}}{I_{max,\ B}} = \sin^2(\delta_B/2)\sin^2(2\chi)\ , \tag{2.6}$$

$$i_G = \frac{\hat{I}_G}{{E_{y,G}}^2} = \frac{\hat{I}}{I_{max,\ B}} = \sin^2(\delta_G/2)\cos^2(2\chi)\ . \tag{2.7}$$

The above equations reflect the fact that most materials have retardations δ_i that depend of the wavelength of the electromagnetic wave. On the other hand, the orientation of the anisotropy does not depend on wavelength, but only on the alignment of the material. It is then possible to obtain an approximate solution for the above equations assuming a solution via a perturbation scheme (see for example Bender and Orszag [26], Chapters 7 & 8). In this case, taking again the blue beam as the reference color, we can write the expansion with ϵ as the small parameter, as

$$\epsilon = \frac{\lambda_G - \lambda_B}{\lambda_G} \tag{2.8}$$

$$\delta_B = \frac{2\pi d}{\lambda_B}\Delta n' = \frac{2\pi d}{\lambda}\Delta n' = \delta \tag{2.9}$$

$$\delta_G = \frac{2\pi d}{\lambda_G}\Delta n' = \frac{2\pi d}{\lambda}\Delta n'(1-\epsilon) = (1-\epsilon)\delta \tag{2.10}$$

$$\delta(\epsilon) = \delta_0 + \delta_1\epsilon + \delta_2\epsilon^2 + \mathcal{O}(\epsilon^3)\ , \tag{2.11}$$

and solve for

$$i_B + i_G = \sin^2(\delta_0 + \delta_1\epsilon + \delta_2\epsilon^2 + \mathcal{O}(\epsilon^3))\sin^2(2\chi) +$$

$$+ \quad \sin^2[(1-\epsilon)(\delta_0 + \delta_1\epsilon + \delta_2\epsilon^2 + \mathcal{O}(\epsilon^3))]\cos^2(2\chi) \; . \qquad (2.12)$$

Using the following expression to reduce equation 2.12

$$\sin^2(\alpha \pm \beta) \simeq \sin^2\alpha \pm \beta 2\alpha + \beta^2(1 - 2\sin^2\alpha) \; ,$$

valid for all $\beta \ll 1$,[3] and collecting terms of increasing order in ϵ we obtain

$$\delta^{(1)} = \delta_0\left(1 + \frac{\epsilon i_G}{i_{\rm tot}}\right) \; , \qquad (2.13)$$

$$\delta^{(2)} = \delta_0\left(1 + \frac{\epsilon i_G}{i_{\rm tot}}\right) + \frac{1}{2i_{\rm tot}}\left[\frac{\delta_0^2(2i_{\rm tot}-1)i_G i_B}{{i_{\rm tot}}^{5/2}(1-i_{\rm tot})^{1/2}} + 2\frac{\delta_0 i_G}{i_{\rm tot}} - 1\right]\epsilon^2 \; . \qquad (2.14)$$

Here, $i_{\rm tot}$ is the sum of the relative intensities of both colors. For the first order approximation, equations 2.6 and 2.7 can be resolved for the birefringence $\Delta n'$ and the orientation angle χ

$$\Delta n' = \frac{\lambda_B}{\pi d}\left[1 + \left(\frac{i_G\epsilon}{i_{\rm tot}}\right)\right]\sin^{-1}(i_{\rm tot})^{1/2} \; , \qquad (2.15)$$

$$\chi = \tan^{-1}\left(\frac{i_B}{i_G}\frac{\sin^2(\pi d\Delta n'(1-\epsilon)/\lambda_B)}{\sin^2(\pi d\Delta n'/\lambda_B)}\right)^{\frac{1}{2}} \; . \qquad (2.16)$$

If the precision of the above formulae is not sufficient for data analysis, then equations 2.15 and 2.16 can be used in conjunction with a numerical algorithm (an iterative method of the Newton-Ralphson type is a good choice for most cases), where the approximate solution is the starting value for the iterative algorithm. For retardation values less than $\pi/2$, we can expect equations 2.15 and 2.16 to yield results within 1 % of the exact value.

2.3 The Optical Arrangement for TCFB

Four important features must be fulfilled for a two-color flow birefringence system to be usable in the study of non-homogeneous flow fields: (1) a stable light source,

[3]Later on we will discuss some limitations of the two-color birefringence equation. When the retardation is reaching values close to $\pi/2$ the expansion for the sin function may not be the most appropriate, for β is no longer small.

(2) the correct complementarity between the two color, in order for the analysis presented in the previous section to be applicable to the measured quantities, (3) a high sensitivity for the optical arrangement to be capable of discriminating against a background with dust particles in the test fluids, and (4) the necessary accuracy to measure the anisotropy of the fluid in a point wise manner. The schematic diagram for the present experiment is shown in Figure 2.1. Firstly, the light source is a Spectra Physics model 2020 Argon-ion laser. The two colors correspond to the 4880 Å blue line and the 5145 Å green line. These are the two strongest, most stable lines of an Argon-ion laser. The laser head, in order to supply the two-color beam, has been equipped with a blue-green output coupler, a flat broadband reflector, an isothermal intracavity etalon and, a polarization rotator at the lasing end. The polarization rotator allows the operator to adjust the polarization orientation of the outgoing beam such that the intensity of both beams when they reach the flow device is equally strong. This is necessary because the Brewster windows of the laser cavity already define the polarization orientation of the exiting beam (vertically polarized), which under the most general conditions is not the most appropriate orientation given that the orientation of the polarizers for the green and blue beams are tilted $+22.5°$ and $-22.5°$ respectively, from the horizontal plane. These initial orientations for the polarizers were chosen so that their bisector lies on the symmetry plane along the gap of the two-roll mill.[4]

For this type of laser, although the total light intensity remains at a constant value, with almost no drift, the intensity of every line will fluctuate within a much wider range due to the competing effects between different modes of the same color, and also because of competition between the different lines. The intracavity etalon

[4]The symmetry plane been chosen based on mechanical considerations that warranty a center of mass closest to the geometrical center of the flow, since the stepping motor represents a large mass off center for other orientations. However, the relative orientation of the flow cell with respect to that defined by the orientation of the polarizes is totally symmetric with respect to the horizontal plane or any other orientation defined by increments of 45° degrees. This condition provides the flexibility and convenience to map the birefringence in the global sense along radial directions starting at the stagnation point in the flow.

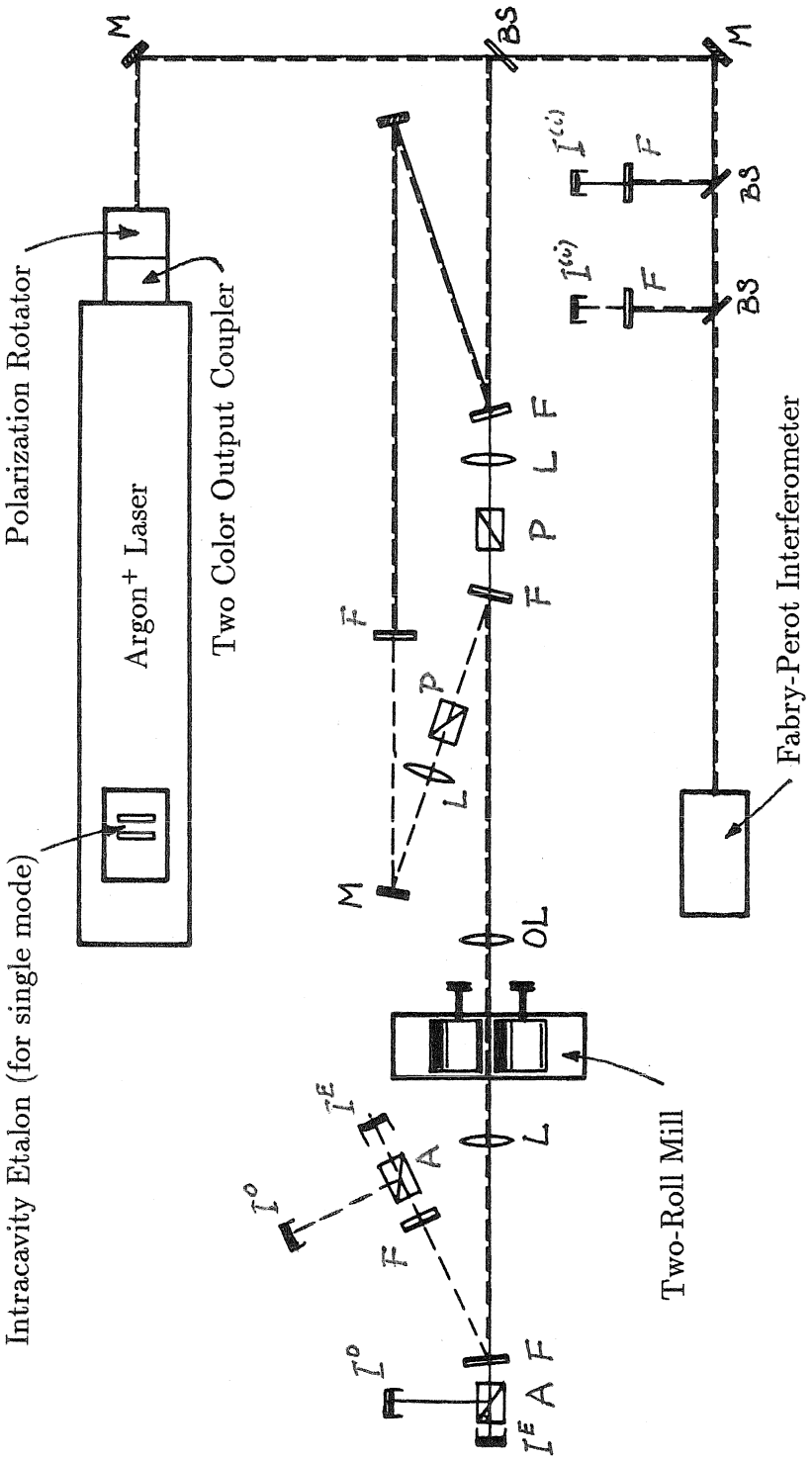

Figure 2.1: Optical arrangement for the Two color Flow Birefringence (TCFB) implemented for this work. Blue laser beam is shown as a continuous line; green beam as a broken line.

is used to operate the laser in single mode for both lines and in this way a more stable operation for the intensity of the two colors is obtained. Furthermore, the stability of the light intensity depends on the gain of the laser cavity (The conversion efficiency for a given mode.) This gain depends on the temperature on the etalon. The control of the temperature of the etalon's oven provides the means of balancing the intensity of both beams so that the most stable operation is achieved for both lines.

The argon laser equipped with these items becomes a light source with the following important characteristics: (a) one laser provides the two colors, and consequently the initial optical characteristics of both beams are identical, (b) both lines operate in single transversal emission mode TEM_{00}, maintaining it for periods up to several weeks at a time. In this manner, the light intensity distribution across the beam is very stable and can be assumed to have a *Gaussian* profile at all times; and, (c) the stability of the light intensity is best for both lines independently, remaining within a percentage point. The Fabry-Perot interferometer indicated in Figure 2.1 provides the necessary monitoring capability for fine-tuning of the laser system.[5]

The present optical arrangement is designed to address two important and different aspects of the flow birefringence experiment: first, the conditioning of both beams with respect to the polarization orientation, and secondly, the conditioning of the green and blue beams so that the element of fluid volume probed is identical

[5]The Fabry-Perot interferometer (see, for example G. Hernandez [20]) is made of a pair of partially reflective flat mirrors that become an optical cavity when properly aligned. If the wavelength of the incident electromagnetic wave, or any other higher harmonic, matches that of the optical cavity then we will have an standing wave with very little loss of energy. The Fabry-Perot interferometer can easily be converted into a spectrum analyzer if the separation between mirrors is varied in a way that the wavelength of the standing wave is also changed. In this manner it is possible to monitor the output of the laser system and tune it for optimal conditions. The interferometer gain (that is, the sensitivity) depends strongly among other things on the parallelism between the two flat mirrors. It also requires a light source with normal incidence to the optical cavity. Consequently, both mirrors of the etalon cavity are perpendicularly aligned to the incident beam as well as possible. On the other hand, a feedback loop into the laser cavity is established if an almost perfect alignment of the interferometer exists; with the stability of the laser output deteriorating significantly. Consequently, in order to have the best of both conditions our Fabry-Perot is slightly *misaligned*!

for both colors in size, positioning and shape. The first part is equivalent to the original optical arrangement of Chow and Fuller. The optical path of both beams is shown in Figure 2.1 as a broken line for the green beam and a continuous line for the blue beam. The blue interferometric bandpass filters are used with the double purpose of reflecting the green beam off the highly reflective surface of the filter, while allowing the blue beam to pass through. Once the two colors are separated, in order to measure the birefringence of a polymeric sample the essential optical elements become the calcite polarizers P_i and A_i. Both incident polarizers P_G and P_B (Glan-Thompson prism polarizers manufactured by Karl Lambrecht Corp. Cat # MGTS8) are adjusted so that the polarization vectors for the green and blue beams have a *relative* angular orientation that is 45° apart. The best way to warrant this condition is by using the calcite polarizer A_B (the blue analyzer) to define the polarization orientation of P_B and then rotate A_B to a new position 45° away and subsequently repeat the procedure for the green beam. The optical mount of A_B was designed such that the angular positioning is adjusted with a micrometer and is capable of defining the relative orientation of 45° within 0.1 minutes of arc resolution. Once the correct orientation for the incident green beam has been defined then the green analyzer A_G is rotated until the maximum extinction is achieved.

For the green beam it is important that the incident beam to the bandpass blue filter makes the smallest possible angle with respect to the main optical axis (the blue beam axis) in order to minimize changes of the polarization orientation of the two beams. Fresnel's law of reflection implies that a rotation of the polarization vector of less than one tenth of a degree will occur for the reflected beam for angles of incidence less than 5°. It is also important in order to obtain the maximum extinction ratios—and consequently the highest sensitivity—to minimize the number of optical elements between the polarizers and analyzers. This is a result of the fact that almost all optical components (including lenses and especially filters), are highly birefringent because of the applied or the residual (intrinsic parasitic) stresses. Consequently, this fact also requires the measurement of the relevant

properties of all optical elements placed between the polarizers and analyzers on the main axis, so that the specific deficiencies can be corrected by using appropriate mounts (in order to reduce the applied stresses) and by adding the necessary degrees of freedom (to reduce the effects of residual stresses).

The latter methodology is adequate for the measurement of birefringence for samples in which the birefringence is only weakly dependent on position. If the birefringence of the sample is a strongly varying function of position then it becomes necessary to have *colinear* beams passing through the sample that also have the same *divergence* angle and the same *focal point.* One way to fulfill these additional conditions for both beams is by using a convergent lens L_i for each color (although not necessarily of the same focal length), so that the optical path differences are taken into account to form a point source just before the objective lens (at point ${S^{(1)}}_{B,G}$). These lenses are positioned at points such that, given their focal lengths, the beam waist for both colors at ${S^{(1)}}_{B,G}$ are *equal.* The objective lens L_{obj} does the final focusing of the two beams into the flow cell. This lens can travel along the main optical axis to position the waist's beam at the center of the flow cell, taking into account the difference of the refractive index of the fluid with respect to that of vacuum. Finally the aligning pin holes $S^{(i)}_{B,G}$ are used to warrant the colinearity of both beams.

In order to calculate the position of the beams' waist, is necessary to use the geometrical optics for a *Gaussian* beam, originally introduced by Kogelnik & Li [21]. The simpler geometrical optics for thin lenses does *not* take correctly into account the diffraction of the laser beam. (See any modern optics textbook such as Yariv [22] or O'Shea [23]). The complete characterization of the optical parameters of a Gaussian beam can be given in terms of the following equalities

$$z_R = \frac{d_0}{\theta} = \frac{\pi d_0^2}{4\lambda},$$

where d_0 is the beam waist diameter, θ is the full angle beam divergence, λ is the laser wavelength, and z_R is the Rayleigh range (that is, the parameter characterizing

the extent of the beam waist region). The initial values for these parameters are determined uniquely by the wavelength of the light, and the optical characteristics of the laser cavity, *i.e.,* the radii of curvature of the reflector and the output coupler, and the separation between these mirrors. The thin lens equation for a Gaussian beam in its Newtonian form [23] is given by

$$(z_2 - f)(z'_1 - f) \;=\; f^2 - f_0^2,$$

where z_2 is the distance from the lens to the new position for the center of the beam waist, f is the focal length of the lens, z'_1 is the distance from the initial position of the beam waist to the lens, and f_0^2 is the term introduced to account for diffraction of the laser beam. Since f_0^2 is a property of the laser beam on both sides of the lens, a symmetric expression for it is

$$f_0^2 \;=\; z'_R z_R.$$

Using the above equalities, in conjunction with the characteristics of the laser cavity, it is possible to calculate the correct positions of the lenses given their focal lengths such that the beam waists for both colors at the location of the first pinhole are almost identical. Because of the uncertainty in defining the *real* focal length of the lenses it is still necessary to adjust the position of one lens (lets say, the green lens) relative to the position of the other lenses on the optical rail. The complete procedure of adjustment requires repositioning of the lens and the blue filter ahead of the pinhole, since the displacement of the lens not only moves the position of the beam waist but changes its size as well.

The final conditioning lens, the objective lens L_{obj}, focuses the laser beams into the central region of the two-roll mill. The size of the beam waist and the length for the waist region can also be calculated by the previous equations. In practice, the final adjustment is done by inserting a pinhole instead of the flow device and translating L_{obj} until the beam waists are focused onto the pinhole.[6]

[6]It is necessary that the pinhole diameter be smaller than the size of the beam waist. In

The pinhole is held in place by a specially designed mount so that it is placed precisely at the geometric center of the flow device; halfway through the fluid and at the stagnation point. In this manner it is possible to align the flow cell with respect to the optical system. It is also important for the reliability of the experiment, to warrant that both beams actually have their waists located at the same point in the fluid, otherwise different elements of fluid will be sampled by the two colors. The characteristics of the two color beam going through the fluid can be indirectly evaluated with a pair of pinholes. When using a 50 μm. pinhole the fraction of irradiance passing through is approximately 60% for both beams, and this fraction is 95% when a 100 μm. pinhole is used. The calculated Rayleigh range is approximately 0.75 cm. and the observed decrease in irradiance is of the order of 35% for a point 0.375 cm. away from the stagnation point.

Finally, the positioning of the objective lens is corrected to take into account the difference of the refractive index—between the fluid and air (with the refractive index for air being equal to 1)—using the paraxial formula (see for example O'Shea [23]) where the waist beam displacement (Δt) along the optical axis by a different medium of thickness t and mean refractive index n' is given by

$$\Delta t \;=\; \frac{n'-1}{n'}\, t.$$

The correction to the beam waist position is no larger than 0.5 cm. when the presence of the fluid and the glass windows is taken into account.

Besides the use of the pinholes ${S^{(i)}}_{B,G}$ to determine the position of the waist beams along the principal optical axis, a secondary use is to "define" the colinearity of the two beams. With this arrangement it is possible to align the relative position on a plane perpendicular to the incidence axis of both beams to within a couple of microns at the center of the flow device. This accuracy (defining the colinearity

this case the position of the waist is "defined" as that when the measured light intensity passing through the pinhole reaches its maximum value. This condition can easily be corroborated because the divergence of the beam will be observed as the separation between the flow cell and L_{obj} is varied.

of the beams) can be maintained with the optical system for periods of several weeks without readjustment. Even though, it appears like a very good, long term colinearity, some of the fluids that have been tested so far appear to show localized birefringence effects over characteristic distances of only a few tens of microns. Therefore it may be necessary to check the optical alignment on a daily basis.

The posterior lens L_D has a focal length such that the laser beam will have the smallest spot size when measured at the detector positions —for the blue as well as the green beams. In this case, the residual birefringence of the blue and green filters (located just in front of the analyzers A_i) is well defined, hence making it possible to rotate the filters into an angle which does not degrade significantly the sensitivity of the apparatus.[7] The photodetectors are located after the analyzers. These analyzers are beam *splitting* Thompson calcite polarizers manufactured by Karl Lambrecht Corp (Cat # SMBTS-8-45 with a multilayered antireflective coating centered at 500 nm.). With these analyzers it is possible to measure simultaneously the intensity of the *ordinary* and *extraordinary* beams for each color.[8] The ability to measure the ordinary and extraordinary components of polarized light is an important part of this experimental set-up, that is different from the standard TCFB originally introduced by Chow and Fuller [16]. The main reasons for this modification are given in length in the following subsection.

The light detectors are located after the analyzers with a light-trap placed in between. The light-trap is necessary to avoid scattered light from the optical mount of the analyzers from reaching the light sensors (photodiodes by Newport Research Corp model 815); the scattered light can be considered totally depolarized. These traps are made of a pair of pinholes separated by a tube that has a much larger

[7]The layers of epoxy used to hold together the interference films that make up the filter have high levels of residual stress. The principal orientation for these stresses varies strongly as a function of position over the surface of the filter. If a large aperture is used, then polarized light passing through the filter will become depolarized to a significant degree.

[8]The extraordinary beam corresponds to the component of the electromagnetic wave propagating with the electric field vector parallel to the optical axis of the material (see for example Born and Wolf [27]).

diameter. In this case only light within a small angle of incidence, and close to the normal, is detected and good extinction ratios are then possible. Otherwise, when the light traps are removed, the signal/noise ratios remain rather low with values of only $\sim 10^3$. The light detector signal goes to a power meter with a bandwidth of 10 KHz and a voltage output (from zero to ten Volts) that is sent into the computer analog to digital converter card (the A/D card—model HP98640A— handles up to 8 differential inputs with its twelve bit converter into a Hewlett-Packard computer models 310 and/or 332).

The complete optical arrangement has extinction ratios of better than 10^{-5}. After the flow device is placed along the main optical beam, the extinction ratios for the blue and green beams degrade slightly: of the order two to three times, with average extinction ratios better than 2×10^{-5}. The optimum values that can be attained in the experiments are always obtained by relieving the residual stresses on the flow cell windows by means of the screws on the window-holder. This procedure was always done before a series of experiments started. This apparatus offers a level of sensitivity, reproducibility, and accuracy that to our knowledge is *not* available anywhere else. In combination with the two-roll mill, it offers a unique experimental system to study the effect of flow on the dynamics of polymer liquids; specifically, under *strong* flow conditions which are most likely to prove the most important dynamic mechanisms for polymer deformation into a highly stretched state.

2.3.1 Considerations for High Signal/Noise Ratios with TCFB

The experimental constraints and/or limitations impose certain requirements upon the data acquisition methodology. Overcoming these difficulties, in order to obtain good signal to noise ratios is considered equally important as the need to obtain accurate values of the relative light intensities as required by equations 2.15 and 2.16. These limitations are associated with the "real" life of the laboratory as the result of: (a) mechanical imperfections of the optical system, as well as those

of the associated electronics; (b) limitations of the laser source; (c) the presence of dust in the polymer solutions, etc. Any of the previous conditions affects the measured values of light intensity in such a manner that, on a daily basis, it becomes difficult to correct these small deviation from the optimum experimental conditions. Each non-ideal condition deteriorates the overall sensitivity of the optical system as observed at the detector point, with the combined effects having sometimes catastrophic results; signal/noise ratios may become poor enough to destroy all meaningful information.

However, these limitations affect the data acquisition in two distinct ways. Those non-idealities associated with mechanical conditions have characteristic times of several hours and sometimes days. For example, not only the light detectors have different efficiencies, but they also have sensitivities that depend on the inhomogeneities of the detector surfaces; thus light intensity measurements depend on the detector used, and on the exact position where the beam reaches each detector. On the other hand, the presence of dust, and/or fluctuations of the intensity of the laser source affect measurements with time-scales that are comparable to those of the polymeric system. Consequently, we can minimize the long time-scale limitations by performing a calibration procedure prior to the execution of an experiment. The calibration procedure (described in the following paragraphs) not only takes care of problems associated with long time-scales, but also permits measurements of the true *relative* light intensities[9].

The limitations associated with the faster time-scale non-idealities can be resolved by adding some extra light detectors to the basic optical set-up for the purpose of sampling the sources of noise, and subsequently, subtracting their effects in order to maintain good signal to noise ratios. The supplementary de-

[9]It is always necessary to calibrate the different detectors for their sensitivities are also wavelength dependent. Furthermore, it is desirable that the calibration procedure allows measurements of optical anisotropy that are *independent* of the detectors used and its associated electronics, or for that manner, of all of the mechanical details of the detection optics; *e.g.*, the size of the pinholes of the light-traps, the difference of the transmission coefficients along two different optical paths through the analyzers, or small misalignments that can occur while setting up the experiment.

tectors are used to allow instantaneous readings of the irradiance falling upon the flow device $I^{(i)}_{max,j}(t)$, together with the total light intensity passing through the fluid sample $I^{(o)}_{max,j}(t)$. The total incident irradiance is measured with the detectors located on the *auxiliary* optical rail in Figure 2.1; before the fluid sample. The total intensity past the flow cell is simply the sum of the intensities of the ordinary and the extraordinary beams.

This calibration procedure also takes into account the fact that the light detectors are *not* ideal detectors with output readings proportional to the *absolute* values of the light intensities. Of course, this scenario is far from being possible. However, the relative values (with respect to the maximum intensity that each detector can receive) are easily determined with very good accuracy. Hence, the calibration procedure necessary to reduce the long time drift effects consists of two sets of measurements done under *no-flow* (*i.e.*, zero flow) conditions. The first set of measurements is taken with the maximum extinction on the extraordinary beam detectors. Under these optical conditions we have

$$I^{E}_{min,j}(t), \quad I^{O}_{max,j}(t), \quad I^{(i)}_{j}(t) \quad j = \text{blue, green} .$$

Here $I^{E}_{min,j}$ is the light received by the detector along the extraordinary beam path, $I^{O}_{max,j}$ falling upon the ordinary detectors, and $I^{(i)}_{j}$ samples the light intensity before passing through the flow cell. These light intensities are "instantaneous" readings. We can then normalize the measured values at the detectors on the extraordinary and ordinary beams using the incident intensities $I^{(i)}_{j}$, and thereby discriminate the temporal fluctuations of the light intensity of the laser output. Thus, we obtain two quantities of interest:

$$i^{E}_{min,j}, \qquad \text{and} \qquad i^{O}_{max,j} .$$

Now a second series of measurements is done after inserting a half wave retarder (with a 90° orientation with respect to the incident polarization) immediately after the flow device. In this way, each detector (and for each color) is used to measure the

maximum and minimum intensities of the ordinary and the extraordinary beams,

$$\frac{i^E_{max,j}}{\kappa_j}, \quad \frac{i^O_{min,j}}{\kappa_j} ,$$

where κ_j are the transmission coefficients of the half wave retarder. Thus, the *proportionality coefficients* or *sensitivity ratios* for the ordinary-extraordinary set of detectors are given by

$$\alpha_j = \frac{i^E_{min,j} + i^E_{max,j}/\kappa_j}{i^O_{max,j} + i^O_{min,j}/\kappa_j} , \tag{2.17}$$

and the total incident irradiance coefficients are:

$$\theta_j = \frac{I^O_{max,j} + I^O_{min,j}/\kappa_j}{I^{(i)}_j(t)} . \tag{2.18}$$

θ_j provides the *scale factor* to determine the maximum light through the fluid sample based on the instantaneous measurements ahead of the flow device. The computation of these coefficients concludes the calibration of the optical system and permits measurements of the *relative* light intensities as required by equations 2.15 and 2.16.

When the flow field is started, and/or meaningful data readings are going to be taken, then

$$I^{(o)}_{max,j}(t) = I^E_j + \alpha_j I^O_j \leq \theta_j I^{(i)}_j(t) , \tag{2.19}$$

where now, superimposed to the temporal variations of the light source, as measured by $I^{(i)}_j(t)$, we also have the fluctuations due to dust particles and other phenomena such as dichroism. That is,

$$I^{(o)}_{max,j}(t) f(\tau, \Delta n'') = \theta_j I^{(i)}_j(t) , \tag{2.20}$$

where τ is the turbidity of the sample due to particles, tiny bubbles, and density fluctuations for systems close to a critical point, etc. [28]. $\Delta n''$ represents contributions of dichroism of the fluid. For most polymeric solutions, measurable level of $\Delta n'' \ll 1$, while the contributions of birefringence are very large, and can be

obtained by using

$$i_B(t) = i_B^E / I_{max,B}^{(o)} , \tag{2.21}$$

$$i_G(t) = i_G^E / I_{max,G}^{(o)} . \tag{2.22}$$

in conjunction with equations 2.6 and 2.7, or equations 2.15 and 2.16. In principle, the light intensity readings with the six detectors of this optical arrangement, can be used to determine not only the birefringence but also the solution dichroism. for it is possible to calculate the anisotropic attenuation based on a simple time dependence (*i.e.*, flow field dependence) of the total incident intensity coefficients $\theta_i(t)$.

In Figure 2.2 we present sample data for a solution that has a very low degree of birefringence, thus showing the effects of the glass windows of the flow cell as well as the noise levels due to $f(\tau,\ \Delta n'')$. The "true" curve is shown at the base of the birefringence data points. The fact that noise increases the minimum levels of detectable birefringence is because scattering centers tend to depolarize the incident light, the net result being a significantly larger intensity of light reaching the extraordinary detectors. Finally, in Figure 2.3, we present a birefringence plot for a case when the values of the retardance go past $\pi/2$. In this case we can expect the calculated birefringence to be an approximation of the *real* birefringence because of the assumptions used, such as the absence of dichroism as well as some of the approximations used for the reduction of the birefringence equations. Nonetheless this optical technique as shown in this chapter, presents the capability of very good sensitivity, together with a large dynamic range of measurable values, as well as the possibility of probing very localized regions of the flow field.

2.4 The Homodyne-Light-Scattering Technique

The second essential experimental technique is one that will allow us to evaluate the effects of the conformation changes of the polymer on the flow field. This is a very important objective in our research program. Earlier studies have failed

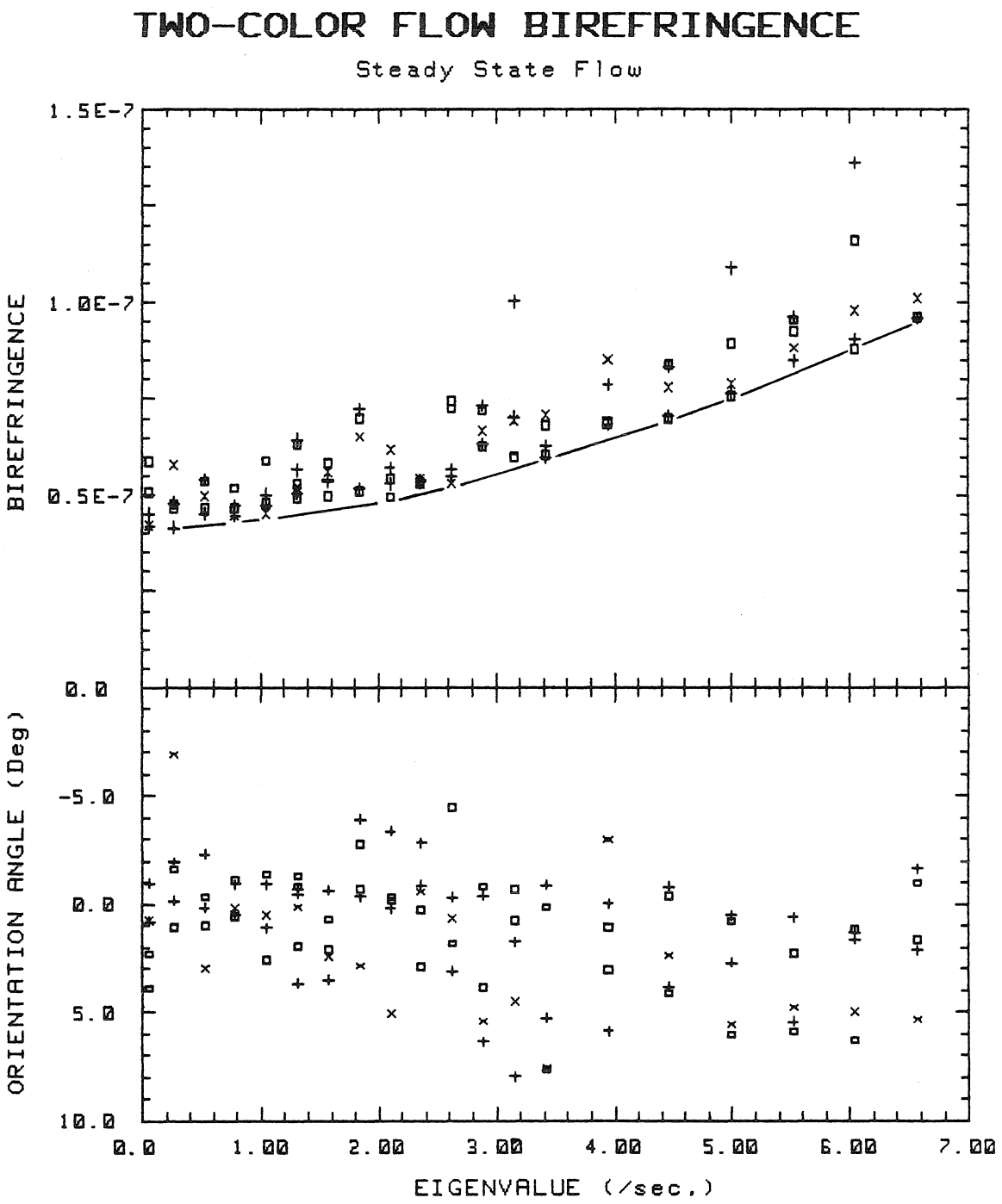

Figure 2.2: Birefringence and extinction angle for the solvent with rollers F ($\lambda = 0.1501$). Different markers represent different experiments consecutively done. The continuous line represents the ideal experiment where noise due to dust, air bubbles, etc., are not present.

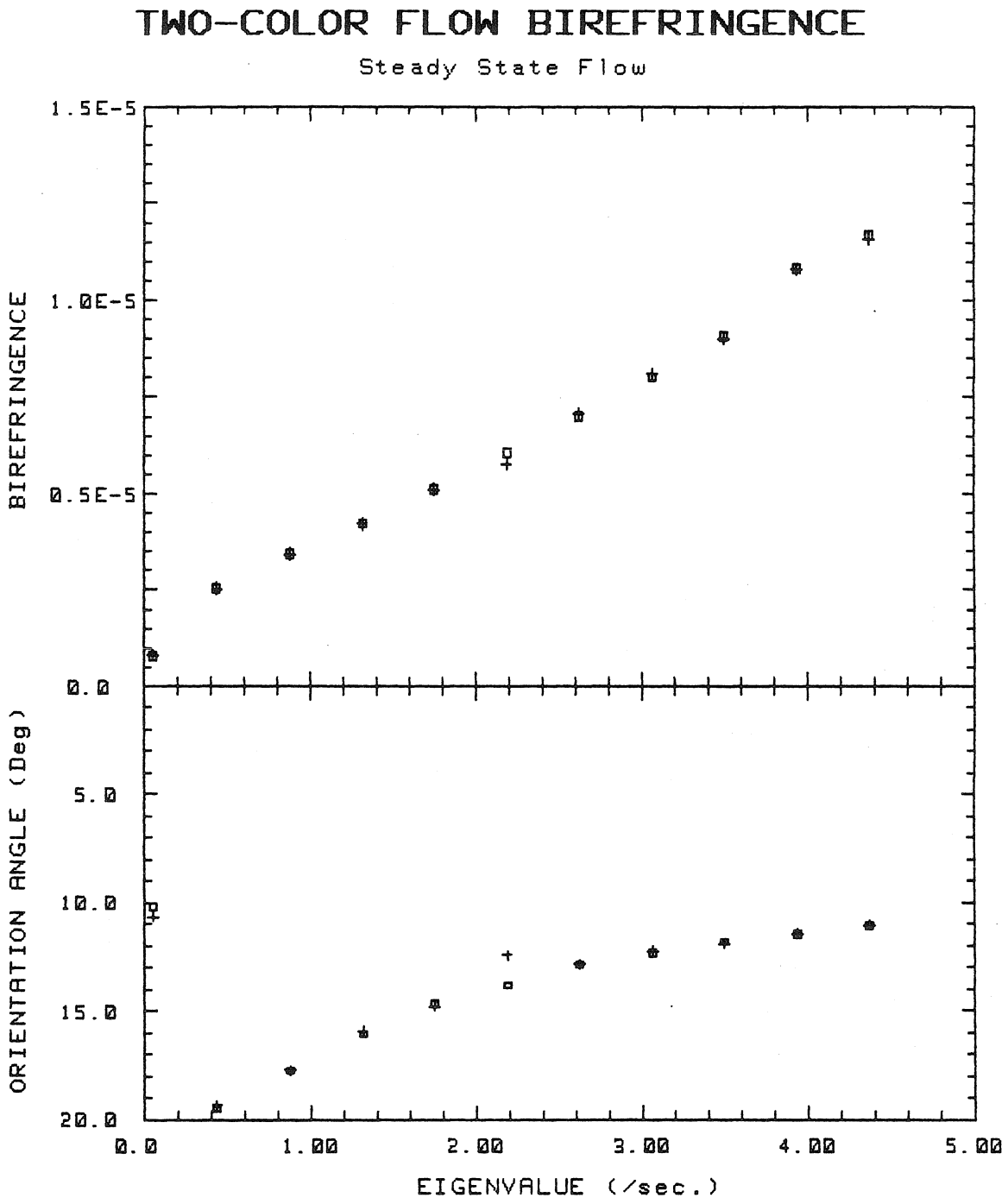

Figure 2.3: Birefringence and extinction angle for a concentrated polymeric solution. The birefringence value that corresponds to a retardance of $\pi/2$ is approximately 9.6×10^{-6}. higher values of birefringence correspond to retardances larger than $\pi/2$.

to show modification of the flow by the presence of the polymer. In these studies, streamline or streakline photography was used to characterize two-dimensional hyperbolic flows (see references [6 – 11, 27, 28]). Although flow birefringence measurements clearly indicated localized regions of the flow containing highly stretched polymers, in general the streamline patterns did not change much. Streamlines are essentially an integral property of the velocity fields and, consequently, a "double integration" property of the velocity gradient. Hence, streamlines are relatively insensitive to localized variations of the velocity gradient field. Furthermore, in flows with a high degree of symmetry, such as a two-dimensional hyperbolic flow, the qualitative streamline pattern tends to be preserved even if the velocity gradients in the streamline direction are changed.

The homodyne-light-scattering technique (HLS) (originally developed in this laboratory by Fuller et al. [17]) has been used to directly—and in a point-wise manner—evaluate the velocity gradient of the flow. This property of the flow is the most critical because it determines the degree of strain that the polymer is subjected to. A significant part of our earlier investigation was, in fact, the development of a theoretical basis for the interpretation of light scattering measurements in a flowing solution. In principle, the HLS technique applies to both steady and time-evolving flows, with the current bandwidth limits being defined by the electronics of the photon correlator.

HLS is also a noninvasive technique. It uses part of the TCFB optical arrangement to align the element of volume on which the measurement takes place at any point in the flow. In this way we can map the spatial variation of the velocity gradient in the plane of the flow. It is also possible to measure the variation of the velocity gradient at any position along the third axis. However, the mathematical manipulation necessary to interpret the data becomes quite complex whenever the components of the velocity gradient tensor along the third dimension become significant due to effects of the boundaries.

Theoretically, the homodyne correlation function is given by [17, 32]

$$G(\tau) = \mathbf{F}_2(\mathbf{q},\ \tau) = \left| \iiint \mathrm{d}^3\mathbf{x}\, I(\mathbf{x}) \exp(-i\mathbf{q}\cdot\mathbf{\Gamma}\cdot\mathbf{x}\tau) \right|^2 , \qquad (2.23)$$

where $I(\mathbf{x})$ is the light intensity distribution across the beam, $\mathbf{q}$ is the scattering vector in the scattering plane and along the bisector of the incident and scattered beams, $\mathbf{\Gamma}$ represents the velocity gradient tensor and τ is the characteristic time of the correlation function. If the incident beam has a radial Gaussian distribution perpendicular to the direction of propagation with mean radius L, and the scattering vector $\mathbf{q}$ is aligned along the $0x$ axis, then the homodyne correlation function is given by

$$\mathbf{F}_2(q_x,\ \tau) = \exp\left(-\frac{1}{2}L^2q^2\dot{\gamma}^2\tau^2\right) .$$

If the alignment of $\mathbf{q}$ coincides with the $0y$ axis, then

$$\mathbf{F}_2(q_y,\ \tau) = \exp\left(-\frac{1}{2}L^2q^2\dot{\gamma}^2\lambda^2\tau^2\right) .$$

Here, λ is the flow field parameter, and $\dot{\gamma}$ is the magnitude of the velocity gradient. Experimentally, the values determined for $\dot{\gamma}$ and λ depend on the auto-correlation function of the scattered intensity:

$$G(\tau) = \lim_{T\to\infty} \frac{1}{2T} \int_{-T}^{T} I(t)I(t-\tau)\, dt .$$

where τ is the characteristic correlation time and T is the time period during which photons arrive at the photomultiplier tubes. Besides the standard requirements for development of the correlation function under steady flow conditions, additional requirements exist if this technique is also to be used for transient flows where Γ, λ may be functions of time. In the latter case it is also necessary (a) to have correlation functions that can be built-up rather quickly;[10] (b) to have the best possible signal-to-noise ratios, and (c) to operate under flow conditions where the particular polymer sample does not degrade. The latter condition is is necessary because the

[10]For the best optical and electronic conditions that are desirable for homodyne scattering experiments see the book by Dahneke [33].

complete correlation is computed by executing the same experimental run several times. The *total* correlation time T is then the sum of several shorter correlation times T_i, all taken with the flow field satisfying exactly the same conditions; *i.e.* identical values for the flow parameter λ, and the shear rate $\dot{\gamma}$. The correlation information is preserved by this summation whenever the characteristic correlation time τ is significantly shorter than T_i. In this case, the generation of a "smooth" correlation function as the sum of correlations taken during several short sampling periods is not affected by the summation of statistically independent correlation segments.

However, the best signal to noise ratios are achieved when on the number of decay times during the sampling time T_i is large. If τ is the characteristic time scale for the correlation function, then the signal to noise ratio is proportional to $(T_i/\tau)^{1/2}$, even when the light level reaching the light detectors is infinite. Therefore, the only way to increase the signal to optimum level is by reducing τ by *increasing* the scattering angle (*i.e.*, through $\mathbf{q}$). This imposes some limitations on the minimum gap with in the two-roll mill, and is one of the factors that has being considered in its design.

The two techniques described in this chapter provide the tools to study the dynamics of polymeric liquids under the most demanding conditions. Most of the data presented in the second part of this thesis is the result of applying the TCFB technique to two polymer solutions. The HLS technique is not yet fully operational and thus no data is reported here. Its importance nonetheless is as high as that of the TCFB, and this is the reason for this short discussion of the HLS technique.

Bibliography

[1] W. Heller; *Reviews of Mod. Phys.*, **14**(4)390-409(1942).

[2] R. M. A. Azzam and N. M. Bashara, *Ellipsometry and Polarized Light*, Section §5.6, North Holland, The Netherlands (1987).

[3] V. N. Tsvetkov, V. E. Eskin, and Ya. S. Frenkel; *Structure of Macromolecules in Solutions.*, Vol III; National Lending Library for Science and Technology, Washington, (1971).

[4] A. Peterlin; *Ann. Rev. Fluid Mech.*, **8**,35-55(1976).

[5] J. L. S. Wales; *The Application of Flow-Birefringence to Rheological Studies of Polymer Melts*, Delft University Press, Rotterdam (1976).

[6] H. Janeschitz-Kriegl; *Polymer Melt Rheology and Flow Birefringence*, Springer Verlag, New York, 1983.

[7] R. Cressely, R. Hocquart and O. Scrivener; *Optica Acta*, **25**(7)559-571(1978).

[8] O. Scrivener, C. Berner, R. Cressely, R. Sellin and N. S. Vloches; *J. Non-Newtonian Fluid Mech.*, **5**,475(1979).

[9] D. G. Crowley, F. C. Frank, M. R. Mackley and R. G. Stephenson; *J. Polym. Sci.: Polym. Phys. Ed.*, **14**, 1111-1119(1976).

[10] F. C. Frank and M. R. Mackley; *J. Polym. Sci.: Polym. Phys. Ed.*, **14**,1121-1131(1976).

[11] M. J. Miles, K. Tanaka and A. Keller; *Polymer*, **24**,1081(1983).

[12] J. A. Odell, A. Keller and M. J. Miles; *Polymer*, **26**(8)1219-1226(1985).

[13] G. G. Fuller; *Ph. D. Thesis*, California Institute of Technology, Pasadena, Ca. (1980).

[14] P. N. Dunlap; *Ph. D. Thesis*, California Institute of Technology, Pasadena, Ca. (1986).

[15] R. C. Ng; *Ph. D. Thesis*, California Institute of Technology, Pasadena, Ca. (1989).

[16] A. W. Chow and G. G. Fuller; *J. Rheol.*, **28**(1),23-43(1984).

[17] Y. Shindo and H. Hanabusa; *Polym. Comm.*, **24**,240(1983).

[18] Y. Shindo and R. Takigaura, *Polym. Comm.*, **25**(12),378-381(1984).

[19] P. L. Frattini and G. G. Fuller; *J. Rheology*, **28**(1),61-70(1984).

[20] G. Hernandez *Fabry-Perot Interferometers*, Cambridge Univ. Press, Cambridge U. K., 1986.

[21] H. Kogelnik and T. Li; *Applied Optics*, **5**,1550-1567(1966).

[22] A. Yariv and P. Yeh, *Optical Waves in Crystals*, John Wiley, New York, (1984).

[23] D. C. O'Shea, *Elements of Modern Optical Design*, John Wiley, New York, (1985).

[24] A. Onuki and M. Doi; *J. Chem. Phys.*, **85**(2)1190-1197(1986).

[25] A. Gerrard and J. M. Burch; *Introduction to Matrix Methods in Optics*, John Wiley & Sons, New York, 1975.

[26] C. M. Bender and S. A. Orszag; *Advanced Mathematical Methods for Scientists and Engineers*; McGraw-Hill, New York, 1978.

[27] M. Born and E. Wolf; *Principles of Optics*, Pergamon Press, Oxford, U. K., 4th. ed., Section §14.4, 1970.

[28] F. Buehler, R. Stadler and W. Growski; *Makromol. Chemie*, **187**(5)1295-1299(1986).

[29] W. W. Graessley, R. Hocquart and O. Scrivener; *Optica Acta*, **25**,559(1978); **26**,1173(1978).

[30] K. Gardner, E. R. Pike, M. J. Miles, A. Keller, and K. Tanaka; *Polymer*, *23*, 1435(1982).

[31] G. G. Fuller, J. M. Rallison, R. L. Schimdt and L. G. Leal; *J. Fluid Mechanics*, **100**(3)555-575(1980).

[32] B. J. Berne and R. Pecora; *Dynamics Light Scattering*, John Wiley & Sons, New York, 1976.

[33] B. E. Dahneke; *Measurements of Suspended Particles by Quasi-Elastic Light Scattering*, John Wiley & Sons, New York, 1983.

Chapter 3

The Real-Time Software Controlling this Apparatus

Chapter 3

The Real-Time Software Controlling this Apparatus

Besides the sometimes well-justified-sense-of-urgency of researchers using computers to do so-called "numerical simulations," the *real* need for an "instantaneous" response by the computer to its user is not a requirement of capital importance. On the other hand, there exist a whole class of uses for modern computers which demand an almost "instantaneous" response from the system. This type of computer use requires programs and algorithms of what is called *real-time* software, where the responsiveness to the execution of different processes by the computer is of great importance for the correct performance of the task at hand. Most of the programming presented here is of the standard type, where the algoritm does not require inputs or outputs at specific times but at specific points. It is only those parts that relate to the control and execution of the experiments that require the use of *real-time* techniques and methodology. These parts for control and execution will by discussed in section 3.3, with a short description of the main characteristics of the real-time type of software that were implemented for this experiment. In the first section a global overview of the different modules is given and their

relationship to the other modules. In the following section, the first level of programming for the birefringence module is described in pseudo-code, in order to show the most important features of this program. The next section deals with the actual implementation of the real-time data acquisition with other code processes in charge of: (a) monitoring the various instruments, and (b) data reduction and graphing. These two complementary codes run concurrently, in the background of the data acquisition. We consider that the level of description of this program at the present level can be a good starting point for a researcher interested in real-time data acquisition, using a similar computer. This type of information is equally difficult to find as the "experts" in this field.

3.1 The Program Main Level.

All necessary tasks related to this work are done within the options specified by the main program AEGAMAIN. This computer program is designed to allow the user (that is, the experimentalist): (a) access and control through the computer, of all instruments involved in the experiments; (b) the execution of birefringence experiments to determine the conformation of polymer molecules when subjected to flows generated by the two-roll mill, and (c) the possibility to read, and/or manipulate experimental data previously obtained. The program has been written using HP Pascal language (Hewlett-Packard Pascal version 3.1 or later), and the communication with the numerous instruments is through an IEEE-488(1986) port.

In order to perform tasks in a "real-time environment," that is where there is a need for synchronization of events in real-time, AEGAMAIN makes extensive use of the computer clock, and user-defined interrupt handlers to execute processes according to the experiment needs. These include both, anticipated needs as well unexpected needs, such as failures or errors that happen within the instruments during the experimental run, that do not directly affect the execution of the experiments but may seriously affect the trustworthiness of the data. Furthermore, only

a user-friendly program is acceptable given the complexity of these assignments, hence, requiring the use of primitive operations for the control of the IEEE-488 interface, keyboard and of the monitor with the goal of developing an efficient program.

The complete program is composed of 13 modules each of which has a set of procedures (subroutines) related to a very specific operation or "global" activity. All of these modules are available to the main program as a "library" named AEXPLIB, and together with some software drivers, which are part of the HP extension for the Pascal language, the software package is complete. These modules are:

```
IODECLARATIONS, GENERAL_1, GENERAL_2, GENERAL_3, DGL_LIB,
AsmMod, UserProc, FileOper, Monitor, Laser, SMI, AD_Converter,
Correlator, Gral_Exp, Bir_library, VelGrad_lib, DataEvaluation.
```

The first five modules are part of the HP Pascal, and all information is given in the manual for the language, specifically the Procedure Library and the Programming and Configuration Topics of the HP Pascal 3.2 .

When the variables of interest are related in a complex manner to the measured quantities and large amounts of data are being generated by an experiment, then, it is most desirable to present the collected information in graphic form, "instantaneously," and in an easily readable format. A quick display of the collected data allows the experimentalist the possibility of rapidly evaluating the goodness of the data by observing possible (unusual) faulty conditions during the experimental run. This is one of the most important characteristics of real-time data acquisition. In order for graphed information to be easily readable by the operator, it should be scaled in a way that optimizes the use of the screen, even though, the best scale is not known until the experimental run is completed. In any case, the current scale should always be the optimum for those data points available. Whenever the current scale is not the most appropriate for a new set of data—that includes the latest data points—then, it is necessary to adjust the scale since otherwise infor-

mation of diminished value is given to the experimentalist. If the total number of displayed points is small, then, it is probably faster to erase, and subsequently to redraw, using the new scale, all data points. On the other hand, if the number of points is large then, it is simpler to discard the old plot and use a new copy of the axes and labels previously stored in memory. Since most graphic displays are high resolution monitors, a large amount of memory space is needed to store and manipulate the information contained in a plot. `AsmMod` deals with the most elementary algorithms necessary for up-dating the graphed information, *i.e.*, with those operations and control of the graphics monitor needed for real-time display of the experimental data. This module is written in Assembler language in order to achieve the fastest execution times.

`UserProc` is a general purpose module to facilitate programming of long pieces of code. The purpose for the procedures in this module is to avoid repetition of frequently used sections of code, and it is consequently used by almost all other modules. `FileOper` deals with the declaration of those variable-types that are specific to this experiment and allows for an efficient and compact use of data structures and of allocation of memory, both in DRAM as well as hard disk storage. These data structures make extensive use of pointers, and linked list and queues, thus allowing allocation of memory during the execution of experiments while still preserving the compactness of code. For example, data readings only take as much memory space as necessary, with the data reduction algorithms processing the first data points at the fastest possible rate and the data acquisition algorithms appending to the list of unprocessed data the latest data readings. We discuss in greater detail, the advantages of the use of linked data structures in the next sections. `Monitor` provides the utilities for the graphing of data in any graphics or plotting device.

`Laser`, `SMI` (Stepping Motor Interface), `AD_Converter` (analog-to-digital converter) and `Correlator` provide the software interfaces to use these particular instruments. These instrumentation modules make extensive use of the HP Pascal

drivers for the IEEE-488 interface and also take into consideration the different idiosyncrasies of the instruments, such as specific formats and/or control sequences. These instruments are all programmable, and the corresponding modules are designed to allow their "manual" operation via the computer or as embedded parts of TCFB or HLS experiments. These modules contain procedures to detect and trap errors or faulty conditions that can occur within the instruments, with the appropriate interrupt handlers to report its status to the computer.

`SMI` is the procedure in charge of programming and controlling the stepping motor interface. This interface drives in turn, the electronics of the motor coupled to the rollers. This procedure reads the operator requested parameters for the motor interface, and since the motor is not capable of operating under every possible combination of parameters, it returns the closest acceptable values for the motor; these being the values saved in the experiment tag for future reference. `AD_converter` contains the procedures responsible for programming the analog-to-digital converter that reads the light intensity values of the photodetectors. This converter is fully programmable, but the power meters used to convert the light intensity measurements into voltage signals have gains settings that are manually operated. This arrangement presented the advantage of faster tracking light intensity measurements and simpler software, although, it reduces the capacity of totally automated control by the computer as will be discussed shortly.

`Gral_Exp` are output procedures to report status and results of the several possible experiments to the experimentalist. `Bir_library` contains all of the procedures necessary for the execution of flow-birefringence experiments and will be discussed more extensively shortly. `VelGrad_lib` is the equivalent module used to evaluate the velocity gradient tensor of flows generated by the two-roll mill. It is listed here to present the global perspective of this project that includes not only measurements related to the conformation of the molecules as induced by the two-roll mill flows but also the determination of the changes in the velocity gradient of the flow because of the presence of highly stretched polymer molecules. To date,

however, this module is not completely operational, and will not be discussed further. `DataEvaluation` allows the subsequent evaluation and analysis of the collected experimental data as a whole, or in part, as numerical results or in a graphical mode.

3.2 Main Level for the Flow Birefringence Procedure.

The main level of the birefringence program is essentially a user-interface. That is, it provides the means to pass information between the computer and the operator in both directions. It displays the choices available to the operator in a menu driven environment, and communicates via the screen and the printer. This first level of the birefringence program is best described by the following pseudo-code (the actual implementation has been done in HP Pascal 3.2).

```
Execution of Birefringence Experiments;
1     Initialization of variables and pointers;
      Read tag of last experiment (old_label);
      Modify parameters? (y/n)
        If yes
5         Display & modify (old_label, new_label);
        Else new_label is old_label;
      Repeat                        { .. until all data has been feed .. }
        Read type of experiment
          Read all necessary parameters for exp;
10    Until no_more experiments to do;
      Input of special parameters for experiment series;
      Execute calibration of light detectors;
      If automatic operation
        Repeat                    { .. until all experiments are done .. }
15        Initialize memory allocation for current experiment;
          Reset error trapping mechanism
            Initialize instrumentation;
            Execute experiment;
            Update experiment tag (new_label);
20          Print hardcopy of experiment report;
            Save new_label + new_data if so requested;
          Recover from errors block
            Clean-up instruments, computer devices, etc.;
            Print status-quo report;
25         END;                        { ..  of error recover block .. }
        Until No_more experiments;
```

```
      END                                  { .. of automatic execution ... }
     ELSE If Mapping of Birefringence
       Initialize memory allocation;
30     Repeat              { .. as many times as manually requested .. }
         Request new coordinates;
         Update new_label coordinates;
         Reset error trapping mechanism;
               .
35             .
         Recover from errors block
               .
          END;                            { ..  of error recover block .. }
       Until Map_done;
40    END                                { .. of birefringence mapping .. }
     ELSE If Degradation of Birefringence
       Initialize memory allocation;
       Repeat               { .. as many times as requested or done .. }
         Reset error trapping mechanism;
45         Initialize instrumentation;
           Execute experiment;
           Update experiment tag (new_label);
           Is degradation exp. series done?
             If not then Degrade_Fluid
50           Else Degradation_done;
           Save new_label + new_data + degradation data;
           Print hardcopy of experiment report;
           degradation cycles + 1;
         Recover from errors block
55             ....
          END;                            { ..  of error recover block .. }
       Until Degradation_done;
      END;                      { .. of degradation of birefringence .. }
   END;          { .. end of execution of birefringence experiments .. }
```

Line 1 of this pseudo-code deals with initialization of all variables involved in this experiment. This is a good programmer practice specially when lower level code pieces receive information through these variables, and a known state for these variables is desirable. The initialization of pointers is also an important element for a program that uses large amounts of memory, where because of the limitation of the operating system, the needed memory space cannot be assigned by the compiler. In lines 2-6, and in order to reduce the number of parameters that need to be specified at the beginning of a experimental session, the operator is presented with the option of modifying a portion of the parameters used during his

(or her) previous experiment. Subsequently (in line 7), the operator must summit the series of experiments that are to be executed. These experiments need not be of the same type, with the computer asking for only those parameters necessary for each of the requested experiments.

Line 11, deals with special conditions that affect the methodology for data acquisition or the execution of the experiments. For example, it presents the operator with the choice of using a default configuration for the optical system. The "default" optical configuration is that which best discriminates noise sources such as dust particles and bubbles, and is thoroughly described in section §2.3.1. In general, the actual birefringence is determined based on the total light intensity past the fluid sample. However, for some solvents such as Chlorwax, because of its large absorption at the wavelengths of the argon laser, there exists a very localized heating of the fluid within the illuminated fluid element, and as a result, there is a strong divergence of the laser beams especially for a fluid at rest, with significantly reduced levels of light reaching the light detectors. Under these circumstances, the strongest effects occur when the absorbed energy is greatest for a given volume element, which of course, happens under no-flow conditions. Thus, the calibration procedure is skewed, and needs to be modified. The second calibration procedure follows those used in the standard TCFB experiments which assumes there is no attenuation of light intensity through the sample, and represents a better solution than when the calibration is done under highly dispersed (no-flow) conditions. Furthermore, the methodology for evaluation of birefringence is also corrected under this conditions. Among the other special experimental conditions useful to the experimentalist are the possibility of running equivalent experiments with the rollers alternating direction of rotation.

The calibration of detectors is done following the algorithms already discussed in Chapter 2. This section of code does the measurements of light intensities, necessary for the calibration, while at the same time prompts the operator to assist with specific tasks such as inserting the half-wave retarder, etc. The computed values for

the calibration constants of the detectors are saved, in order to be used subsequently in normalizing all readings taken during the measurement of birefringence.

The next lines of code (beginning in lines 13, 28 and 41) provide specific environments for three possible objectives for a sequence of experiments. The first type of environment corresponds to the case of a series of experiments done sequentially, without modifying any of the common parameters for the series. For example, the location of the laser beam in the flow cell remains identical for all experiments in the series. The series may be composed of a variety of different experiments where the instrumentation parameters may be different for the purpose of studying a supplementary range of values, or the type of experiment is actually different such as steady, start-stop, etc.[1] In this manner, series of experiments can be arranged so that a specific study can be done quickly, while a set of parameters maintain constant values.

The second environment (line 28) allows the operator to repeat the *same* experiment at a different position in the flow field. Given the fact that the flow field of a two-roll mill does not have identical deformation histories for different streamlines, an understanding of the anisotropy of the fluid as a function of position is an important objective for rheological studies. It is possible to study the flow field within the vicinity of the stagnation point, with distances no further than 1.0 cms. away.

Finally, the third environment (line 41) is most useful when studying degradation of the fluid sample. Some polymeric fluids degrade rather easily when subjected to this type of flows. In order to obtain a measure of degradation, it is necessary to perform a series of "characterization" experiments intercalated with "degradation" runs. The "characterization" parts should be designed to affect the polymer sample the least, while the "degradation" section is always done under known,

[1]This type of environment can eventually be upgraded to the point of being totally automated, where all possible parameters are directly accessible via the computer. Currently the light detector power meters have gain setting that need to be set manually. However, it is not difficult to design programmable gain amplifiers.

reproducible conditions, where most of the possible degradation of the fluid occurs, and in a manner that does not directly affect the results obtained under the characterization part. Simply, the independence of these two parts is best assured by allowing enough time between them, especially, before the characterization section.

Each environment allows the operator to proceed through the complete set of experiments by means of an outer loop (`repeat... until done`). The outer loop executes the experiments originally requested under the supervision of the operator, specifically, the program prompts the operator when new information is required (*e.g.*, the laser beam coordinates after the flow device has been re-positioned). However, for all three environments there are several common blocks of code, with small pieces of code handling specific differences. For example, beginning in line 13, different experiments require different types, and amounts of memory allocation; dependent on the number of data points to be read. The next block of instruction are enclosed by the error trapping mechanism provide by HP Pascal. In this manner, all error occurrences within the error-recover block are reported and returned to the program with the purpose of taking, immediately, the appropriate action. In the following section we discuss some of the ideas and necessities for such mechanisms in real-time environments.

The initialization of the instrumentation is done according to the parameters required by the next-in-line experiment. Before the initialization is considered complete, all instruments must respond as operational; otherwise after an attempt is made to reach the requested values, it is called to the attention of the operator that his request failed, or is not acceptable. Once the instrumentation is ready, the execution of the experiment takes place. Errors that occur in this portion of the code are handled within this procedure. If the error reported does not invalidate the data previously taken, an attempt is always made to preserve the previously obtained data. However, a list of error codes is appended to the experimental label for reference by the experimentalist. After termination of the experiment the `new_label` is updated with those parameters used for the execution of the

experiment. Subsequently, a printed report is done, and, finally the data is stored in hard disc memory. The experimental label represents a *complete* record of all experimental data in relation to all of the important parameters relevant: (a) the fluid, such as the composition and characteristics of each one of the components (*e.g.*, type of polymer, molecular weights, etc); (b) the flow-field, such as type of time history for the flow, and values for the flow parameter λ, and rollers speeds; and (c) various other experimental conditions such as temperature, orientation of the flow device with respect to the optical axes, gain settings used for the evaluation of the light intensities, or the computed values obtained during the calibration procedure, etc. Furthermore, this label also contains a list of exceptions and errors that occurred during the experiment. A partial copy of the label is always printed at the completion of the experiment together with a copy of the experimental data in graphical form. In Figure 3.1 an example of such a report is given.

3.3 The Real-Time Software for Birefringence. General Properties

There are several important features that real-time software must have [1, 2]. Besides the obvious characteristic of real-time systems being able to work in a time-critical environment, these systems must be *responsive* to changes in the environment in an "instantaneous" manner; where sufficiently fast reaction for an apparatus like this is of the order of one hundredth of a second. Nowadays, computers have faster response times. However, the peripheral instrumentation is always significantly slower, with the programmable clock possibly being the most important bottleneck, mainly because, without it, there is no easy alternate method to achieve the desired synchronization of events. The programmable clock used in this computer, provides intervals no smaller than 0.01 seconds. Furthermore, our stepping motor is not capable of responding to transient conditions in a time increment shorter than 2/100 of a second. On the other hand, the light intensity tracking

TWO-COLOR FLOW BIREFRINGENCE

Enrique Geffroy.

FLUID CHARACTERISTICS:

Polymer type	NONE
Polym. Mol. Weight	0.000E+000
Pol. Concentration	0 PPM
Solvent type	KER/PBUTENE
Sol. Concentration	1.0000
Fluid Temperature	20.00 °C

FLOW FIELD PARAMETERS:

Flow type	Steady State
Flow Geometry	Two-Roll F
Flow Parameter	0.1501
Gear Ratio red.	5.000:1
FCell Xposition	0.000 in.
FCell Yposition	0.000 in.
FCell Angle Rot	67.50°
Rollers Dir.Rot.	Clockwise

EXPERIMENTAL CONDITIONS:

LIGHT DETECTORS and LASER:

VoltG Blue Ref	3
VoltG Green Ref	3
VoltG Blue Det	5
VoltG Green Det	6
Laser Intensity	0.2490 W
Blue Light Imin	0.00005 mW
Blue Light Imax	1.77620 mW
Green Light Imin	0.00002 mW
Green Light Imax	1.71538 mW

ADC and STEPPING MOTOR:

# Data Readings	500
Sampling time	0.0050 Sec.
Number of Steps	11
Acceleration	24000 S/sec2
Minimum speed	2000 S/sec.
Maximum speed	4800 S/sec.
Number of Runs	1
Step Duration	10 Sec.

Errors Detected:

WARNING: Dangerous experimental conditions ...
Transient behavior expected. Increase mintime!
BAD data statistics, values defined as zeros!
Total # Warnings: 2

Figure 3.1: Birefringence report. The experimental label.

electronics has a combined bandwidth of better than 10 kHz.

The control system must also be *correct* and *complete*. That is, it must be capable of catering to all possible events and situations that may arise in the experimental environment or the software itself. In reality, it is extremely difficult to reach optimum levels in this field, for a well prescribed action must always correspond to each event. As a result, the program must have "defensive" code with the specific purpose of trapping error conditions and exceptions. In this manner, the system reliability may be improved to the desired degree. Furthermore, the defensive code must take actions that degrade the performance of the system in a "soft" way. That is, the system must provide a useful degraded service, in the event of a failure of the peripheral instrumentation. For example, a degraded service may be the possibility of salvaging previous data taken before the failure was detected, or the possibility of tagging data corrupted during the failure of the system while still managing to complete the task. A weaker alternative will be to report the failure of the system, by issuing a failure report. All three techniques of defensive code are used within this program.

The specification of the software problem (*i.e.*, the program) is most easily done in terms of a virtual machine, which corresponds to the idealization of the designer without considering the limitation of the computer upon which the program is going to be executed. In practice there are several constraints upon which the virtual machine is built, specially when the software requires utilities provided by the operating system, such as the system clock, I/O ports, etc. In order to define the virtual machine associated with the control system it is necessary to define the processes to execute, the level of synchronization and information sharing among different processes, and the mechanism by which the computer resources are going to be shared.

The problem at hand is the concurrent use of one CPU by four processes: (a) data acquisition, (b) control of instrumentation, (c) processing of experimental data, and (d) display of data for operator supervision. Data acquisition involves

reading voltages at precise time intervals in order to determine the light intensities for all detectors as a function of time. Control of instrumentation relates to requesting specific tasks from these instruments such as inception of the roller rotation in order to generate the flow field. Processing of data corresponds to manipulation of data to convert voltage readings to meaningful relative light intensity measurements. And finally, display of data requires evaluating the anisotropy of the sample with given mathematical formulae such as those discussed in the previous chapter, and displaying this information in a graphic form.

Data acquisition, processing of data, and its display in graphic form are all interelated processes. The lack of the first de-activates the others. Furthermore, their interelationship also requires common variables or parameters to be shared in a safe way, where concurrency of processes is such that the process controlling the CPU should never corrupt the information being used by other process. This requirement is most easily resolved by double variables, where the current status is only accessible to the fastest process, and other processes only read/write to the second variable. Data transfer is done using so-called channels implemented as linked list and queues of data [3], where the first element passed to the channel will be the first element removed from the other end. The priorities for execution of these three processes are very different with priority for data acquisition being the highest. Furthermore, the level of synchronization is low, that is, there is no need for channels that can only take one value. Consequently, it is best if raw data channels can grow in size if the rate of data reading exceeds the rate of data processing. Thus, no real compromise is made by forcing the other two processes to run in the background, while allowing the data reading and control of the instruments to have the highest priority.

Data acquisition and control of instrumentation are tightly couple operations and thus, their synchronization becomes essential. For example, during transient flows, the onset of data readings must coincide with the start-up of the rollers rotation. Actually, these two events must *always* run in synchrony, and under

scheduling defined by the programmable clock. The clock ticks according to the largest time interval common to all processes, and the interrupt handler operates as a dispatcher deciding which process will be serviced. The use of the longest time lapse possible provides the most CPU time for those processes running in the background, while still executing all of the necessary high priority tasks. Therefore, at the beginning of the program, the best time interval for the programmable clock is chosen and the dispatcher is called whenever there is an interrupt caused by the cyclic clock. This type of interrupt must be differentiated from those interrupts caused by other devices, for none of the interrupts should be masked (there is possible generation of interrupts done by internal devices to the computer, as well as those associated to the instrumentation). Once the interrupt is identified by the system as belonging to the cyclic timer, the appropriate interrupt handler takes over the CPU. In this case the CPU enters in the *supervisor* mode of operation in order to service the interrupt. This is a high priority processing mode available to the Motorola CPU's, that allows a quick service response, but with same drawbacks such as no debugging mechanisms, etc. (for more details see [4]). In this supervisor mode, the last instruction being executed by the lower priority process is stored, for future use, and the control is passed to the dispatcher. The function of the dispatcher is to choose the top priority task and sequentially execute all the others that are also needed.

The simplest interrupt handler is that used by the steady state birefringence. In this case the experiment consists of a series of steady state flow conditions, with the angular speed of the rollers starting at a low speed, and incremented by a prescribed amount after a period of time. The number of steps for the series, the initial low speed, the speed increment, and the period of time at a given speed, are parameters given by the operator at the first level of the program. The following lines present such an interrupt written in HP Pascal (this procedure is part of the procedure executing the Steady State birefringence).

```
PROCEDURE SS_INTR_HDL(VAR STATBYTE, DATABYTE: BYTE; VAR DOIT: BOOLEAN);
```

```
{- - - - - - - - - - - - - - - - - - - - - - - - - - - - - - - - - - - - - -
 This sub-procedure of BirP_BSS takes over the CPU when an interrupt occurs.
 It is in charge of doing the data acquisition thru the ADC and triggering
 of the SMI to generate the step ramp.              EGA Rev. 1.0, 25/Nov/86.
 - - - - - - - - - - - - - - - - - - - - - - - - - - - - - - - - - - - - - }
 VAR   i : NATURAL;

 BEGIN
   IF (ODD(STATBYTE DIV 32) AND ODD(DATABYTE DIV 32)) THEN BEGIN
       CYCLICCOUNT := CYCLICCOUNT + 1;
       IF (CYCLICCOUNT MOD 20 = 1) THEN BEGIN
           TRIGGER(SMI_isc);          { .. trigger SMI. Speed incremented! }
         END;
       IF (CYCLICCOUNT MOD 20 = 0) THEN BEGIN{.. Data acquisition begins.. }
         TRY
           measurement_lib_random_scan(name, c_size, channel,
                     d_size, ADC_Dptr, REPT, p_size, pace, g_size, gain);
           i := 4 * REPT + 1;
           WHILE i <= d_size DO BEGIN
               ADC_Dptr^[i] := -11.0;
               i := i + 1
             END                                 { .. Data acquisition done! }
         RECOVER BEGIN
             IF (ESCAPECODE = IOESCAPECODE) AND (IOE_ISC = 18) THEN
               Add_Error(ErrorLT, ADC3)
             ELSE IF (ESCAPECODE = -1) THEN
                    Add_Error(ErrorLT, ADC4)
                 ELSE ESCAPE(ESCAPECODE);
             ADC_Dptr^ := arrayconst {.. Failed, all elements equal to -13.}
           END;
         Save_dpoint(datqueue, ADC_Dptr); {.. ADC readings stored in queue.}
         STEPCOUNT := STEPCOUNT + 1;
        END
     END
   ELSE CALL(SAVEISRHOOK,STATBYTE, DATABYTE, DOIT);
 END;      { - - - - - - - - - - - - - End of Procedure BirP_BSS.SS_INTR_HDL.}
```

CYCLICCOUNT keeps track of real time by counting the number of ticks of the cyclic timer. CYCLICCOUNT is initialized by the higher level procedure before the cyclic timer is started. After the first interrupt, the interrupt handler commands the stepping motor interface to start the motor, (maintaining a constant speed) and requests it to increase its speed after 20 ticks, repeatedly, until the complete sweep of speed is executed. The data acquisition is always done just before the speed is incremented (during tick #19) allowing the longest possible time for the flow to reach a steady state before reading the light intensities falling upon the detectors.

`random_scan` actually takes 500 readings (or less if requested by the operator) per light detector, with the purpose of increasing accuracy of the measurements by doing statistical data reduction of the experimental data. The data reading takes place in an error trapping block. In this way, failures of the A/D converter are reported to the system and the data is invalidated before it is actually used by the data reduction process. Afterwards, the data `ADC_Dptr` is stored in the raw data channel: `datqueue`, and the step counter incremented. When exiting the interrupt handler, all registers, and the program counter are restored by the CPU in order for the lower priority process—initially interrupted—to continue running. The possible conflict of changing the rollers speed before all data is taken never arises. The occurrence of another cyclic timer interrupt, while reading data, is always saved in queue, and only executed after the completion of the previous one.

3.4 Execution of Birefringence. The second level

The second level programming actually corresponds to the line of pseudo-code for "execution of the experiment" of section §3.2, lines 18, 46. There are three specific procedures for each one of the three possible birefringence experiments: Steady-State, Start-Stop and Double-Step birefringence. The transient flow birefringence is intrinsically more difficult mainly because of the strict synchronization required. In the following paragraphs, the Pseudo-code for Double-Step birefringence is given, together with its interrupt handler, written in Pascal code.

This experiment's objective is the evaluation of fluid birefringence under transient flow conditions. This transient flow condition is the result of two identical changes of the roller speed; the first change is from a low to a high speed and the second is from the high speed bach to the low speed. Hence, we are interested in the *time* evolution of the birefringence and the experiment tracks this evolution by reading the light intensities at discrete time intervals, or points in time. Because

of the fact that it is not possible to take enough experimental data during a single run, this procedure executes a series of identical low-high and high-low changes until enough data is collected and the statistical reduction of data improves the accuracy of the experiment. During each one of the "partial" runs, the A/D card reads at the fastest possible rate 10 values of light intensity for each point in time. In this manner if the requested number of readings per point in time is 100, then only ten partial runs are actually performed. Furthermore, the code allows a complete series of low speeds to be tested where the high speed remains the same in all cases. Here is a pseudo-code of such an experiment.

```
1  PROCEDURE Bir_Proc_Double_Step;
       initialization of variables;
       initialization of graphics;      { .. monitor in graphics mode .. }
       initialization of data channels;
5      calculate cyclic timer period (t_tick);
       convert times into number of t_ticks;
       save default interrupt handlers;
       install cyclic interrupt handler(LH_INTR_HDL);
       Reset error trapping mechanism
10       Repeat                   { ... for all low speeds requested ... }
           initialize SMI;
           initialize double variables;
           enable cyclic timer;

15             { .. data reduction and plotting run in the background .. }
           Install graphic mode for birefringence;
           While experiment not completed do
               If data reading finished
                   stop motor;
20                 disable cyclic timer;
                 END;
               update double variables for background processes;
               Fetch data point from raw data channel;
               Normalize raw data;
25             Statistical analysis of data;
               If birefringence plot
                   compute orientation angle and biref;
               plot data;
             END;            { .. of do loop for background execution .. }
30       Until all low speeds done;
         Store experimental data;
         Force exception (error = no_error);
       Recover from errors block
           disarm and replace cyclic interrupt;
35         clean dynamic variables (data channels);
```

```
        reset SMI to initial state;
        print hardcopy of bir. plot;
        reset monitor to alpha mode;
      END;                              { ..  of error recover block .. }
END;                        { .. end of procedure Bir_Proc_Double_Step. }
```

Initialization of the system is always the first operation. Replacement of the standard interrupt handler by the desired one is done only after the previous one is saved. The following section of code is completely guarded by an exception trapping block, and in this manner, all the necessary clean-up operations are still available before the experiment is aborted to a higher level of code. At this point the complete apparatus should be ready to start execution of the experiment. It commences by enabling the cyclic clock, where now there are two pieces of code sharing the CPU "concurrently." The other piece of code corresponds to the interrupt handler which is described shortly. The background code consists of (a) the normalization and conversion of voltages to relative light intensity values; (b) statistical reduction of data; and (c) presentation of data in graphed format to the operator. These three operations are done sequentially, and process all data available to the background loop as provided by the last update of double variables. This does not mean that the raw data channel is empty, since the update of double variables occurs much less frequently than the rate of data acquisition.

It is required that the statistical reduction algorithm calculates mean values and higher order moments of the *partial* data sets, permitting the operator to monitor the time evolution of the data readings as the number of "partial" runs progresses. At this point two conditions are important to take into account. The first is the necessity to use algorithms that preserve the accuracy of the *partial* sums of the moments of the distribution without incurring least-significant-bit errors by the computer [6, 5], and secondly to compute the variances and covariances of the experimental data in order to be able to calculate the uncertainties of the dependent variables, i.e., birefringence and orientation angle (see for example Bevington [7]). This scenario implies that the best way to preserve the integrity of the data is by

permanently storing the mean values as well as the variance and covariance of the relative light intensities. Storage of the raw data requires approximately 100 times more memory space, and storing the birefringence data provides no means of retrieving the experimental values, if other equations for computation of birefringence are to be used.

Once all data readings are done, the program releases the interrupt code and the background program takes full control of the CPU. The statistically reduced data is saved along with some small tags, and before the control is passed to the higher level procedure, the code forcefully executes clean-up operations in order to restore the computer resources to the existing state before entering this code. The Pascal code for the interrupt handler is as follows:

```
PROCEDURE LH_INTR_HDL(VAR STATBYTE, DATABYTE: BYTE; VAR DOIT: BOOLEAN);
{- - - - - - - - - - - - - - - - - - - - - - - - - - - - - - - - - - - - -
 This sub-procedure of BirP_BLH takes over the CPU when an interrupt occurs.
 It is in charge of doing the data acquisition thru the ADC and synchroniza-
 tion of the Stepping motor.                          EGA Rev. 1.0,  1/Sep/87.
   datagood    : boolean variable used to decide when to store data,
   IntrCOUNT   : keeps track of the number of interrupts trap by the handler,
   CYCLICCOUNT: interrupts after high or low speed flow,
   Read_pts    : is a counter for the number of points read,
   RunCounter : Counter to guarantee the minimum number of data readings,
   Flow        : boolean describing the flow condition based on counters.
- - - - - - - - - - - - - - - - - - - - - - - - - - - - - - - - - - - - - - }

 BEGIN
   IF (ODD(STATBYTE DIV 32) AND ODD(DATABYTE DIV 32)) THEN BEGIN
     datagood := TRUE;
     IntrCOUNT := (IntrCOUNT + 1) MOD MaxCOUNT;
     CYCLICCOUNT := CYCLICCOUNT + 1;
     IF (IntrCOUNT  = 1) THEN BEGIN
         Read_pts := 0;    CYCLICCOUNT := 0;
         RunCounter := RunCounter + 1;
         IF RunCounter <= runs THEN BEGIN
             TRIGGER(SMI_isc); {.. start HIGH speed section of program! .. }
             HighFlow := TRUE
           END
         ELSE BEGIN
            TRIGGER(SMI_isc);  { .. ENDS the flow condition of program! .. }
            HighFlow := FALSE;
          END
       END;
     IF RunCounter <= runs THEN BEGIN
       IF (IntrCOUNT  = StopCOUNT + 1) THEN BEGIN
```

```
        TRIGGER(SMI_isc);     { ... begins LOW speed steady flow !  ... }
        HighFlow := FALSE;  CYCLICCOUNT := 0
      END;
    IF (RunCounter > 0) THEN
       {i. e., first lap is for warming up! or no more data than needed.}
      IF                  {   ....... data Acquisition begins  .... }
        (HighFlow AND((CYCLICCOUNT <= N1)OR
        ((CYCLICCOUNT > N1)AND((CYCLICCOUNT - N1) MOD 3 = 0)))) OR
        (NOT(HighFlow) AND((CYCLICCOUNT <= M1)OR
        ((CYCLICCOUNT>M1)AND((CYCLICCOUNT - M1)MOD 3 = 0)))) THEN BEGIN
        TRY
          measurement_lib_random_scan(name, c_size, channel,
                      d_size, data, REPT, p_size, pace, g_size, gain);
        RECOVER BEGIN
            datagood := FALSE;
            IF (ESCAPECODE = IOESCAPECODE) AND (IOE_ISC = 18) THEN
              Add_Error(ErrorLT, ADC3)
            ELSE IF (ESCAPECODE = -1) THEN
                   Add_Error(ErrorLT, ADC4)
                 ELSE ESCAPE(ESCAPECODE)
          END;
        Read_pts := Read_pts + 1;
        IF Read_pts > totalpoints THEN totalpoints := Read_pts;
        IF datagood THEN
          Save_dpoint(Datlist, data^)  {.. ADC readings stored in queue.}
       END;
   END
  END
 ELSE CALL(SAVEISRHOOK,STATBYTE, DATABYTE, DOIT)
END;       {- - - - - - - - - - - - - End of Procedure BirP_BLH.LH_INTR_HDL.}
```

The interrupt handler bases synchronization of data readings and triggering of the stepping motor in terms of the `t_tick` here expressed as `IntrCOUNT`. A *partial* run is completed when the number of interrupts reaches `maxCOUNT`. At this point the partial run counter is incremented and the next run is executed. The data acquisition starts only after the first partial run is completed. That is, this first run is executed to erase the previous memory of the fluid sample. In this manner, the second run, commences with a known flow history. When `IntrCOUNT` $= 1$, the roller rotation changes to a high speed, and this speed is altered only after the interrupt counter reaches `StopCOUNT` $+ 1$.

The data acquisition part of the interrupt handler, is similar to the one previously discussed for the Steady-state experiments; the main difference being that

data is not always read for every clock interrupt. The highest density of points in time is needed when the sample anisotropy is most rapidly changing. Thus, three times more points in time are read for the first one third of the experimental run when changes of the roller speed occur and transient effects should be most important.

Bibliography

[1] S. T. Allworth and R. N. Zobel; *Introduction to Real-time Software Design*, Second ed. Springer-Verlag, New York, 1987.

[2] D. A. Mellichamp, ed.; *Real-Time Computing*, Van Nostrand Reinhold, New York, 1983.

[3] A. M. Tenenbaum and M. J. Augenstein; *Data Structures Using Pascal*, Prentice-Hall, Englewood, N. Y., 1981.

[4] Motorola Inc.; *Manual for the MC680xx Family of Microprocessors.*

[5] D. L. Smith; *Rev. Sci. Intrum.*, **54**(7)818-824(1983).

[6] A. D. Forsythe; *Byte*, **4**(1)182-184(1979).

[7] Bevington; *Data Reduction and Error Analysis*, McGraw-Hill Book Co. New York, 1978.

Part II

Transient Flow Birefringence of Polymeric Solutions

Chapter 4

Flow Birefringence Studies in Transient Flows of a Two Roll Mill for the Test-Fluid M1 *

Enrique Geffroy
California Institute of Technology
Department of Chemical Engineering

and

L. Gary Leal
University of California, Santa Barbara
Department of Chemical and Nuclear Engineering

*Presented at the International Conference of Extensional Flow in Combluix, France; March 1989. Accepted for publication in the Journal of Non-Newtonian fluid Mechanics, September, 1989.

Flow Birefringence Studies in Transient Flows of a Two-Roll Mill for the Test-Fluid M1

Abstract

We have studied the test-fluid M1 in flows generated by a two-roll mill. These flows are linear, and two-dimensional, and the magnitudes of the strain-rates are greater than the vorticity. The polymeric solution is shown to degrade significantly, even for small values of the velocity gradient, as measured by the changes in the macroscopic relaxation time-scales. Consequently, the determination of macroscopic properties such as elongational viscosity based upon the overall pressure difference, or the total force as measured in a spin-line rheometer, may *not* be representative of the properties of the fresh, undegraded fluid. In this work, the degradation of the test-fluid has been studied as a function of the strength of the velocity gradient for different values of the ratio of the strain-rate to vorticity of the flow. Furthermore, the observed relaxation time-scales have been evaluated based on data for steady state flows, and several transient flow histories such as start-up and cessation of flows, and double-step flows. These flow histories provide us with some insight into the relaxation dynamics of the polymeric structure for different initial conformation states.

Chapter 4

Flow Birefringence of the Test-Fluid M1

4.1 Introduction

In this paper, we report a birefringence study of the polymer solution M1, in two-dimensional strong flows that are generated in a two-roll mill. The designation *strong* in this instance is taken from the general criterion as expressed by Olbricht *et al.* [2] and others (see for example Tanner [4].) In two-dimensional flows this criteria implies that the magnitude of the strain-rate exceeds the vorticity. Previous studies of both dilute and concentrated polymer solutions have shown that polymer extension and orientation is qualitatively (and even quantitatively) similar for *all* strong flows, including pure extension, provided that the polymer orientation is compared with the principal eigenvector of the velocity gradient tensor, and the effective strain rate (i. e., the magnitude of the principal eigenvalue) along this direction is used instead of the velocity gradient itself (see for example Dunlap and Leal [7]).

Birefringence provides a measure of the degree of optical anisotropy, and of the orientation of the principal axes of the refractive index tensor, that is induced in a polymeric liquid by the imposed flow (see for example Janeschitz-Kriegl [1]). This

is a reflection of changes in the polymer conformation due to the flow, and for weak departures from the state of equilibrium, it is also directly related to changes in the stress. Most of the other studies of the fluid M1 that are reported in this volume are designed to provide a measure of extensional viscosity via measurements of overall pressure differences or exerted force in spin-line and opposing jet configurations. The birefringence data reported here provides a direct measure of polymer conformation in an extensional flow. We are able to study both steady and transient flows of various types, i. e., start-up, relaxation from a steady flow, or double-steps, etc. We shall describe these flows in the next section.

The present study was carried out using a new experimental system that was designed to study birefringence in time dependent strong flows, and that also allows detailed measurements, via dynamic light scattering, of the velocity gradient field as a function of time and spatial position. The latter, in our view, is *essential* for any *quantitative* interpretation of the birefringence data (that is, of the response of the polymer to the "real" strain-rate imposed by the flow,) because significant departures from the equilibrium conformation will not only be accompanied by measurable amounts of birefringence, but also usually, by significant changes in the flow compared with the motion of a Newtonian fluid in the same flow device, at the same Reynolds number.[1] In spite of this, however, measurements of the velocity gradient field were *not* made in the present study because it was found that the polymer solution degraded on a time-scale that made it infeasible to do both birefringence and light-scattering studies in a reasonable amount of time with the somewhat limited amount of test fluid that was available.[2]

In this paper, we briefly summarize the main features of the experimental system (a more detailed description will be published elsewhere, and may be obtained upon request from the authors), and then report data on both the solvent and the polymer test-fluid M1. Finally, we discuss our views on the significance of our results.

[1] Of course, the same is true of the flows in "extensional" rheometers.

[2] Degradation of the solution required the fluid sample to be frequently changed so that it was under flow only for a short time.

4.2 A Brief summary Description of the Experimental System

The experimental system used for this work is new and has not yet been described elsewhere. However, a complete, detailed description would be inappropriate in the present context, where the focus is the measured behavior of the test fluid M1. Thus, we limit ourselves to a brief summary of the experimental set-up with enough detail to allow the reader to understand what we have done.

4.2.1 The Flow Device: A Two-Roll Mill

All of the birefringence and light scattering studies carried out in this laboratory over a number of years have utilized either a two- or a four-roll mill to generate the flow fields. These devices consist of either two or four parallel cylinders (situated, in the case of the four roll mill, in a square pattern) with the flow generated by rotation of the cylinders. When properly designed, these flow devices produce a good approximation to a linear flow in the region between the rotating cylinders, with the ratio of strain-rate to vorticity and the magnitude of the velocity gradient *independently* controlled. In the case of the two-roll mill, with cylinders co-rotating at the same angular velocity (as in this work), the flow type is controlled by the geometry of the flow device, i. e., by the ratio of the cylinders' radius to the gap width between the cylinders, and the magnitude of the velocity gradient is proportional to the angular velocity of the cylinders.

It is convenient to parametrize the (approximately) linear flow that exists in the region between the cylinders by expressing the velocity field in the form

$$\mathbf{U} = \frac{G}{2}\begin{bmatrix} (1+\lambda) & (1-\lambda) & 0 \\ -(1-\lambda) & -(1+\lambda) & 0 \\ 0 & 0 & 0 \end{bmatrix} \cdot \mathbf{X}, \tag{4.1}$$

where the position vector $\mathbf{X}$ is measured from the origin of a coordinate system that is centered at the geometric center of the two-roll mill. Thus, the flow is completely characterized by the two parameters G and λ, where G is the magnitude of the

velocity gradient (often called the shear rate), and λ determines the ratio of strain-rate to vorticity (i. e., the flow type) by the expression

$$\frac{\|E\|}{\|\Omega\|} = \frac{1+\lambda}{1-\lambda} . \tag{4.2}$$

Clearly, λ varies from -1 to $+1$, with $\lambda = +1$ representing a pure straining flow, $\lambda = 0$ a simple shear flow, and the range of possible *strong* flows (as defined earlier) corresponding to $0 < \lambda \leq 1$. The two-roll mill can generally produce flows with λ values in the range of $0 < \lambda \leq 0.25$. Another critical feature of the flow generated by a two-roll mill as indicated by equation (1) is that it contains a stagnation point at its geometric center. Thus, in contrast to many extensional flow devices, the polymer molecules near the stagnation point are subjected to very large total strains, and consequently can achieve the maximum change in conformation that is consistent with the particular strain-rate.

The two-roll mill used in the present study is shown schematically in Figure 1. It was built with 8 pairs of rollers of different diameter, so that eight λ values between $0.01 \leq \lambda \leq 0.2$ could be obtained by simply using different pairs of rollers. In the present study, the M1 fluid was evaluated with roller pairs C, and F. The dimensions of these two sets of roller pairs, together with the gap width and the length-to-gap ratio are listed in Table 1. The two-roll mill used here was designed so that both

Roller ID.	radius (cm)	gap (cm)	height: gap ratio	λ	$\sqrt{\lambda}\dot{\gamma}_{max}$ (sec^{-1})	$\dot{\gamma}_{max}$ (sec^{-1})
C	1.570	0.260	9.8:1	0.0403	74.2	461.2
F	1.278	0.844	3.1:1	0.150	32.9	105.8

Table 4.1: Characteristics of the Two-roll Mill

rollers are driven simultaneously by a single stepping motor. The motor electronics is interfaced with a computer, so that a variety of different transient flow-histories can be produced, as well as an automated sweep through a series of steady flows with different values of G. Among the transient flows used in this study were: (a)

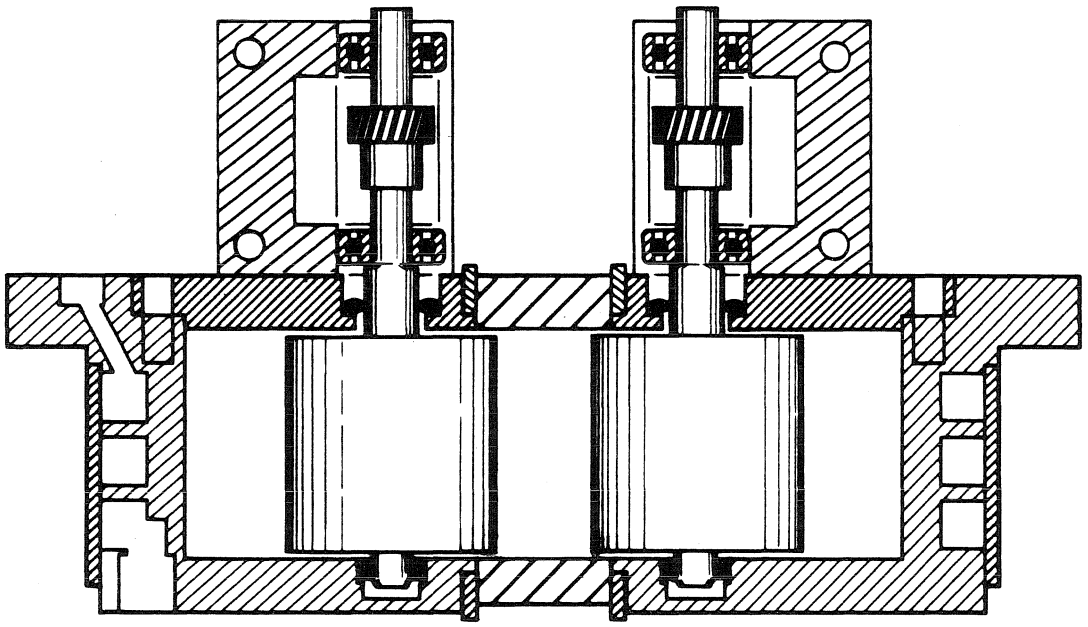

Figure 4.1: The two-roll mill flow device. The rollers are driven by a single stepping motor coupled to them via identical worm-and-gear assemblies. The rollers are supported by three sets of bearings to guarantee colinearity of the axis of rotation and to minimize excentric wobbling of the rollers.

a start-up flow, where the fluid at rest is put abruptly into a condition of steady flow[3], (b) stop flow, which corresponds to an "instantaneous" cessation of a steady flow condition, and (c) double-step flows where a steady flow condition is stepped into another.

4.2.2 Two-Color Birefringence System

In order to perform birefringence measurements in time dependent flows, we have adopted the two-color birefringence technique that was originally developed by Fuller and coworkers [15]. The basic problem with transient birefringence measurements is that both the degree of birefringence (i. e., the difference of the principal values of the refractive index tensor in the plane of the flow), and the orientation of the corresponding principle axes of the refractive index tensor are unknown and varying in time. Clearly, two independent measurements are necessary to determine both the degree of optical anisotropy and the time-dependent orientation angle. The two color system is designed to provide these two independent measurements simultaneously by using the two main colors of an Argon-ion laser[4] (respectively, with wavelength of 4880 Åand 5145 Å). The retardance of the sample is determined by

[3]Actually, all flow conditions are achieved via an acceleration ramp for the angular velocity of the rollers that although quite high, is still finite. The motor always requires less than 1/20th of a second to reach any prescribed angular speed; mean values for the ramp-time are less than 1/100 of a second for the experiments reported here. The fastest intrinsic time-scales observed for this particular fluid sample were at least an order of magnitude longer. The acceleration ramp is one of the various parameters that the experimentalist has control of through the computer. The observed behavior was always checked for possible dependence on the ramp-time.

[4]The laser head in order to supply the two-color beam has been equipped with a blue-green output coupler, a flat broadband reflector, an isothermal intracavity etalon and, a polarization rotator at the lasing end. The intracavity etalon is used to operate the laser in single mode for both lines and in this way a more stable operation for the intensity of the two colors is obtained. Furthermore, the stability of the light intensity depends on the temperature of the etalon. The control of the temperature of the etalon's oven provides the means of balancing the intensity of both beams so that the most stable operation is achieved for both lines. The argon laser equipped with these items, becomes a light source with the following important characteristics: (a) one laser provides the two colors, and consequently the initial optical characteristics of both beams are identical, (b) both lines operate in single transversal emission mode TEM_{00}, maintaining it for periods up to several weeks at a time. In this manner, the light intensity distribution across the beam is very stable and can be assumed to have a *Gaussian* profile at all times; and, (c) the stability of the light intensity is best for both lines independently, remaining within a percentage point.

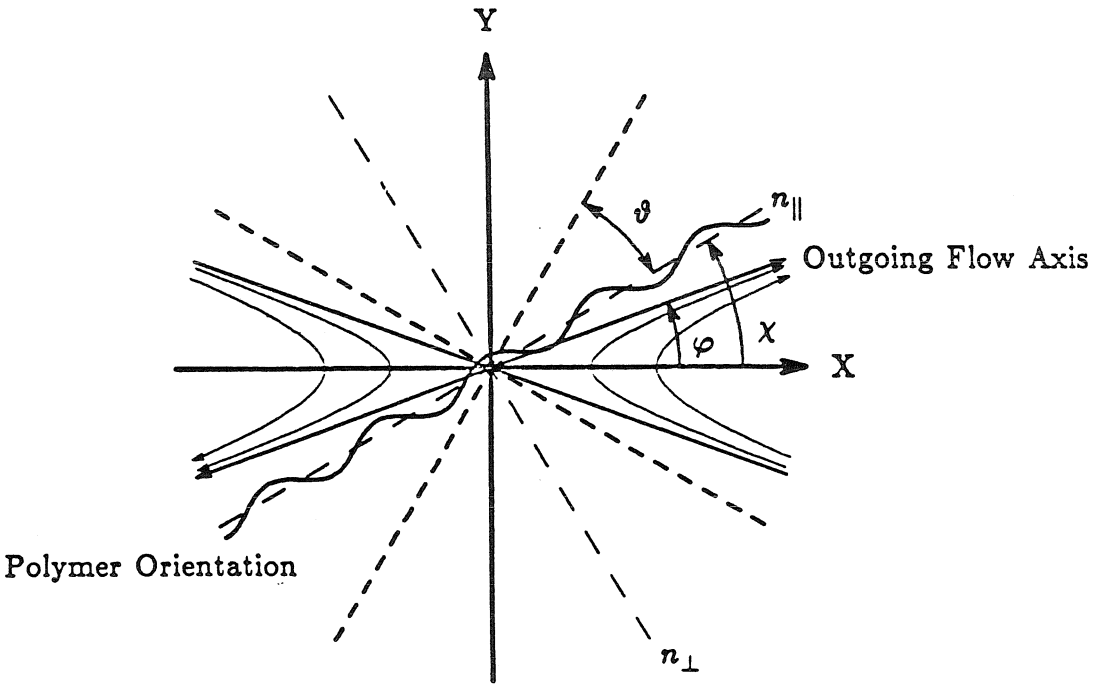

Figure 4.2: Relative orientation of the Optical system and the flow cell

measuring the light intensity that passes through crossed polarizers for both colors separately, with the relative orientation of the incident polarization of the green beam –with respect to that of the blue beam– rotated to some fixed angle. The most convenient angular separation for the polarization of the two beams is 45°, and for the experiments reported here the initial polarization of the green and the blue beams is at angles of +22.5° and −22.5° respectively, relative to the symmetry plane which bisects the two-roll mill. Figure 2 shows the relative orientation of the blue and green analyzers, as well as the principal optical axes of the solution and the symmetry axes of the flow field. The general principles for the two-color measurements, including the general basis for data analysis, are discussed by Chow and Fuller [15] and will not be repeated here.

However, a few details of our present system are worth stating, specifically as they relate to measurements that have been done on the test liquid M1. First, the

current system is extremely sensitive, with extinction ratios in the absence of the flow device of $\mathcal{O}(10^{-5})$. In the presence of the flow device, the residual birefringence of the glass windows is the primary limitation on sensitivity, since it can be larger than the birefringence of a slightly anisotropic fluid. With our flow device it is possible to rotate the glass windows (perpendicular to the incident beam), and pre-load them (at three different points along their perimeter) so that the residual birefringence is minimized prior to the execution of the flow-birefringence experiments. The lowest detectable values for the glass birefringence depend on the minimum detectable values of the measured light intensities past the analyzers. The maximum extinction ratios detectable with our device, for both colors, are typically $\mathcal{O}(5 \times 10^4 : 1)$, which represents the maximum sensitivity of our optical arrangement. Within this range of sensitivity, the residual glass birefringence always exists, and, in fact varies (specially in its orientation angle) from day to day, due mainly to changes of the room temperature. The possibility of pre-stressing the glass windows is an important advantage of this system especially when the fluid sample is only slightly anisotropic, such as for the solvent data that is presented later on.

Another important characteristic of this two color system is that the beam waists for both the green and blue beams are approximately 75 microns in diameter, and the extent of the beam waist regions is about 0.75 cm. Thus, the birefringence measurements are very localized, relative to the dimensions of the flow device. A typical beam dimension of this size is not particularly difficult to achieve for a single color birefringence system. On the other hand, for the two-color system, the optical set-up must not only provide a narrow beam, but the dimensions, shape and location of the blue and green beams must be as nearly identical as possible across the flow device. This is a difficult task when both beams are 75 microns in diameter and the above conditions are to be maintained for long periods of time.

The flow device is mounted on a support with four degrees of freedom (x, y, z, θ) in order to adjust the relative position of the two-roll mill with respect to the

incident beams. The translating stages (three) for these degrees of freedom are driven by differential micrometers with a resolution of 0.00005 inches, while the azimuthal orientation is adjusted with a micrometer providing an angular accuracy of 0.0003 radians. The re-positioning of the flow cell is always better than 0.001 inches and 0.001 radians, even when the flow device is dismounted for the purpose of replacing the solution.

The speed of data acquisition is mainly limited by the electronics in the experimental apparatus. It takes about 1 msec. to execute all the necessary irradiance readings to obtain a data-point for the extinction angle and the birefringence of the fluid sample. In order to increase the signal to noise ratio, the computer program performs several readings sequentially, at full speed, and performs the appropriate statistical analysis on the data sample. For the steady state flow conditions, the average number of readings per data point was about 500. For the transient flows, ten readings are taken sequentially (at the fastest pace possible) for every point in time, and the sum of results from ten repetitions of the experiments are used for the statistical analysis. The flow conditions were kept identical for each one of the ten different experimental runs.

The chief limitation of the M1 solution for the birefringence studies is that it is relatively dirty for optical work. Thus, we have found that there is a significant loss of intensity from the incident light beams as they traverse the sample due primarily to scattering of light from small dust particles that exist in the fluid M1. Although dust can normally be removed from liquid samples—by filtration, for example—this is difficult at best when the fluid is as viscous as M1. We were also hesitant to filter the sample due to the potential for significant changes of the fluid properties via degradation. On the other hand, in order to remove some of the largest and most troublesome dust particles, our samples were centrifuged in a Serval S-6 centrifuge at approximately 5000 rpm., for approximately four hours. The top and bottom of the sample were discarded, and the remaining fluid was allowed to rest for several days at room temperature before being used.

It is also likely that the M1 fluid exhibits measurable dichroism, which increases with increasing values of the velocity gradient, but this is difficult to distinguish from the loss of intensity due to scattering from the dust or dirt. This combination of factors leading to less light intensity makes the data analysis extremely difficult when the birefringence becomes strong enough to produce multivalued light intensity values with increase of G (the measured light intensity is proportional to the square of the sign of the retardance, i. e., $i \sim \sin^2(\delta/2)$). Furthermore, for the flow geometries and values of G reported in this work, the degradation of the fluid samples was already significant in the vicinity of the first maxima of the retardance. Rather than attempting to deconvolute the light intensity data which requires a knowledge of the dichroism for fluid samples that are difficult to characterize because of the fast degradation that is taking place, we have limited ourselves to the limited range of values for the velocity gradient where the light intensities are monotonically increasing functions of G. Furthermore, instead of normalizing the measured intensities with the intensities of the incident beams, as would be "normal" for the two-color system, we measure the total maximum light intensity *after* the beams pass through the fluid sample, and normalize with that value rather than the incident beam intensity in order to reduce fluctuations and noise contributions due to the presence of the dust particles.

The measurements reported below were primarily made at the central region, around the stagnation point of the flow. However, some measurements were also done in the plane that passes through the two roller axes, that is, across the gap between the cylinders. These measurements were necessary in order to locate the region of maximum birefringence and also provide a basis which could be used to evaluate the degree of localization of the birefringence zone for the various flow rates. However, in the present paper, we only report on data from the point of maximum birefringence.

As a general practice and whenever a fresh solution is used, the relative orientation of the symmetry axes of the flow cell with respect to the bisector defined by

the azimuthal orientation of the blue and green analyzers was also fine-tuned based upon the measured orientation angle for the polymer for two sets of experiments at the stagnation point in which the direction of roller rotation was reversed.[5]

4.2.3 Homodyne Light Scattering

Our experimental system is also designed to do homodyne (dynamic) light scattering measurements at any position within the flow device, using the scheme originally developed in this laboratory by Fuller *et al.* [18] to relate this data to the local velocity gradient in the flow. As indicated in the introduction, our goal is to *directly* measure the velocity gradient in the flow in order to correlate with the measured birefringence levels. Indeed, the current experimental set-up is designed to perform measurements of the velocity gradient in both steady and time-dependent flows. In general, if the polymer undergoes a change of conformation, the flow will also change, and measurements of the velocity gradient become an essential part of any study of the birefringence involving polymer solutions (or melts) that are not ultra-dilute. Without flow measurements, for example, any tendency towards non-linear dependence of the birefringence on roller rotation rates cannot be ascribed in an unambiguous way to changes in the polymer response to the flow, as opposed to changes of the flow. Nevertheless, no measurements of the velocity gradient were made for the M1 fluid. Even for steady state flows, where no repetition of the experiment is necessary, the addition of light scattering measurements increases significantly the time the material must be subjected to large strains. For M1, we found that the solution degrades rapidly and this precluded additional measurements beyond the birefringence measurements reported below, both because the limited amount of available test-fluid limits the number of "recharges" that it is

[5]The azimuthal calibration was done with a clean solution of polystyrene in toluene. With this solution, data for the orientation angle is reproducible within $\pm 0.25°$ for the complete range of speeds of the rollers. The flow device and optical system orientation are considered to be equivalent when the absolute value of the extinction angle of the measured anisotropy coincides within 0.5°, for the clockwise and counterclockwise rotation of rollers. It may be noted that the flow cell mount is capable of positioning the flow device with a reproducible azimuthal orientation of ± 0.05 degrees.

possible to do, and because of the excessive time required to evaluate the flow field characteristics of a sample that, because of dust particles has poor signal-to-noise ratios. Since, no measurements were made, we postpone any detailed description of the light scattering system to a later publication.

4.3 Results for the Test-Fluid M1

The complete characterization of the flow-induced anisotropy of a polymeric fluid requires determination of the birefringence Δn, as well as the orientation angle χ of the principal axes of the refractive index tensor with respect to the flow field. Two typical data sets are shown in Figure 3 and 7. In the upper part of these figures, the birefringence is plotted as a function of the principal eigenvalue of the velocity gradient tensor, *i. e.*, $G\sqrt{\lambda}$ for steady flow. The graph on the bottom of the figures shows the orientation of the principal axis of the refractive index tensor measured relative to the bisecting symmetry axis for the two roll mill. A positive value for this angle, corresponds to the optical axis lying between the symmetry axis and the outflow axis along the direction of the principal eigenvector of the velocity gradient tensor (see Figure 2). Previous studies of polymer solutions in this lab have shown that the degree of orientation (and presumably extension) of the polymer molecules is a function solely of $G\sqrt{\lambda}$ for all values of $\lambda > 0$. Thus, in the current studies we plot all results, including those for the solvent, versus $G\sqrt{\lambda}$. Surprisingly, the birefringence data for the solvent shows a reasonable correlation with this parameter even though there can only exist a (presumably) weak orientation of the solvent molecules.

4.3.1 The Solvent

In order to unambiguously interpret birefringence data for a polymer solution, it is necessary to independently measure the birefringence properties of the solvent. Thus as a preliminary to the main body of experiments, a set of results was

obtained for the solvent used in the preparation of M1. Figure 3 presents the optical properties of the solvent as a function of $G\sqrt{\lambda}$ for rollers F. It may seem surprising at first that the solvent shows a measurable and easily reproducible level of birefringence as a consequence of the flow in the two-roll mill. Rheological studies reported in these proceedings, using mechanical rheometers showed no measurable level of non-Newtonian behavior for the solvent at comparable values of the velocity gradient of the flow. The birefringence measurements show the existence of a flow-induced anisotropy in the solvent that is usually associated with non-Newtonian fluid properties. However, the birefringence is very weak (almost two orders of magnitude smaller than measured for a fresh sample of M1 solution at the same value of $G\sqrt{\lambda}$), and presumably represents too little conformational anisotropy to be reflected at measurable levels in macroscopic mechanical properties.

The initial values for the orientation angle, and the birefringence shown in Figure 3, reflect the presence of the residual stress birefringence of the glass windows of the flow device. Thus, the observed behavior (at low values of the velocity gradient eigenvalue) is the result of a weak anisotropy of the fluid that is comparable in magnitude to the anisotropy of the glass windows, but with the principal direction of the refractive index tensor for the glass (which may change on a daily basis) being quite different from that of the fluid. Not withstanding this complication, the solvent birefringence shows a linear increase with $G\sqrt{\lambda}$ for values beyond 5 $\sec^{-1}$. The glass birefringence is only significant at the lowest values of $G\sqrt{\lambda}$ and affects the measured values of Δn for the fluid in a way that changes the zero shear-rate intercept (no flow conditions) relative to the extrapolated solvent birefringence line.

Once the measured birefringence is dominated by the contributions of the solvent, it is seen that the measured orientation angle is relatively close to the principal axis of strain of the flow, which corresponds to an orientation of 45° with respect to the symmetry axis of the flow cell. This is the same orientation that has been observed for other fluids of small asymmetric molecules, and is equivalent to the expected initial orientation of a slightly deformable sphere (corresponding to a 45°

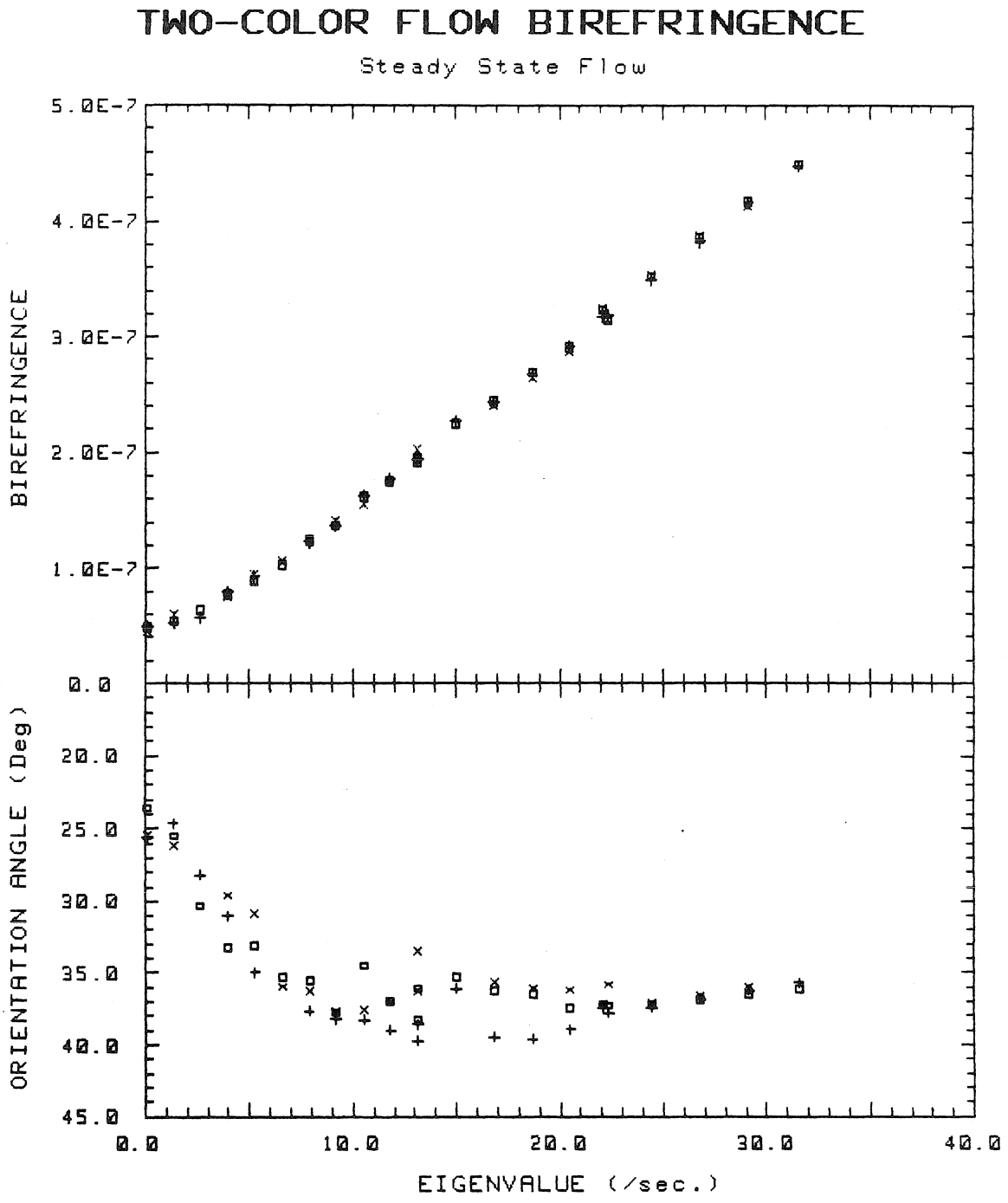

Figure 4.3: Birefringence and extinction angle for the solvent with rollers F ($\lambda = 0.1501$). The three markers represent three different experiments consecutively done.

orientation in these plots). For larger values $G\sqrt{\lambda}$, the orientation angle shown in Figure 3 appears to rotate slightly towards smaller values. This behavior was observed for all flow geometries and values of $G\sqrt{\lambda}$ accessible to this flow cell. There exist two possible reasons for the rotation of the measured orientation angle: (a) the "initial" orientation of the solvent molecules rotates slightly toward the outflow axis as the value of the velocity gradient increases, in a manner reminiscent of the behavior of a slightly more elongated deformable body (note that a sufficiently elongated body will align along the direction of the principal eigenvalue of the velocity gradient); or (b) there is a stress build-up on the glass windows due to the flow which does not contribute significantly to the total birefringence, but may induce a slight rotation of the measured orientation angle. There is no way at the present time to distinguish between these two possibilities. Figure 4 shows results obtained using two different flow geometries (that is, for different values of the flow parameter λ). The two sets of data show a good correlation when plotted against $G\sqrt{\lambda}$. Furthermore, they show an almost linear increase of the birefringence as a function of the eigenvalue of the velocity gradient up to the maximum values possible with this flow device. These facts indicate that any change in the relationship between the shear rate and the roller speed is negligible, *i.e.*, the solvent is responding as a Newtonian fluid for two different flow geometries (λ values of 0.04, and 0.15).

We also examined the abrupt start-up of steady motion of the solvent for two flow geometries: $\lambda = 0.15$ and 0.04 using a linear ramp-up of the cylinder rotation-rate from rest to the final steady value in a time interval less than 0.01 seconds. Relaxation experiments from steady flow to rest were also done. Two typical results for the solvent are shown in Figure 5 and Figure 6. In the first, we see results for start-up to, and cessation from, a steady flow at an eigenvalue of 24 sec^{-1} and $\lambda = 0.15$. The start-up of flow always follows a prescribed "rest-time." Changes in transient effects at the onset of flow, following different rest-times can often be used to probe for the presence of relaxation phenomena that may not be easily detectable in birefringence data after cessation of flow; see for example Liu *et al.*,

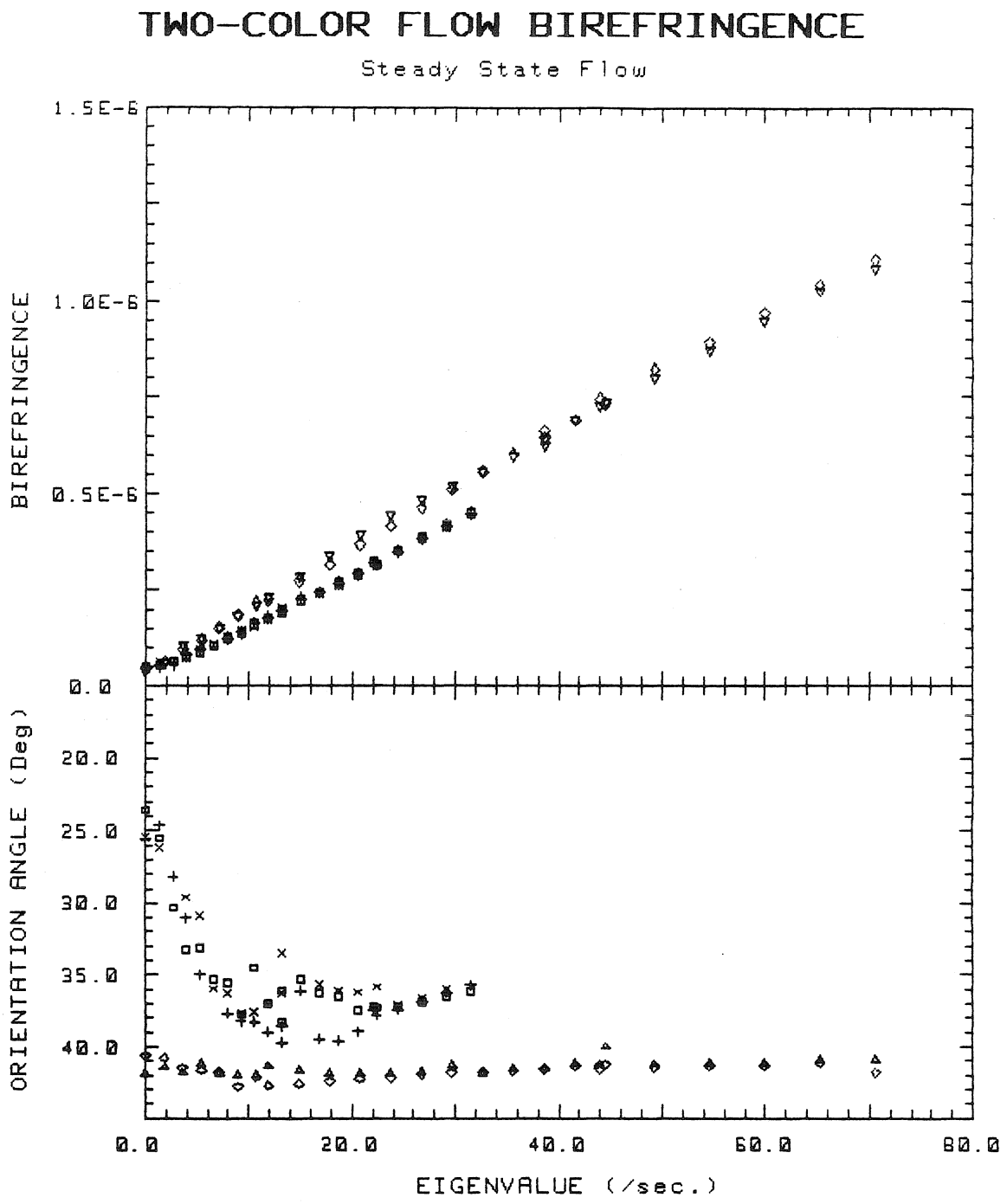

Figure 4.4: Solvent birefringence and extinction angle for two distinct pairs of rollers as a function of $G\sqrt{\lambda}$. The flow parameter are $\lambda = 0.0403$ ($\diamond$, $\triangle$) and 0.1501 ($\square$, $+$, $\times$).

[7, 8] and Dealy and Tsang [9, 10]. In Figure 5 there are four sets of traces of birefringence measurements which correspond to two different experiments for start-up and cessation. In both experiments the duration of the steady flow is 10 seconds, while the "rest-time" (after cessation of flow) is 5 seconds in one case and 20 seconds in the other. However, there is no evidence of any dependence of the start-up of flow on the duration of the rest-time for the solvent.

It may also be noted that the start-up of flow is quite fast as there is only a single reproducible data point at $\Delta t = 2 \times 10^{-2}$ sec. which is indicative of the transient behavior of the fluid during onset of the flow. However, the apparent time-scale for transition to steady state based on this data point (between 0.01 to 0.05 sec.) is of the same order as the expected start-up time scale for the flow based on diffusion of vorticity. Since the length scale for the roller gap is of the order of 0.5 cm for $\lambda = 0.15$, and the solvent viscosity is reported by other investigators in this symposium to be $\mathcal{O}(15$ poise), then the vorticity diffusion time scale is $\mathcal{O}(l^2/\nu) = \mathcal{O}(0.017)$ sec. Consequently, the single transient data point for onset of birefringence may be due to vorticity diffusion rather than any type of molecular re-orientation. The same characteristic behavior can be observed for the orientation angle.

For cessation of flow, there is a fast observable relaxation of the solvent birefringence that happens within the first data point (2×10^{-2} sec.). There is also a fast and small reorientation of the extinction angle. The slight upward drift observed in the orientation angle for large times ($t > 1$ sec.) is probably due to stress relaxation in the glass windows—produced by the previous shearing conditions of the flow field—that without changing significantly the total birefringence, rotates the principal axis of the refractive index tensor. This qualitative behavior, observed for start-up and cessation of steady flow, is generally present at all accessible roller speeds. However, it is interesting that the orientation angle provides a more sensitive probe of flow-induced conformation changes than the birefringence. For example, in Figure 6, we consider a case in which the flow-induced birefringence

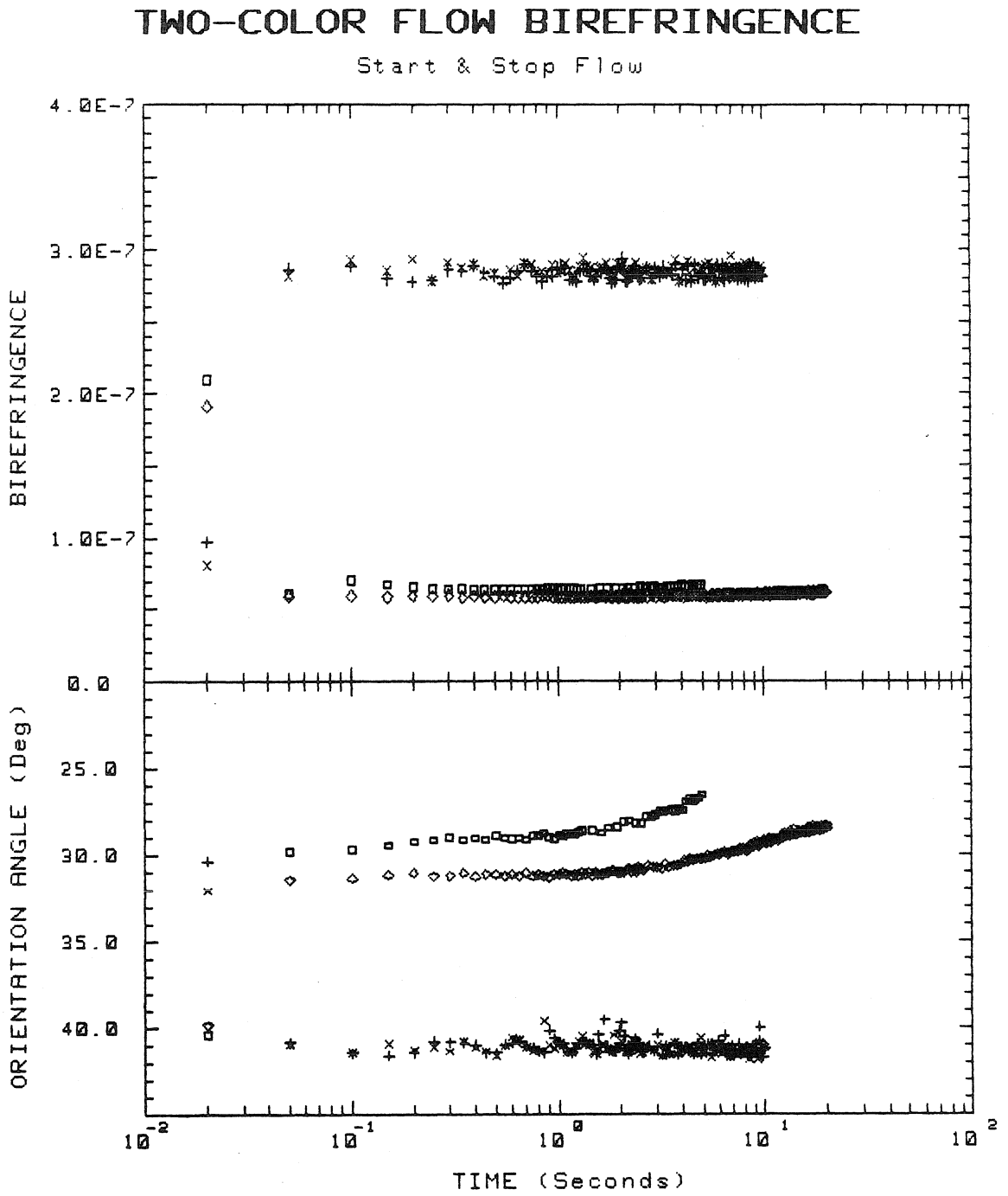

Figure 4.5: Solvent birefringence and extinction angle for inception and cessation of steady flow with $\lambda = 0.15$, and $G\sqrt{\lambda} = 23.7\ s^{-1}$. Inception of steady flow after 5 sec. "rest-time" (+), and cessation of flow after 10 sec. of flow (□). Inception of flow after 20 sec. "rest-time" (×), followed by cessation of flow (◇).

is only slightly higher than the lowest measured levels under no-flow conditions, but it is still possible to detect changes of the extinction angle within ±2 degrees. Double-step experiment (for $\lambda = 0.04$) were also performed for the solvent with results that are similar to the transient flows described above.

4.3.2 The Test-Fluid M1

Birefringence measurements do *not* directly yield the corresponding changes in bulk stress, except for simple and weak flows. Nevertheless, birefringence data for positive values of the flow parameter λ, can contribute to our understanding of the fluid behavior in extensional flows. Among the fluid properties that can be determined is the longest relaxation time for both near-equilibrium and non-equilibrium conditions. Birefringence is also sensitive enough to detect relative changes in the molecular weight distribution for a given sample, including changes in a very small percentage of the highest molecular weight portion of the distribution [23, 24].

The relaxation times for a polymer fluid can, in principle, be measured in several ways. The most straight-forward, with a transient birefringence device like the two-color system, is simply to examine the relaxation of birefringence from an initial steady value to an isotropic rest state when the flow is suddenly removed. Another approximate method that has been used by other investigators, based upon *steady state* flow data, is to estimate the characteristic time-scale from the critical effective strain-rate $G\sqrt{\lambda} = \gamma_{s,c}$ for onset of birefringence. This later method appears to work especially well for dilute solutions of (narrow MW distribution) polymers that are highly coiled in the rest state, and has even been applied with some success (though less justification) to semi-dilute solutions. Other measurements of relaxation times can be obtained from overshoot or relaxation data in double-step and/or start-up experiments [9, 10].

The results actually obtained here for M1 are somewhat less comprehensive than suggested by the above list of possible measurements. The main limitation for experimental studies of the test-fluid M1 is that it undergoes *irreversible*

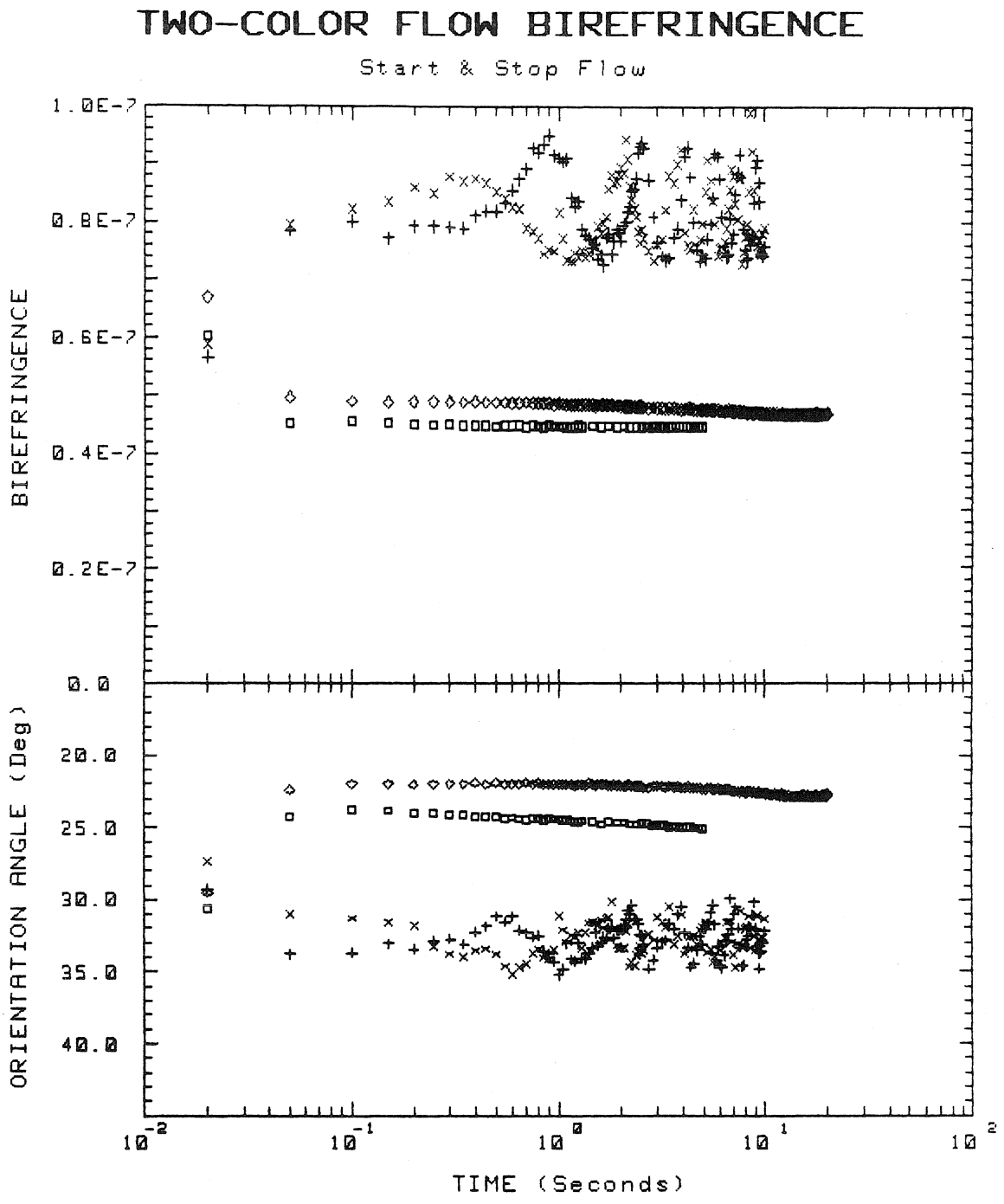

Figure 4.6: Solvent birefringence and extinction angle for inception and cessation of steady flow with $\lambda = 0.15$, and $G\sqrt{\lambda} = 4.0\ s^{-1}$. Inception of steady flow after 5 sec. "rest-time" (+), and cessation of flow after 10 sec. of flow (□). Inception of flow after 20 sec. "rest-time" (×), followed by cessation of flow (◇).

degradation at very low effective strain-rates, $G\sqrt{\lambda}$. Hence, many measurements that one would like to make, involving multiple steps or runs, are rendered more or less futile, and were not pursued. Consequently, in this section we concentrate on a series of experiments that were done to evaluate the effects of degradation. It is this data that we believe to be the most pertinent to the other investigations reported in this volume, because it suggests strongly that any flow which induces significant stretching of the polymer will tend to introduce degradation. However, we have carried out a number of measurements involving M1 that appear to be of general interest in the context of a fundamental understanding of the dynamics of polymeric liquids in time-dependent flows.

Flow Degradation of the Test-Fluid M1

The presence of flow-induced degradation of the polymer even at very low shear rates, is perhaps the most important result of our study, insofar as it relates to the other work reported in these proceedings on the M1 fluid. One clear example of degradation is shown in Figure 7, where we plot the birefringence and orientation angle for steady flow corresponding to $\lambda = 0.15$ and a *small* range of values of $G\sqrt{\lambda}$. Two distinct plots of birefringence are clearly evident. The upper set of birefringence data corresponds to a *fresh* sample of M1, while the lower data set was taken using the same solution after flowing at $G\sqrt{\lambda} \simeq 6.6$ sec^{-1} for a total period of 50 minutes. Although this is a long period of time, and corresponds to a large total strain of approximately 2×10^4 (as calculated for a fluid element that is at the stagnation point), the velocity gradient is very low, indeed, *substantially less* than values that we have previously studied with no sign of degradation for *narrow* MW distributions of polystyrene or polystyrene sulfonate of a comparable average molecular weight in a solvent of a similar viscosity! We conclude from this, that the M1 fluid must exhibit a *very* broad molecular weight distribution (MWD), because it can only be the very high MW portions of the MW distribution of the polymer, that are 'destroyed' at these very low values of $G\sqrt{\lambda}$. Also shown in Figure 7 is the

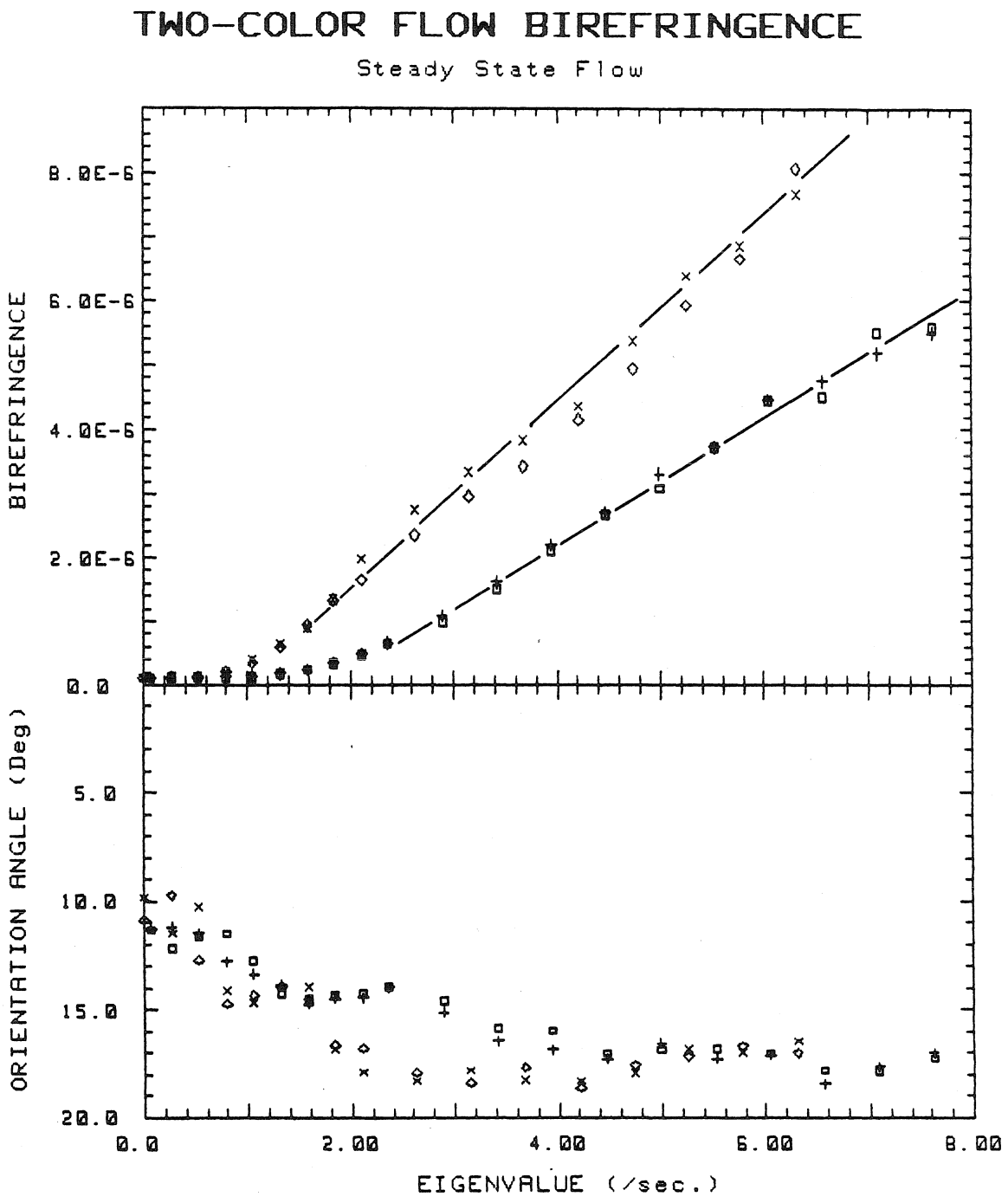

Figure 4.7: Flow induced birefringence of the test-fluid M1 as a function of $G\sqrt{\lambda}$ for rollers F ($\lambda = 0.1501$). Experiments 1 and 2 for a fresh solution ($\diamond$, $\times$), and experiments 3 and 4 for the same fluid sample after been sheared for approximately 50 minutes at $G\sqrt{\lambda} = 6.6\ s^{-1}$. ($\square$, $+$).

measured orientation angle for both the fresh and degraded fluid M1. However in both cases, the orientation angle simply undergoes a transition from the residual initial value of about 10° to a final orientation of 17° which is 4° under the expected orientation for alignment along the principal axis of $\nabla\mathbf{U}$ for $\lambda = 0.15$.

We have noted above that the onset velocity gradient for significant birefringence has often been used to estimate the relaxation time for the polymer in an equilibrium (or near equilibrium) configuration [12, 24]. This process is based upon the theoretical prediction from *linear* (bead-spring) models for dilute solutions that polymer stretching commences when $|\nabla\mathbf{U}|\,\tau_R = \mathcal{O}(1)$, ($\tau_R$ being the characteristic relaxation time) and requires extrapolation of the birefringence data back toward the horizontal axis in order to minimize the effects of the residual glass birefringence. This extrapolation is obviously subject to significant arbitrariness, especially if the polymer has a broad MW distribution that will tend to smooth out the onset of birefringence over a wide range of values of $G\sqrt{\lambda}$, or if the data is noisy as for the "fresh" solution in Figure 7.[6] In any case, it is clear from Figure 7 that there is a substantial ($\sim 2\times$) decrease in the relaxation time when the solution is degraded. Indeed, based upon the straight-line extrapolations shown in Figure 7, we estimate the polymer relaxation times in terms of the apparent critical value of $G\sqrt{\lambda}$ as approximately 1 sec. for the fresh solution and 0.6 sec. for the degraded fluid. We shall shortly show how this compares with the relaxation time obtained in a direct relaxation experiment, but we may note that the quantitative values obtained in this way, depend significantly on the somewhat arbitrary choice of the extrapolated line. For example, in Figure 8 we show a second pair of lines based on the same data set but within a more limited range of values for the velocity gradient. Although it

[6]The rather noisy data set for the fresh solution in Figure 7 is a consequence of (a) tiny bubbles generated while loading our flow device; and (b) a seemingly poor initial mixing of the polymer in the solvent. Normally these conditions would be removed by running the two-roll mill for a period of time before taking any data. However, for experiments designed to characterize the degradation of the fluid this is no longer an acceptable procedure, and one is forced to accept more noise than usual in this data set for the fresh M1. The noise level for the data set of the degraded fluid taken after 50 minutes of elapsed run-time is more nearly typical of the expected results for our apparatus.

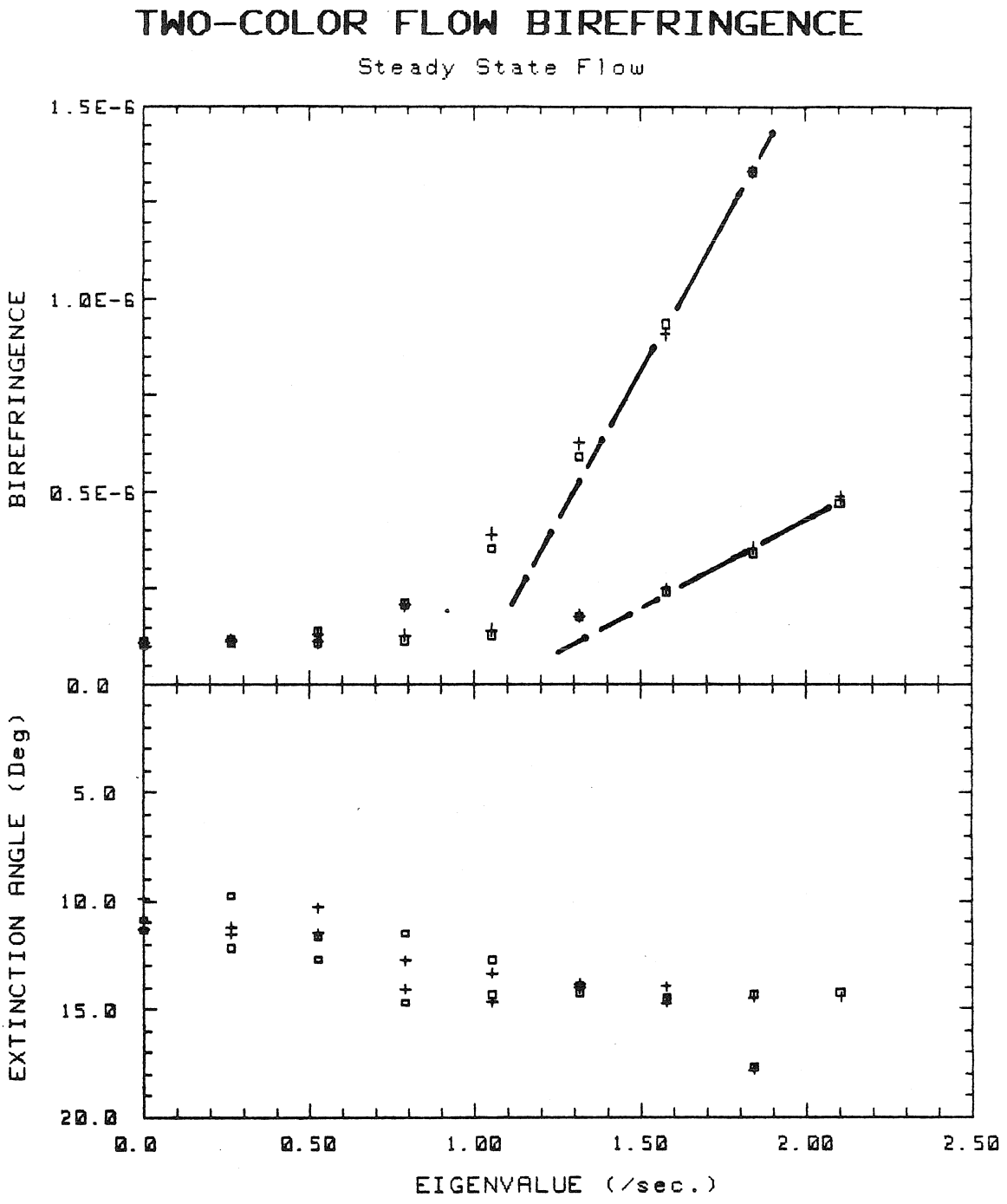

Figure 4.8: Flow induced birefringence of the test-fluid M1 as a function of $G\sqrt{\lambda}$ for rollers F ($\lambda = 0.1501$). The fresh solution ($\diamond$, $\times$), and the degraded sample after been sheared for approximately 50 minutes at $G\sqrt{\lambda} = 6.6\ s^{-1}$. ($\square$, $+$).

is still clear that the relaxation time for the degraded solution is much shorter that that of the fresh fluid, the numerical values are significantly modified.

A much more accurate and reliable estimate for the characteristic relaxation time of the polymer is obtained by a *direct* study of birefringence relaxation from steady-flow to a state of rest, though this would generally depend on the initial polymer conformation. At the same time, a more detailed view of the *rate* of polymer degradation can be obtained by combining such relaxation studies with a succession of steady flow periods of known length. Some selected results for this type of experiment are shown in Figure 9, and a complete set of relaxation times obtained from Figure 9, and a series of related studies is presented in Figure 11, which will be discussed shortly.

As indicated above, the data in Figure 9 was obtained by performing a series of relaxation experiments each separated by a period of continuous flow (when the most significant flow degradation of the fluid occurs). The relaxation data shown in Figure 9 represents an average over five repetitions of a "characterization" sequence, in which a steady flow was maintained for 30 seconds at $G\sqrt{\lambda} = 1.18$ sec^{-1} followed by a 40 seconds relaxation period with the rollers completely stationary. Furthermore, for each such relaxation sequence, each "instantaneous" data point represents an average of ten data readings taken over a sampling period 2 msec. Thus, each data point in Figure 9 corresponds to an average of 50 independent readings. It is important to emphasize that the velocity gradient during this characterization portion of the experiment was very low, $G\sqrt{\lambda} = 1.18$ sec^{-1}, and the total strain corresponding to the complete start-up cessation sequence, *i.e.*, $G\sqrt{\lambda}\, T_f$ with T_f being the total flow time for the sequence, was only 213. In contrast, the period of continuous steady flow *between* each set of relaxation experiments was $T_s = 300$ seconds, corresponding to a total applied strain equal to $G\sqrt{\lambda}\, T_s = 2664$. Two additional details of these relaxation time-scale experiments may by worth mentioning. One is that a significant period, with the system completely at rest, separated each steady flow and relaxation "characterization" sequence; one minute

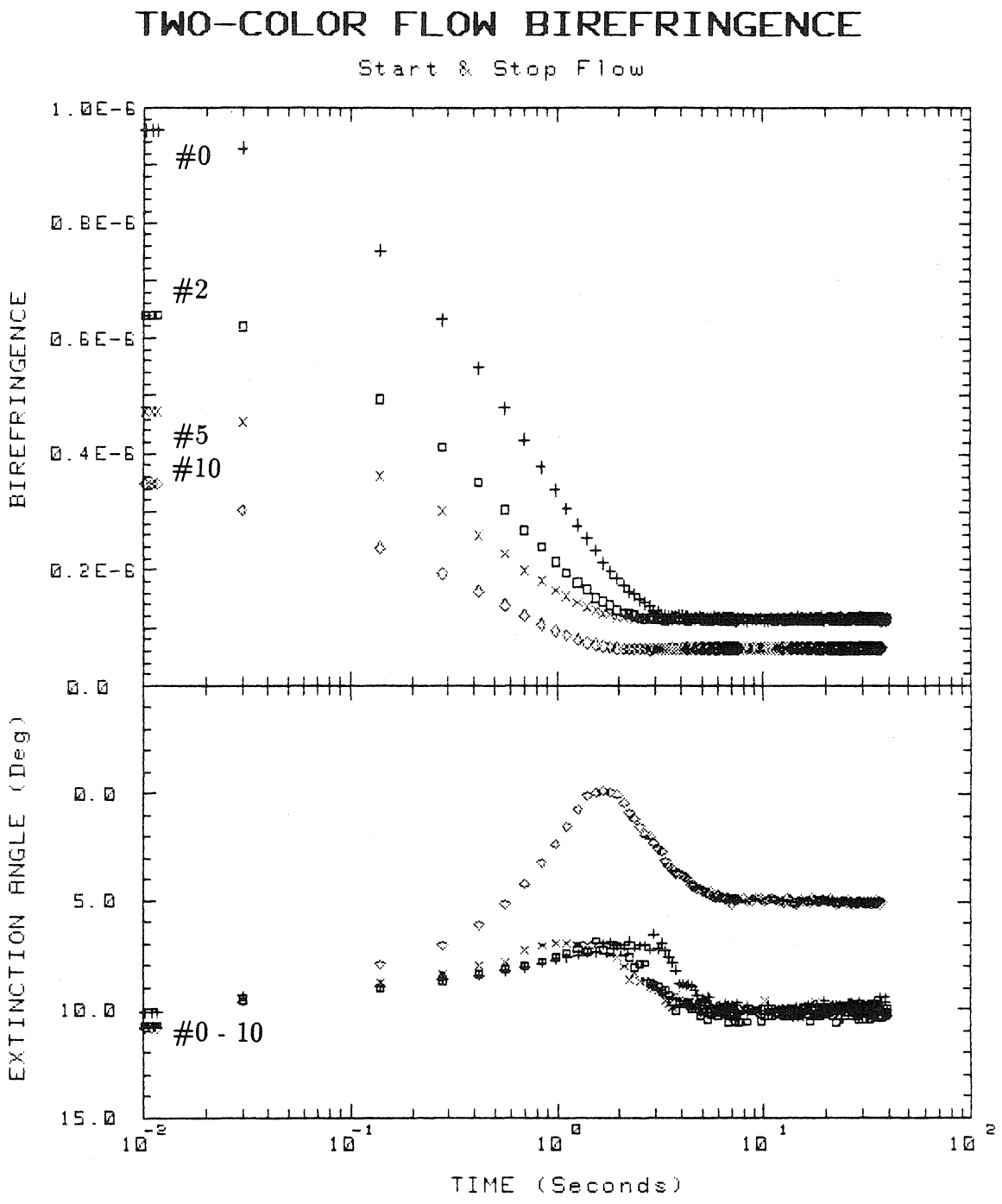

Figure 4.9: Relaxation of birefringence and orientation angle vs. time for the test-fluid M1 for cessation of steady flow (with a λ value of 0.0403 , that corresponds to rollers C.) Different traces corresponds to the fresh solution (#0, +), and different time periods after been sheared at $G\sqrt{\lambda} = 8.9\ s^{-1}$ for 600 (#2, $\Box$), 1500 (#5, $\times$), and 3000 (#10, $\diamond$) seconds.

after each steady flow and three minutes after each relaxation time-scale sequence. Second, one start-up/cessation segment was run prior to any data being taken in each relaxation time-scale sequence in order to 'erase' the previous history of the fluid (*i.e.*, each sequence actually consisted of six inception-cessation segments with data collected during the last five).

Returning to Figure 9, the numbers corresponding to each set of data indicate the sequence number, where #0 is the fresh solution, #1 is the relaxation data taken after one $T_s = 300$ sec. flow period, #2 follows the second period of steady flow and so on. The markers (+, $\Box$, $\times$, $\diamond$) on the left hand side, next to the ordinate, correspond to measured levels of the birefringence and orientation angle for experiments #0, 2, 5, and 10, just prior to the abrupt cessation of flow at $t = 0$. Clearly, as the polymer is sheared for an increasing period, the steady birefringence level at $G\sqrt{\lambda} = 1.18$ sec^{-1} (the value used for the relaxation experiments) decreases due to degradation. It may be noted that the final apparent value for experiment #10 is lower than the other cases because a higher gain was used for the light detectors and the minimum detectable levels thus improved; the final orientation angle is also different for the same reason. To a first level of approximation, the relaxation data in Figure 9 decays as a single exponential. Thus, an estimate of the relaxation time for this process can be obtained from the value of t where the magnitude of birefringence is $1/e$ times the initial value. The values obtained in this way, from the experiments in Figure 9, as well as additional cases carried out at different values of G for the same $\lambda = 0.0403$ are plotted in Figure 11 and will be discussed shortly. Clearly, it it evident that there is a *decrease* in the relaxation time due to degradation as the total elapsed flow time is increased.

Also shown in the lower part of Figure 9 is the corresponding behavior of the orientation angle as the polymer sample is subjected to the degradation process. The "initial" orientations—reached just before the abrupt termination of the steady flow—are also plotted along the left side ordinate. The traces for the birefringence and orientation angle show a quite different time evolution, with the apparent

characteristic time-scale for the evolution of the orientation angle being significantly longer than that observed for birefringence. That is, a characteristic time scale for relaxation based upon a complete return of the polymer fluid to an isotropic state (*i.e.*, no preferential orientation other than that of the glass) is significantly longer than the time-scale observed for the relaxation of birefringence alone. In a macroscopic sense, it appears that the final state of equilibrium is achieved via two distinct relaxation mechanisms; a fast contraction and second, a later rotation towards the "final" orientation angle along the roller gap (at 0 degrees).[7]

The difference in the behavior of the birefringence and orientation angle though perhaps initially surprising, does appear to be consistent with prior rheological measurements of stress components in simple shear flow. To see that this is true, we rely on the so-called stress-optical law which relates birefringence and stress. Even though the stress-optical law is *not* an acceptable methodology for a *quantitative* evaluation of the shear stress and/or the first normal stress difference from birefringence data except for weak and slow flows (*cf.* Janeschitz-Kriegl [1]), it is likely that it can be used for low values of $G\sqrt{\lambda}$ [8]. Certainly, it can be used to provide a *qualitative* comparison between the birefringence measurements described in the previous paragraph, and earlier *rheological* measurements for semi-concentrated polymer solutions in relaxation from simple shear flow. The proposed relationships

[7]For times longer than those past the minima in the orientation trace, the sensitivity of the light detectors and glass birefringence always determine the experimentally measured asymptotic values of the extinction angle.

[8]The stress optical law is widely used to determine the components of the stress tensor for simple shear flows when birefringence data is available, even for transient flows. One should expect this relationship to be an approximation valid only under the following assumptions: (a) the total strain for the molecule must be small; and (b) the molecule must be slightly birefringent. If the stress is a non-linear function of the polymer conformation then for large strains the stress-optical law will not be valid because the birefringence only varies linearly with the polymer deformation. If the polymeric fluid has a strong optical anisotropy, then, again the "law" fails mainly because birefringence only corresponds to the real part of the refractive index tensor, while the imaginary part (that is, dichroism) must also enter into the relationship with the stress tensor. Whenever large retardances are involved, the macroscopic birefringence is a multivalued function of the measured light intensities and a unique determination of the birefringence—as well as the extinction angle—at higher orders can be quite difficult, even when only small amounts of dichroism are detected.

between the shear and first normal components of the stress tensor and the optical anisotropy, based on the orientation of the optical axis and the flow field shown in Figure 2, are

$$\sigma_{xy} = \left(\frac{\Delta n}{2C}\right) \sin(2\chi)$$

and

$$\sigma_{xx} - \sigma_{yy} = \left(\frac{\Delta n}{2C}\right) \cos(2\chi) \ ,$$

where C is known as the stress-optical coefficient of the material, and σ_{ij} are the components of the stress tensor. Given the fact that the relaxation time scale based on birefringence is much faster than the relaxation time for the orientation angle χ, then, we infer from these stress-optical relationships that the shear stress should decay faster than the first normal stress difference. This type of behavior is characteristically observed in semi-concentrated polymeric solutions when subjected to simple shear flow [15].

It is tempting to try to extract a *rate* of degradation from the data we have collected, and determine the dependence of this rate on the flow parameters G and λ. For this purpose we can plot the measured relaxation times, or the steady-state birefringence values as a function of time for various constant values of G and λ. These results are shown in Figures 10 and 11, respectively, with time non-dimensionalized using the eigenvalue of the velocity gradient tensor: $G\sqrt{\lambda}$. Evidently, the continuous decrease in both the steady-state birefringence and the relaxation time reflect a continuous degradation with time of the polymer in the birefringent region of the flow. It is noteworthy and especially obvious in Figure 10, that the most rapid degradation occurs at early times.

The two somewhat surprising features of the data shown in Figures 10 and 11 are: first, that the apparent degradation continues for such a long period, and second, that the data does not correlate with $G\sqrt{\lambda}$. The idea that the latter might be expected is suggested by the fact that a large number of previous measurements have shown that the *birefringence* level correlate to a single curve for each fluid

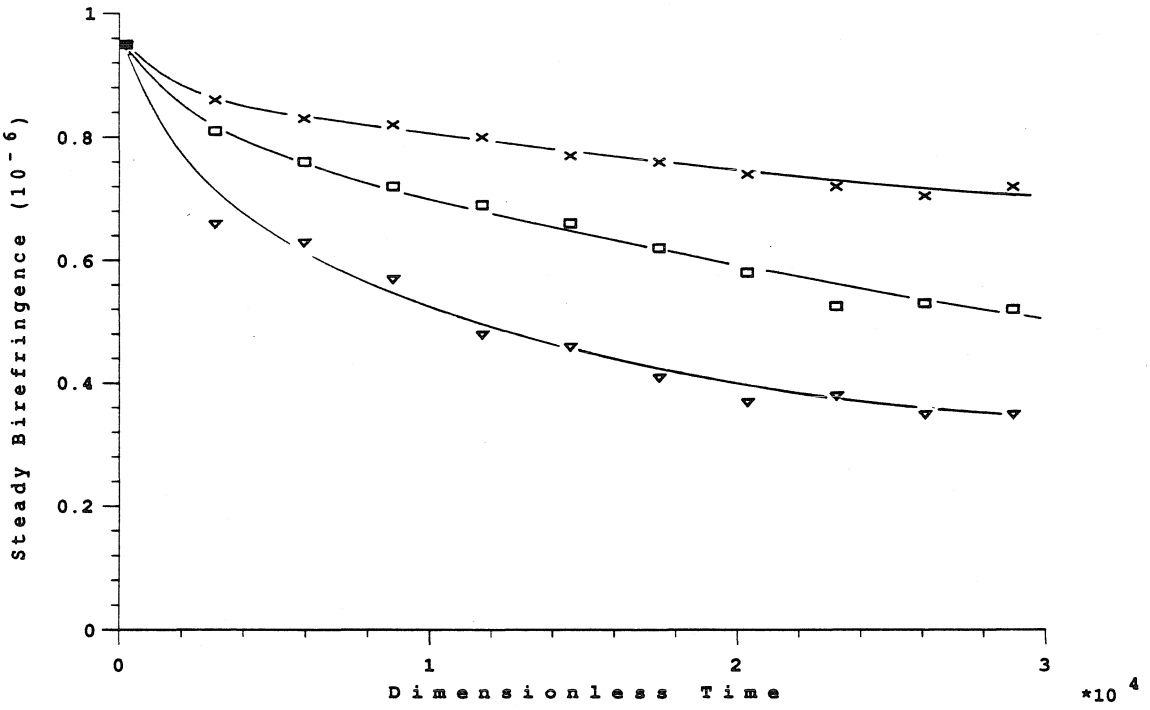

Figure 4.10: Steady state birefringence after inception of flow, as a function of degradation (time non-dimensionalized by $G\sqrt{\lambda}$). Data was taken for rollers C, $\lambda = 0.0403$. $G\sqrt{\lambda}$ are $4.44s^{-1}$ ($\times$), $6.66\ s^{-1}$ ($\square$), and $8.88\ s^{-1}$ ($\diamond$).

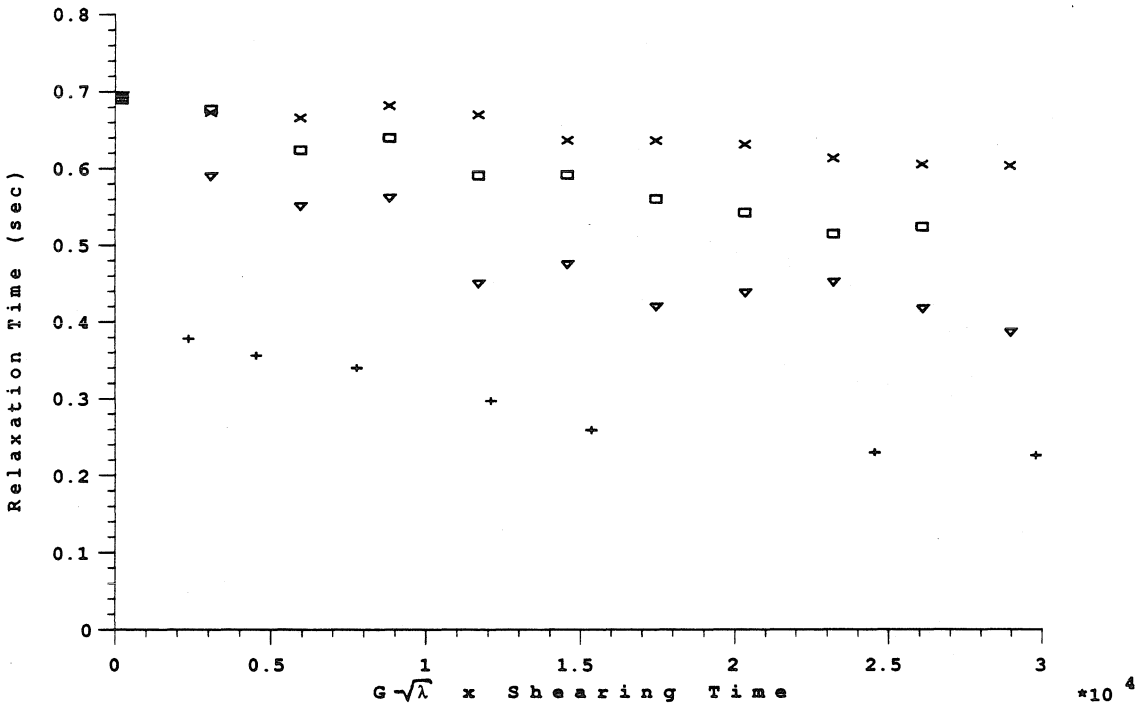

Figure 4.11: Characteristic time-scales of the test-fluid M1 as a function of time (non-dimensionalized by $G\sqrt{\lambda}$). $\lambda = 0.0403$ and $G\sqrt{\lambda} = 4.44\ s^{-1}$ ($\times$), $6.66\ s^{-1}$ ($\square$), and $8.88\ s^{-1}$ ($\triangledown$); and for $\lambda = 0.1501$ with a shear rate of $G\sqrt{\lambda} = 6.57\ s^{-1}$ ($+$).

when plotted versus $G\sqrt{\lambda}$ [9] (see for example references [7, 16, 17] dilute solutions and [8] for a concentrated polymeric fluid). Since birefringence is a measure of polymer deformation, and degradation is thought to arise from deformation, it seems reasonable to expect that *degradation* should also correlate with $G\sqrt{\lambda}$. As already noted, however, the data in Figures 10 and 11 does not correlate in this manner.

In our view, there are two essential reasons why the degradation data do not correlate in the "expected" manner. The first is that existing models of degradation phenomena suggest that to achieve a significant degree of deformation it is necessary not only to stretch the polymer, but to subject the stretched polymer to strain-rates that exceed the critical strain value for stretching by some amount that depends on molecular weight. Thus, though the degree of polymer extension does correlate with $G\sqrt{\lambda}$, there is no reason to think that degradation rates will also correlate for a sample that has a very broad molecular weight distribution.

The second reason for lack of correlation with $G\sqrt{\lambda}$ is, quite simply, that the two-roll mill, operated in the manner described above, does not provide a *direct* measure of degradation for a fixed sample of polymer. Thus, even if the polymer were completely monodisperse, the suggested correlation would probably not occur. Ideally, to establish an unambiguous degradation rate, one would like to subject a fixed body of the polymeric liquid to a constant rate-of-strain for a known period of time. However, the two-roll mill does not work in this idealized manner. The "strong flow" region, with approximately uniform strain rates, is only a local part of the flow, and fluid elements are convected continuously through this region. Consequently, there exists a distribution of residence times (or total strain per pass) that depends strongly on proximity of the particular streamline to the stagnation point of the flow. Thus, any measurement of birefringence or relaxation time in the vicinity of the stagnation point as a function of time can only represent an *averaged*

[9] This correlation also exists for M1 when birefringence data is graphed versus $G\sqrt{\lambda}$, and *fresh* samples of the fluid M1 are used.

degree of degradation for a continuously changing polymer sample that has actually experienced wide range of accumulated times in the strong flow part of the fluid domain.

The net conclusion from the preceding discussion is that it is extremely difficult with the two-roll mill to establish a credible measure of degradation *rates*, at least as understood by the kinetics of the rate-theory of unimolecular decomposition [14]. In fact, the long time inherent in Figures 10 and 11 may be primarily a reflection of time-scales for "averaging," rather than time-scales inherent to the actual degradation process.

Earlier studies of degradation by Odell and Keller [23, 24] for dilute solutions in similar flows were generally focused on much higher strain-rates and narrow molecular weight distribution polymer samples. Although the G values in the present experiments are order of magnitude smaller than the critical values reported by Odell and Keller [23, 24], the solvent viscosity of approximately 15 poise in the present work is much larger, and thus $|G\sqrt{\lambda}\ \nu|$ is within the same range of values here as in the earlier experiments. In view of the broad molecular weight tail, it is therefore not surprising that there is significant degradation apparent in our results even at very low values of $G\sqrt{\lambda}$.

Other Measurements of Characteristic Time-Scales for the Test-Fluid M1

Thus far, the determination of a relaxation time-scale has only involved the decay of birefringence after an abrupt termination of steady flow, and/or the onset point for birefringence in a steady flow. In this section, we briefly consider the response of M1 to other transient flow histories. Our objective is to simply highlight some qualitatively interesting dynamical effects. Figures 12, 13, and 14 present a series of start-up and cessation of flow experiments for different values of $G\sqrt{\lambda}$ but with the same basic pattern of "flow history" in all cases. This basic flow pattern consists of a 30 seconds in steady flow following a "step start-up," followed by a 40 seconds

"rest-time" and so on. The data shown corresponds to a complete cycle for the inception and cessation of steady flow, but for convenience, the traces for both inception and cessation are plotted on a logarithmic scale beginning at $t = 0$

It is clear for all the values of $G\sqrt{\lambda}$ shown in Figures 12-14, that *inception* of flow produces well defined *overshoots* which could, in principle, be used as another basis to evaluate a characteristic dynamic time-scale for the polymer. However, the particular data set shown in these figures, was obtained using a single sample of the test-fluid M1, and thus includes an unknown, though presumably small degree of degradation. For this reason, we focus on qualitative features of the results that do not appear to depend strongly on the degradation of the sample, but are still extremely interesting for the new insight that they provide on the dynamics of this particular fluid at a fundamental macromolecular level.

It is evident, upon examining Figures 12-14 that level of complexity of the start-up flow is much higher,—for both the time evolution of the birefringence and the orientation angle— than what is seen for the abrupt termination of flow. For the three experiments in Figure 12 the values of $G\sqrt{\lambda}$ are 1.18, 1.48 and 1.78 $\sec^{-1}$. Even at these extremely low values of the principal eigenvalue of the velocity gradient the birefringence shows a well-defined overshoot, thus providing evidence of *large* changes of the polymer conformation and consequently of the likely presence non-linear viscoelastic effects (*cf.* Ferry [19]). These overshoots appear earlier in time as $G\sqrt{\lambda}$ increases, in agreement with previously reported data in the literature for simple shear flows and many other polymeric systems. The maximum for these overshoots appears only after the total strain is larger than 7, where the total strain is defined by the product of $G\sqrt{\lambda} \times \tau_p$ and τ_p is the time for the birefringence maximum in the overshoot. These strains are of the same order of magnitude as values already reported in the literature (see for example some recent results by Pearson *et al.* [20] for a narrow MW distribution of polyisoprene using a Couette device). However, in the present context, they are surprising and thus quite important. One might have suspected that the steady-state birefringence levels at these

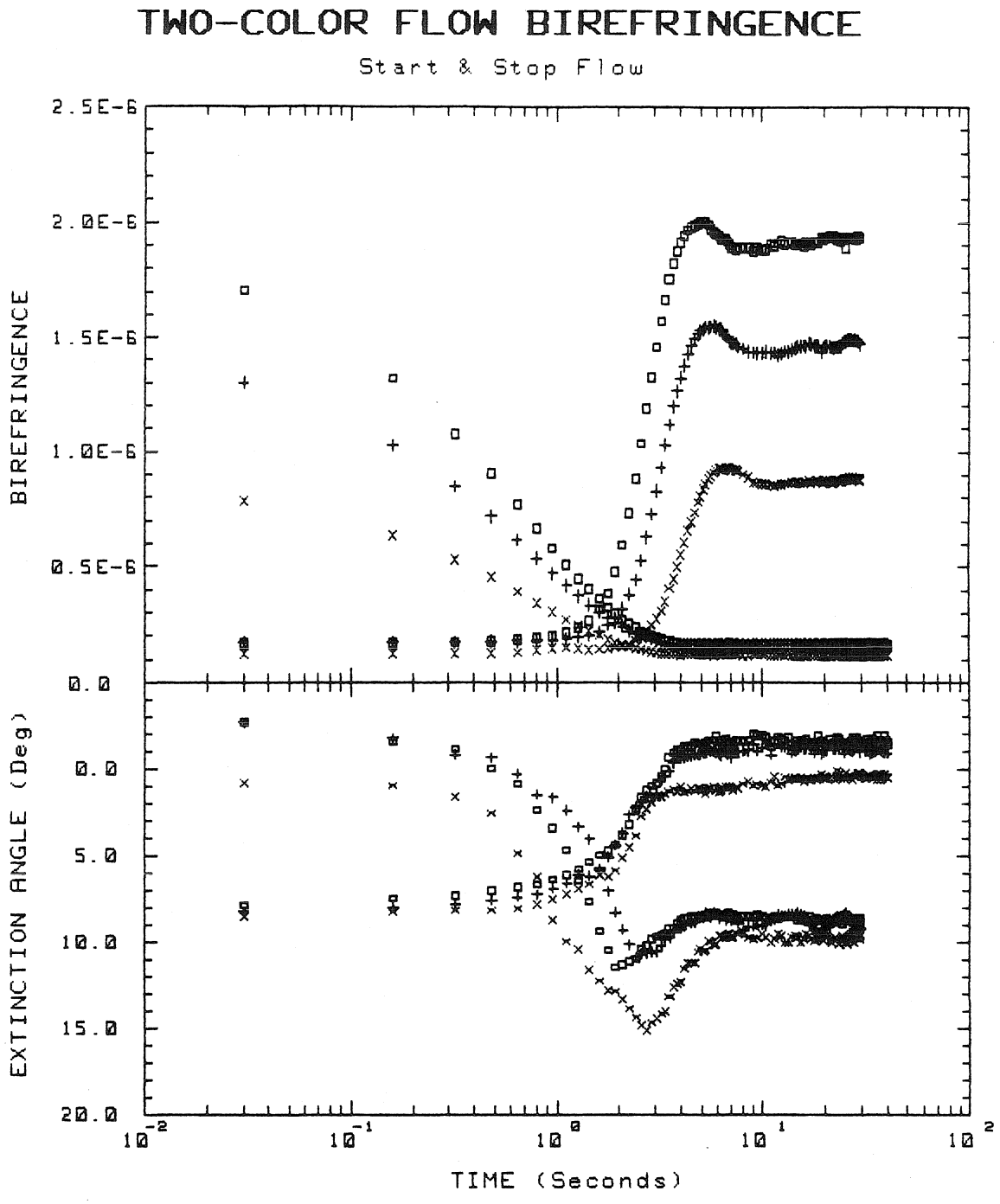

Figure 4.12: Inception and cessation of flow birefringence for the test-fluid M1 and rollers C. $G\sqrt{\lambda} = 1.18$ sec^{-1} ($\times$), 1.48 sec^{-1} ($+$), 1.78 sec^{-1} ($\square$).

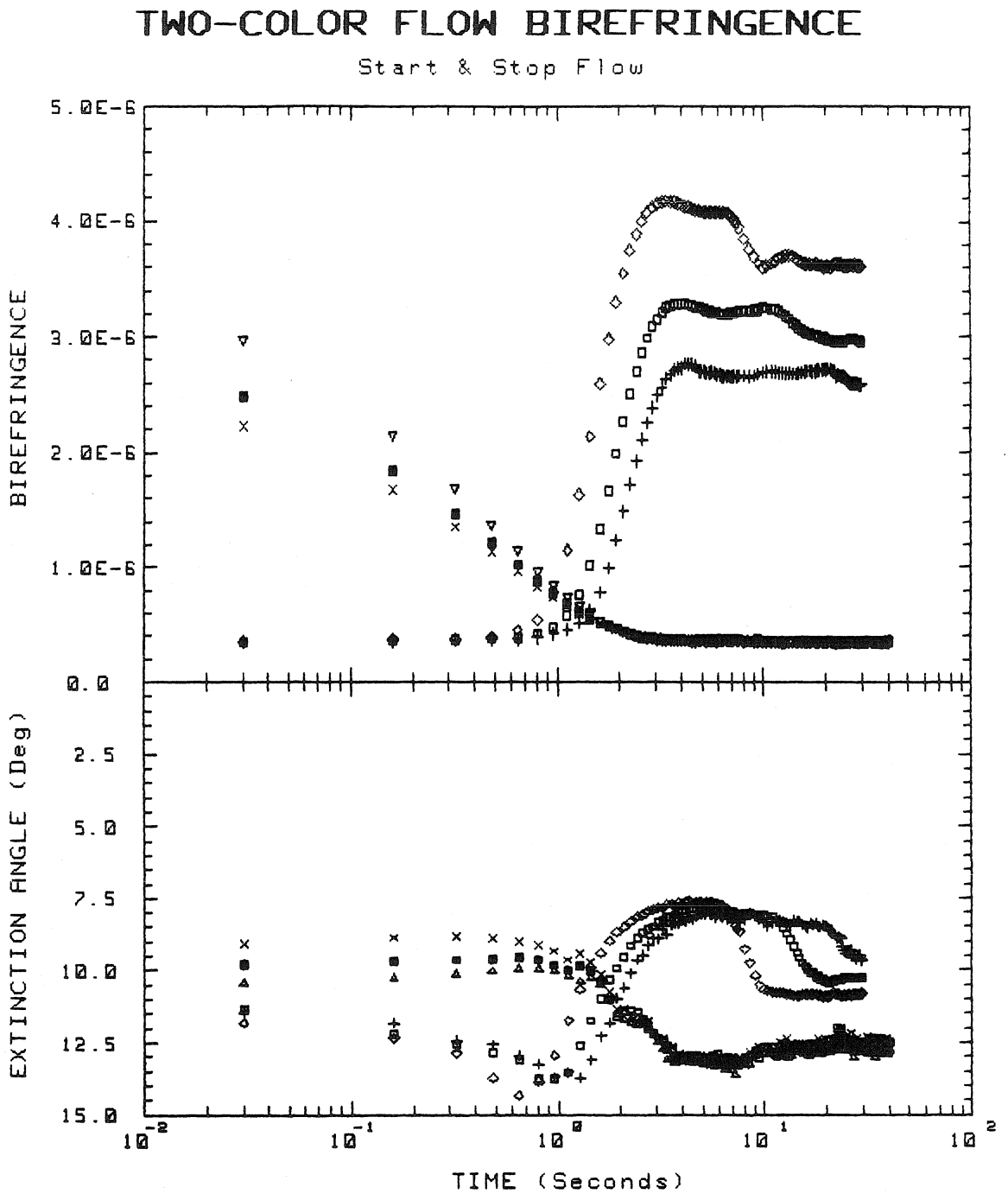

Figure 4.13: Inception and cessation of flow birefringence for the test-fluid M1 and rollers C. Inception to: $G\sqrt{\lambda} = 2.08$ sec^{-1} (+), 2.52 sec^{-1} (□), 2.97 sec^{-1} (◇). Cessation from: $G\sqrt{\lambda} = 2.08$ sec^{-1} (×), 2.52 sec^{-1} (□), 2.97 sec^{-1} (▽).

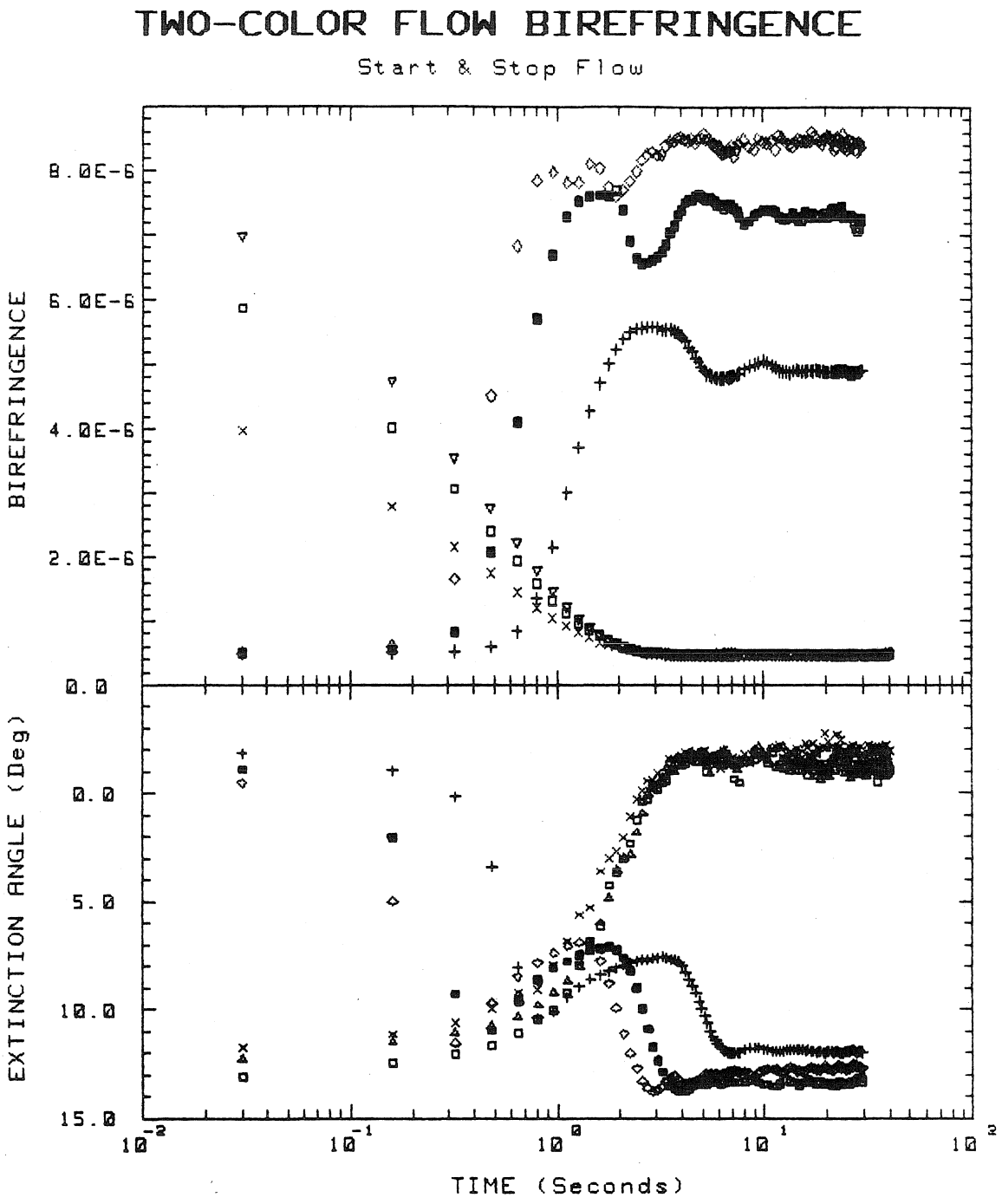

Figure 4.14: Inception and cessation of flow birefringence for the test-fluid M1 and rollers C. Inception to: $G\sqrt{\lambda} = 3.71$ sec^{-1} (+), 5.93 sec^{-1} (□), 7.42 sec^{-1} (◇). Cessation from: $G\sqrt{\lambda} = 3.71$ sec^{-1} (×), 5.93 sec^{-1} (□), 7.42 sec^{-1} (▽).

very low velocity gradients, in an extension dominated flow, would be due primarily to a very small fraction of the highest MW polymer being highly extended, with the rest of the polymer, more or less, in and equilibrium state. Certainly, dilute solution models would support this point of view because they suggest that a polymer molecule remains near equilibrium until a critical strain-rate is reached (that depends strongly in MW), after which they achieve nearly full extension. However, the data in Figure 12 is *not* compatible with this picture. The steady birefringence is reached at such a relatively short time (*i.e.*, small total strain from $t = 0$) that only very modest extension is possible.

Although the data in Figure 12 seems quite straightforward, and consistent with previous studies in shear flow, a complete understanding of the mechanisms involved in the generation of overshoots may be quite difficult, as seen by a comparison of the data sets in Figures 12 and 13. It appears from Figure 12 that whenever $G\sqrt{\lambda} < 1.8$ sec^{-1} a steady birefringence value is reached after only about 8 seconds of shearing. On the other hand, it can be seen from Figure 13 that the situation becomes more complicated as $G\sqrt{\lambda}$ is increased. In particular, for $G\sqrt{\lambda} > 2$ sec^{-1}, the birefringence undergoes a *second* step down to a "final" steady birefringence, but this final level is not reached for approximately 20 seconds. It appears that this second step becomes the dominant "mechanism" for overshoot at the higher values of $G\sqrt{\lambda}$, in the sense that the initial peak is gradually suppressed. We are not aware of previous experimental evidence for this type of complicated multi-time-scale structure in overshoot data. Although we believe that it may be a consequence of the broad distribution of molecular weights, as well as the semi-dilute character of the M1 sample, it is difficult to be more definitive in the absence of the same type of data for a *narrow* molecular weight distribution version of the M1 fluid. We are currently attempting to obtain such a fluid for further investigation.

For all cases, the orientation angle for the start-up of flow shows a very complex and well defined "signature"—that is completely reproducible even when the birefringence is very weak—which is very different from the signatures previously

reported in the literature for start-up of simple shear flow. It is also important to notice that there exists a strong correlation in time between the significant changes that occur in the birefringence and in the orientation angle. In every case the orientation angle begins at the residual value for the glass windows, and oscillates through one very sharp maximum appearing when the total strain $G\sqrt{\lambda}\ t \sim 3.5$, and which corresponds to the onset of birefringence and is present for all values of $G\sqrt{\lambda}$. For longer times, and at low shear rates (shown in Figure 12), the steady value for the orientation angle is reached by a monotonic decrease to a smaller angle. If $G\sqrt{\lambda} \geq 2.08\ \text{sec}^{-1}$, (as shown in Figures 13 and 14) then, the orientation angle goes through a distinct minimum, which corresponds to the time interval of the birefringence overshoot. Subsequently, the orientation angle reaches a second maximum corresponding to a small overshoot before settling quite close to the expected asymptotic orientation for the particular flow.[10] The orientation response beyond the first maximum, is clearly due to the polymer.

The small *overshoots* observed just before the steady orientation value, (whenever $G\sqrt{\lambda} \geq 3.7\ \text{sec}^{-1}$) are reminiscent of the behavior of a quite viscous drop which is also found to overshoot to an orientation that is nearer to the principal *strain* axis before settling on the final asymptotic orientation along the principal axes of the velocity gradient tensor. The significant broad *undershoot* that is observed for $G\sqrt{\lambda} \geq 2.08\ \text{sec}^{-1}$, corresponds to the time period when the birefringence is increasing at the fastest rate and/or is actually above the steady asymptotic value due to the overshoot. That is, the observed decrease of the orientation angle reflects an average among the fully stretched high MW molecules that are well aligned with the out-flow axis, and the lower MW fraction that is in the process of being stretched and appears to have initial orientations close to the symmetry plane at 0°. Of course, an initial alignment near 0° does not correspond to expectations for a deformable sphere which is usually aligned initially along the principal strain axis,

[10]The theoretically calculated angle for the principal axis of $\nabla\mathbf{U}$ for a Newtonian fluid is 11.6° when the λ value is 0.0403 .

but is more reminiscent of a slightly non-spherical rigid spheroid. As the imposed strain becomes larger and the chains are significantly stretched, the orientation angle rotates towards the outflow axis. The rotation, as a function of time, of a measured extinction angle that represents an average over a broad MW distribution has also been observed by Zebrowski and Fuller [21] on the relaxation after cessation of simple shear flow The regions prior to $t \sim 1$ sec^{-1} although having well defined time-histories are not currently understood by the authors, and may only represent the effects of residual glass birefringence.

For even higher shear rates ($G\sqrt{\lambda} > 6$ sec^{-1}) shown in Figure 14, the relative size of the birefringence *overshoot* (normalized by the steady birefringence level) begins to decrease, although there is still significant oscillation around the mean. The obvious question is whether the apparent saturation of the optical anisotropy is an artifact of the experimental conditions or truly represents a decrease in the magnitude of the overshoot due to saturation of the degree of stretching. Unfortunately it is not possible to resolve this question due to degradation, dust particles in solution, and the possible presence of flow-induced dichroism for the test fluid M1. Since the birefringence levels reach values where the retardance is close to $\pi/2$, it is necessary to evaluate the possible contributions of dichroism of the sample, for a very small level of dichroism may cause large variations of the retardance for only minute decrements of the measured light intensities (thus leading to significant uncertainty in the measured Δn). In spite of the difficulties evaluating the magnitude of birefringence, however, the calculated values for the orientation angle show a "signature" for the trace that is almost identical to those observed for lower shear rates, leading us to believe that the birefringence and orientation angle in Figure 14 do represent the correct transient behavior. On the other hand, saturation of the optical anisotropy in steady flow was *not* observed for the test-fluid M1 even for the highest shear rates used for these experiments, and by then a significant rate of degradation was already present. Indeed, in steady state flow experiments we were able to reach levels of Δn of 1.4×10^{-5}, that are approximately 50% larger than the

level where the overshoot in the birefringence disappears, with no clear indication that a saturation level is in sight. The fact is that M1 does not appear to overshoot beyond a shear rate of $G\sqrt{\lambda} = 6.0$ sec^{-1}, even though there is no saturation of the optical anisotropy of the sample. Consequently, any overshoot of the stress under these transient flows will most likely be the result of polymer reorientation rather than changes associated with the end-to-end distance of the molecules.

Figure 15 presents a second type of transient experiment, the so-called double-step consisting of step changes from a steady flow at low $G\sqrt{\lambda}$ to a higher steady value, followed—after a prescribed time at high shear—by a step change towards the original low value. Here again, the complete flow history is a sequence of identical runs where the duration at high-flow (high shear) and low-flow, although distinct, is the same for all the runs. In a similar manner to the other transient experiments, the first run is always used to erase any previous conditioning of the fluid. Every point plotted in Figure 15 is thus the average of 100 readings taken in sets of 10 during each run. For the three experiments in Figure 15 the *high-flow* condition is always $G\sqrt{\lambda} = 1.19$ with a duration of 30 seconds, but with each experiment having a different low shear value of $G\sqrt{\lambda} = 0.74,\ 0.15$ and 0 respectively, with a fixed duration of 40 seconds for all three cases. The observed relaxation of birefringence for zero shear corresponds to that already seen for start-up and cessation of steady flow, and represents the outer envelop for the traces of birefringence Δn and orientation angle χ.[11] The relative size of the plotted overshoots for the two experiments with the lowest values of the *low-flow* $G\sqrt{\lambda}$ do not appear to be significantly different. However, as the low-flow shear rate increases, the overshoot upon re-starting the flow almost disappears, and the long time magnitude of the birefringence drops considerably. We believe that this "secondary" level for the birefringence corresponds to the steady limit of the previously described *secondary*

[11]The slight difference in levels at large times for the two weakest low-flows is, mainly the result of polymer degradation requiring the use of fresh solutions for all experiments. Please also note that the experiment with zero shear rate during the low-flow part of the experiment has shorter time periods for the high and the low-flow sections of the experiment.

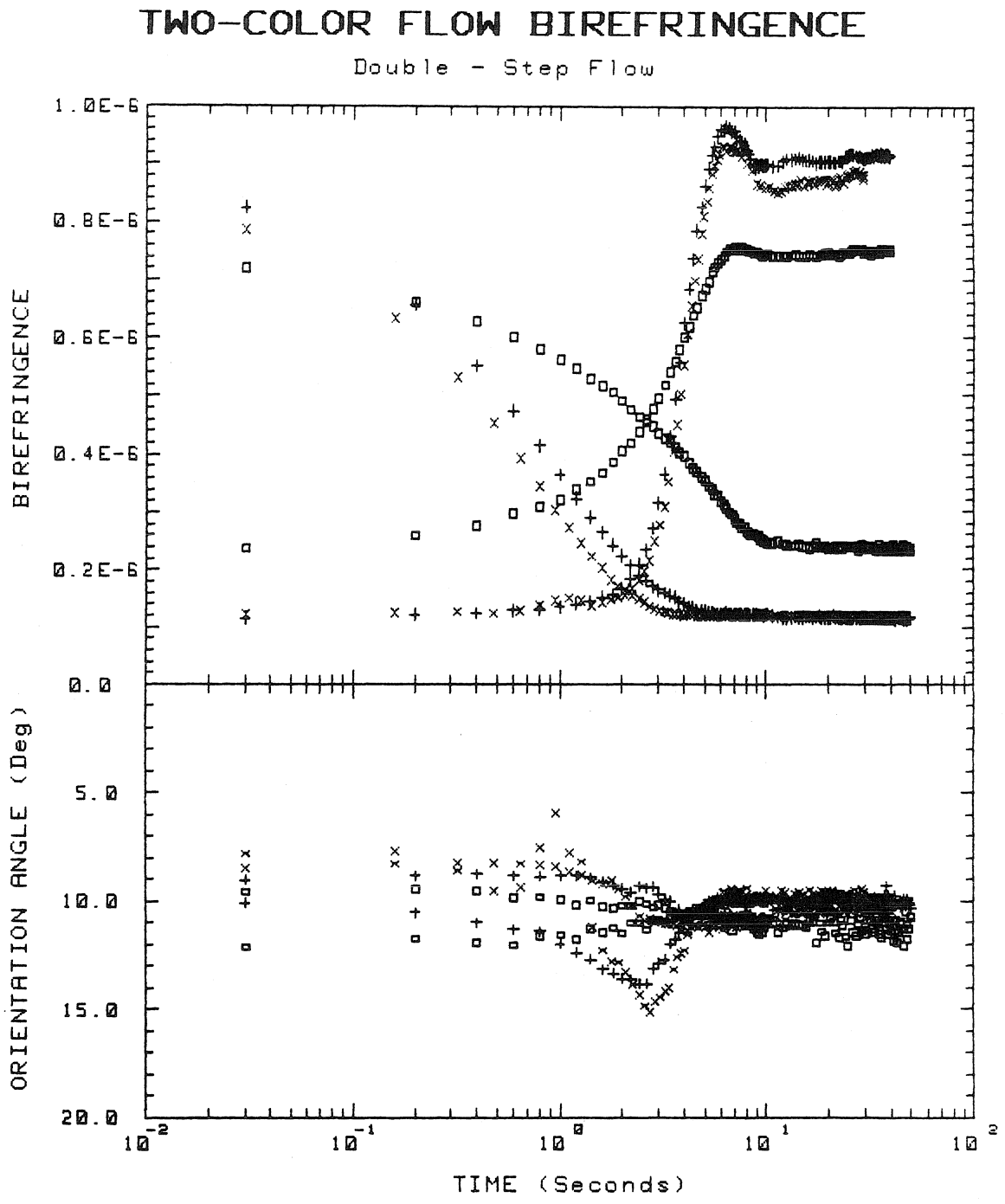

Figure 4.15: Double-step flow birefringence for the test-fluid M1 with rollers C ($\lambda = 0.0403$). The high-flow $G\sqrt{\lambda} = 1.19$ sec^{-1} and low-flow values of 0 ($\times$), 0.148 ($+$), 0.74 ($\square$) sec^{-1}.

relaxation process that appears quite clearly whenever $G\sqrt{\lambda}$ is greater than 2.07 sec^{-1} as shown in Figure 13. The fact that it did not appear upon inception of flow at the lower values of $G\sqrt{\lambda}$ is apparently a result of the fact that the time period for flow was too short, even though the steady rotation of the rollers was imposed for up to 30 seconds.

Figure 16 shows another double-step experiment, but performed at significantly higher shear rates (for these experiments the value for $G\sqrt{\lambda}$ at high-flow is 4.45 sec^{-1} with low-flow shear values of 2.23, 0.74 and 0 sec^{-1}; the time periods are those reported for the previous double-step experiment). In this case, the levels at long times appear to be the *same* for all experiments, and the step towards the high-flow shear rate loses all trace of an overshoot for the low-flow shear of 2.23 sec^{-1}. Even the low-flow shear rate of 0.74 sec^{-1} seems to affect the start-up of flow in the sense that the magnitude of the overshoot decreases, even though no significant steady-state birefringence is seen in Figure 8 for the same value of $G\sqrt{\lambda}$.

Even more interesting than the behavior upon start-up of flow, however, is the relaxation from the high to the low-flow condition. Clearly, as seen in Figures 15, and 16 the relaxation process is slowed significantly when there is a step change to a weaker extensional flow, rather than to the fluid at rest. This effect is present for the whole range of shear rates that we tested using M1. Indeed, for Figure 15 a step-down to 0.15, or 0.44 sec^{-1} increases the apparent relaxation time from approximately 0.81 to 3.22 sec., respectively, compared to $\tau_R \sim 0.61$ sec^{-1} for the step-down to a complete rest state. Similarly, for the data presented in Figure 16, the increments in τ_R are 0.34, 0.44 and 0.62 sec. as the low-flow shear rate is increased from 0, 0.74, and 2.22 sec^{-1} respectively. The variation of the orientation angle is qualitatively similar to the equivalent start-up and cessation of flow experiment, until the low-flow shear rate is high enough to maintain the polymer molecules sufficiently stretched and aligned close to the orientation observed during the high-flow regime so that the time evolution is simply a monotonic change to and from the long time asymptotic limits.

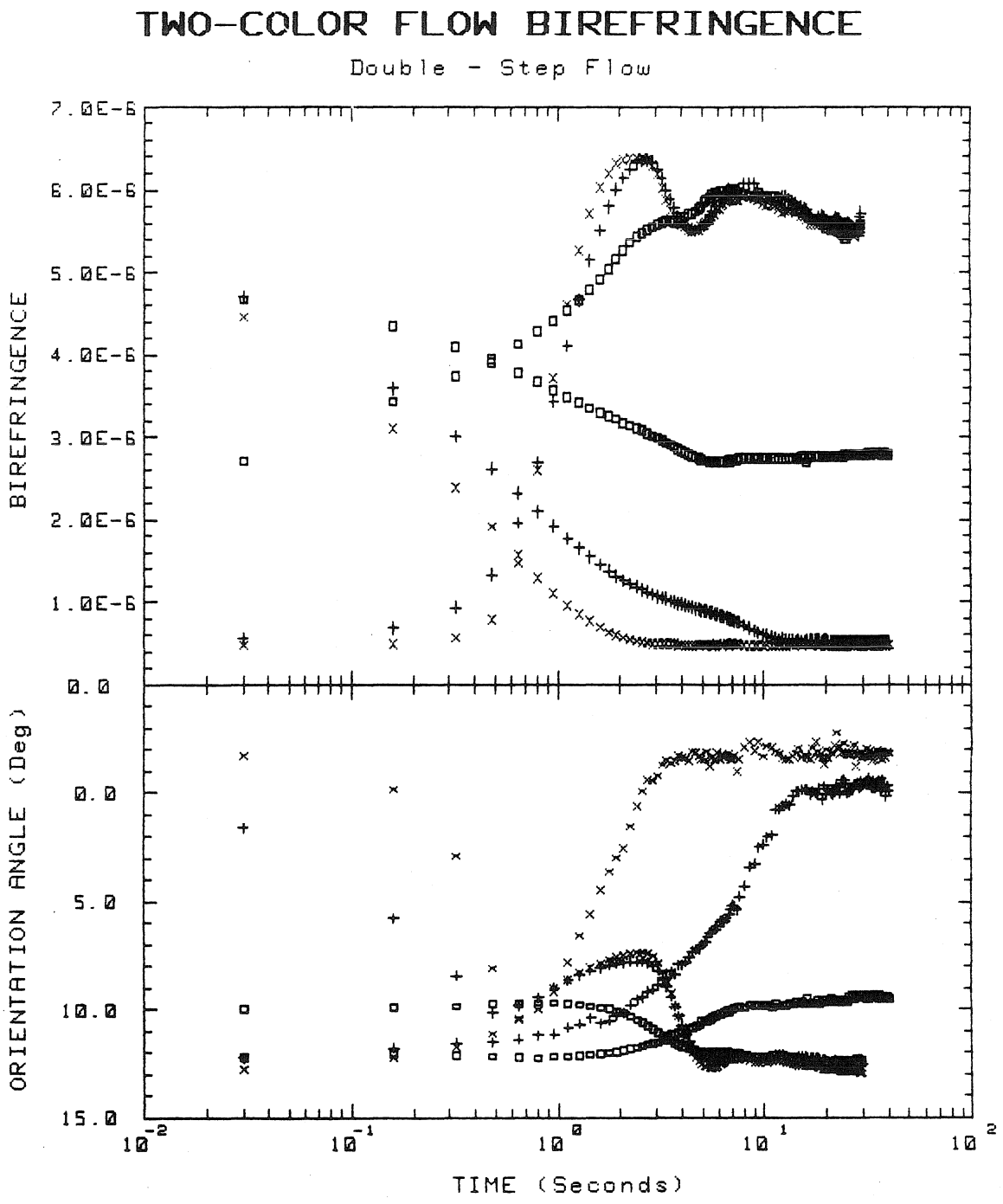

Figure 4.16: Double-step flow birefringence for the test-fluid M1 with rollers C ($\lambda = 0.0403$). $G\sqrt{\lambda}$ at high-flow is 4.45 $\sec^{-1}$ with low-flow shear values of 2.23, ($\Box$), 0.74 (+) and 0 $\sec^{-1}$ ($\times$).

4.4 Discussion

The solvent properties do *not* seem to affect the observed properties of the test-fluid M1, apart from the fact that they provide for a high monomeric friction coefficient. The solvent appears to have characteristic time scales that are at least two orders of magnitude faster that those observed for the test-fluid M1 under the same flow conditions. The solvent birefringence always showed a linear dependence on $G\sqrt{\lambda}$. Furthermore, the magnitude for the solvent birefringence is almost constant for a wide region between the rollers, and decreases only slowly for points far away from the stagnation region. This global region actually has a length scale similar to the roller radii, and for the larger rollers is several times the roller gap width. We have measured a slight asymmetry of the birefringence data within this wide region, say between the right and the left sides of the stagnation point, which we believe corresponds to spatial variations of the residual glass birefringence that is always superimposed upon the solvent birefringence. The characteristics within the central region of the flow reported in this work in Figures 3-6, as well as the spatial mapping of Δn for the solvent, lead us to postulate that: the solvent behaves as a "quasi-Newtonian" fluid within the time-scales observed for the test-fluid M1.

On the other hand, there are many interesting features of the data for the test-fluid M1. To begin with, the spatial behavior for the test-fluid M1 is quite different from that of the solvent. There exists only a narrow gap that includes the central stagnation region of the flow that is highly birefringent. In fact, the width of the birefringent region is not much greater ($\sim 2\times$) than the linear dimension of the cross sectional area of the laser beam. This thickness is much smaller than the gap width between the rollers implying that it is only those molecules moving along streamlines close to the stagnation region and thus subjected to a sufficiently large total strain—at a high enough shear rate—that become stretched. The width of this birefringent region depends also on the values of the principal eigenvalue, and grows wider as G increases. However, when the spatial variation is normalized with

respect to the level of birefringence at the stagnation point, the apparent width appears almost constant and independent of G. The width of the birefringent region decays to one half of the maximum birefringence level over a distance less than 100 microns.

This localized behavior for the birefringence of the test-fluid M1 is similar to that reported by Dunlap and Leal [7] and by Odell *et al.*, [24, 23] for *dilute* solutions of polystyrene with different types of solvents. However this similarity between the dilute solutions of polystyrene and the solution M1 is quite surprising, because the characteristic behavior for a semi-dilute solution such as the test-fluid M1 (with a nominal concentration of 2440 PPM) should resemble that of a more concentrated solution where intermolecular interactions are dominant and the birefringent zone is less localized. On the other hand, the characteristic relaxation time, based on the relaxation of birefringence after cessation of steady flow as shown in Figures 12, 13, and 14, depends on $G\sqrt{\lambda}$ in a matter that is characteristic of concentrated solutions. In particular, the relaxation time *decreases* as the eigenvalue increases. As stated above, this behavior is characteristic of truly concentrated polymeric systems where entanglements are the dominant physical phenomena. For an example, see the results by Zebrowski and Fuller [21].

Dunlap and Leal [7] have also measured the *velocity gradient* for dilute solutions of polystyrene, using the HLS technique previously described, and constructed a "global" map for the velocity gradient within and around the stagnation region. They found that even though birefringence is very localized, the effects of highly stretched molecules on the flow are important; as seen by comparison with the flow field of a Newtonian fluid, over domains significantly larger than the well defined birefringent regions. This phenomenon has also been observed in our laboratories for solutions of polystyrene but at much higher concentrations. One implication is that the real value of $G\sqrt{\lambda}$ around the stagnation region, is actually lower than the values "assigned" for the test-fluid M1, which are based solely on the values for a Newtonian fluid at the same rate of roller rotation. If this is the case, then

the relaxation times determined from plots of the birefringence vs. $G\sqrt{\lambda}$ as shown in Figures 7 and 8 would be longer than suggested earlier. This conjecture is also corroborated by the fact that overshoots on start-up of flow appear for values of the shear rate as low as 1.2 sec^{-1}, which implies a non-linear viscoelastic behavior with a characteristic time-scale for the fluid as long as 0.8 seconds. The possibility of flow modification also has other important consequences. In particular, since the largest changes in the flow would be correlated with the largest values of birefringence, the transient behavior measured for the flow-birefringence in this paper may be considerably smoothed as compared to what it would be if the velocity gradient remained constant. Furthermore, characteristic time-scales based on the inverse of $G\sqrt{\lambda}$, given as a function of roller rotation, may also be underestimated.

It is also important to note that the degradation observed with our apparatus is essentially *irreversible.* The degraded solutions did not show any recoverable birefringence even after remaining at rest for more than 90 hours. In particular, the total degradation, based on the birefringence values reached at long times for the steady flow, and the measured relaxation time after 90 hours of rest was determined to be equal within 10% of the original "degraded" value. It should be noted, however, that some exchange of polymer between fluid elements that occupy the stagnation point, where measurements are made, and the surrounding fluid occurs in a period of 90 hours.

The fact that we have observed significant degradation of the test-fluid M1 for quite small values of G, implies that conformational changes of the macromolecules are important, and that there must be a significant fraction of the polymer with a very high MW. This is also consistent with the fact that (a) the measured relaxation times for steady flow appear to be longer than those measured by cessation of steady flow; (b) that birefringence increases monotonically and quasi-linearly for a wide range of values of $G\sqrt{\lambda}$; and (c) that overshoots appear even at the lowest values of shear rate.

Of course, the interesting phenomena reported in this work are all a consequence

of the extension of the polymers. In order to achieve a transition from coiled to stretched state, it is necessary to impose upon the polymer a large enough strain rate ($G\sqrt{\lambda} > \gamma_c$ a quite low but nonetheless critical value as measured with our apparatus) for a sufficiently long time period in order to stretch it to the point where its elastic effects are important. This is precisely the advantage of the two-roll mill, where the residence time of polymer molecules at the stagnation is extremely long and even shear rates very close to the critical values are capable of significantly extending polymer molecules of sufficiently high MW. Therefore, the observance of degradation at *very low* shear rates may not be possible except in flows with stagnation points. On the other hand, degradation *will* occur whenever the fluid mechanics are such as to induce major departures from the equilibrium configuration of the polymer.

Consequently, in view of the degradation levels observed here at very low strain-rates, we believe that the use of spin-line or other type of extensional rheometers does *not* guarantee a trustworthy characterization of the test-fluid M1 in regions of high extensional viscosity. Even for the smallest strain rates, given the very broad MW distribution, significant degradation should be expected.

In a more general vein, we believe M1 to be a useful first step toward a test-fluid for extensional rheometry that could be improved significantly if the disadvantage of a broad molecular weight distribution were removed. It would also be useful to provide the system with a solvent that is chemically characterizable in a less ambiguous manner than kerosene. Such solutions similar to the test-fluid M1 offer considerable potential for future rheological as well as rheo-optical studies. For optical measurements however, special care should be taken in the preparation of the sample in order to avoid dust particles in the solution and thus insure highly reproducible and accurate data.

4.5 Conclusions

We have measured the optical anisotropy induced by flow fields generated by a two-roll mill for the test-fluid M1, and also separately, for its solvent. The flow conditions that were studied include steady state flows, as well as two transient flow histories: (1) inception and cessation of steady flows; and (2) the so called double-step steady flows. One of the most important characteristics of these flows is the fact that the strain rate is always larger than the vorticity of the flow. These flows are classified as strong flows and share many of the features of other (purely) extensional flows, the main characteristic being the capability of inducing significant changes in polymer conformation into a highly anisotropic state. The two-roll mills are capable of producing large *strains* near the stagnation region located between the rollers even when the fluid is subjected to rather small shear rates.

The experimental data presented here comprises measurements of birefringence—or degree of deformation of the polymer molecules—and the orientation of the polymer with respect to the outflow axes. The relative complexity of the phenomena associated with the orientation angle as well as that observed for the birefringence, represents a unique opportunity for subsequent detailed analysis of polymeric fluids under flow conditions that are of the strong type but also include vorticity within the velocity gradient. However, to carry out this analysis, it will be necessary to obtain corresponding data on a narrow MWD version of M1.

The solvent birefringence does not show any measurable time dependence for the transient flows presented in this work. It does not show any localize phenomena and is always weakly birefringent, even at very high strain-rates. On the other hand, the test-fluid M1 shows a very localized and strong birefringence along the outflow axes. The fluid M1 showed appreciable degradation, even though the shear rates used in this study were quite low, making it very difficult and time consuming to perform a complete characterization. We also present in this work a series of characteristic time-scales for the fluid evaluated by means of flows with different

time histories. The variations observed between these time-scales show the importance of the polymer conformation—at the molecular level—on the dominant dynamic processes and their relationship to the macroscopic behavior. Among the features presented are (a) a birefringence that slowly increases—up to very high values—as a function of the flow strength, (b) relaxation time-scales that decrease as a function of shear rate, (c) two mechanisms for the presence of overshoots: one seen whenever the shear rate is very small and of the same order of magnitude as the relaxation time-scale of the fluid and the second one with quite different characteristics, being the dominant mechanism at higher shear rates. Also, step flows (from a high to a low flow conditions) show a significant increase of the relaxation time. These transient histories provide some insight into the complex nature of the fluid as well as the fluid mechanics under experimental conditions that are well characterized and highly reproducible.

Acknowledgement: This research was supported by a grant from the Polymer Program in the Division of Materials Research of NSF.

Bibliography

[1] W. L. Olbricht, J. M. Rallison and L. G. Leal; *J. Non-Newtonian Fluid Mechanics*, **10**,291-318(1982).

[2] R. I. Tanner; *Engineering Rheology*, Section §5.4; Clarendon Press, Oxford, 1985.

[3] P. N. Dunlap and L. G. Leal; *J. Non-Newtonian Fluid Mech.*, **23**,5-48(1987).

[4] H. Janeschitz-Kriegl; *Polymer Melt Rheology and Flow Birefringence*, Springer Verlag, New York, 1983.

[5] A. W. Chow and G. G. Fuller; *J. Rheol.*, **28**(1)23-43(1984).

[6] G. G. Fuller, J. M. Rallison, R. L. Schimdt and L. G. Leal; *J. Fluid Mechanics*, **100**(3)555-575(1980).

[7] T. Y. Liu, D. S. Soong and M. C. Williams; *J. Polym. Sci.: Polym. Phys. Ed.*, **22**,1561-1587(1984). and references therein.

[8] T. Y. Liu, D. S. Soong and M. C. Williams; *J. Rheol.*, **27**,7-35(1983).

[9] J. M. Dealy and W. K. W. Tsang; *J. Appl. Polym. Sci.*, **26**,1149-1162(1981).

[10] W. K. W. Tsang and J. M. Dealy; *J. Non-Newtonian Fluid Mechanics*, **9**,203-222(1981).

[11] J. A. Odell, A. Keller and M. J. Miles; *Polym. Comm.*, **24**(1)7-10(1983).

[12] M. J. Miles and A. Keller; *Polymer*, **21**,1295(1980).

[13] J. A. Odell, and A. Keller; *J. Polym. Sci.: Polym. Phys.*, **24**,1889-1916(1986).

[14] R. S. Berry, S. A. Rice and J. Ross; *Physical Chemistry*, John Wiley, New York, 1980.

[15] R. B. Bird, R. C. Armstrong and O. Hassager; *Dynamics of Polymeric Liquids, Vol 1: Fluid Mechanics*, John Wiley, New York, Second Ed. 1987.

[16] P. N. Dunlap, C. -H. Wang and L. G. Leal; *J. Polym. Sci.: Polym. Phys. Ed.*, **25**,2211-2238(1987).

[17] G. G. Fuller and L. G. Leal; *Rheol. Acta*, **19**,580-600(1980).

[18] G. G. Fuller and L. G. Leal; *J. Polym. Sci: Polym. Phys. Ed.*; **19**,557-587(1981).

[19] J. D. Ferry; *Viscoelastic Properties of Polymers*, Third Ed., John Wiley, N. York, (1980).

[20] D. S. Pearson, A. D. Kiss, L. J. Fetters and M. Doi; *J. Rheology*, **33**(3)517-535(1989).

[21] B. E. Zebrowski and G. G. Fuller; *J. Pol. Sci.: Polym. Phys. Ed.*, **23**,575-589(1985).

Chapter 5

Birefringence Studies in Transient Flows of a Two Roll Mill for a Concentrated Polystyrene Solution.

Enrique Geffroy
California Institute of Technology
Department of Chemical Engineering

and

L. Gary Leal
University of California, Santa Barbara
Department of Chemical and Nuclear Engineering

Birefringence Studies in Transient Flows of a Two-Roll Mill for a Concentrated Polystyrene Solution.

Abstract

We have studied a 5 percent solution of polystyrene of 3.84×10^6 MW in flows generated by a co-rotating two-roll mill. These flows have a stagnation point at the midpoint between the roller axes, are linear, two-dimensional, and the magnitudes of the strain-rates are greater than the vorticity. The observed characteristic times-scales are mostly dominated by the polymer relaxation dynamics of a highly *anisotropic* conformation since, around the stagnation point, fluid elements are subjected to very large deformations.

In this work, point-wise birefringence data is presented for steady and transient flow histories, such as inception of steady flow. The steady and transient data are used to analyzed the *linear* and *non-linear* viscoelastic regions of material behavior. A set of macroscopically defined characteristic relaxation times were measured and a correspondence is made with the relaxation mechanisms suggested by reptational models for concentrated polymers. A time-scale for the onset of non-linear viscoelastic behavior is determined as well as a characteristic time for significant deformation of the polymer structure. The main objective of this work is to provide a better understanding of how the macroscopic relaxation mechanisms are affected by the relative amount of vorticity and by the magnitude of the principal eigenvector of the velocity gradient tensor. Thus, this work provides a basis for understanding the strikingly different predictions of the reptational dynamics for simple shear flows and for elongational flows.

Chapter 5

Transient flow Birefringence of Concentrated Polystyrene Solution

5.1 Introduction

In this paper, we report a flow-birefringence study of a concentrated polystyrene solution with an average molecular weight of 3.84×10^6, a narrow MW distribution, and a concentration of 5 percent. Birefringence provides a measure of the degree of optical anisotropy, and of the orientation of the principal axes of the refractive index tensor, that is induced in a polymeric liquid by the imposed flow (see, for example, Janeschitz-Kriegl [1]). This is a reflection of changes in the polymer conformation due to the flow, and for weak departures from the state of equilibrium, it is also directly related to changes in the stress (via the so-called stress-optical law). The birefringence data reported here provides a *point-wise, instantaneous,* and *direct* measure of polymer conformation in an extensional flow.

The flows used for this report are two-dimensional strong flows that are generated in a co-rotating two-roll mill. The designation *strong* in this instance is taken from the general criterion as expressed by Olbricht *et al.* [2] and others (see, for

example [3]-[6]). In two-dimensional flows this criterion implies that the magnitude of the strain-rate *exceeds* the vorticity, and therefore, large conformational changes are possible for the polymer molecule. Previous studies of both dilute and concentrated polymer solutions have shown that polymer extension and orientation is qualitatively (and even quantitatively) similar for *all* strong flows, including pure extension, provided that the polymer orientation is comparable with the principal eigenvector of the velocity gradient tensor, and the effective strain rate (i. e., the magnitude of the principal eigenvalue) along this direction is used instead of the velocity gradient itself (see for example Dunlap and Leal [7] and Fuller and Leal [8]).

On the other hand, the conformational changes that are possible with steady shear flows (such as those produced in Couette devices) are only marginal for it is a weak flow in the sense of Olbricht *et al.* For simple shear, it is necessary to imposed a exponentially increasing shear rate in order to achieve a strong flow condition [9]. In the laboratory environment it is only possible to maintain such a flow for a limited amount of time, and therefore, one can only achieve a small total strain. The same laboratory constraint applies to existing steady uniaxial extensional flow experiments where the Hencky strains commonly have maximum values of about 4, except for a few cases where Hencky strain measures ≤ 7 have been reported [10]-[12]. This latter limitation does not apply to fluid elements in the neighborhood of the stagnation point of the two-roll mill, where the residence time is very long, and very large strains are possible. Indeed, strains as high as 100 are possible with this system; we will discuss in length, these and other related ideas shortly. Furthermore, with our two-roll mill, we were able to study both *steady* and *transient* flows of various types, *i.e.*, start-up, relaxation from a steady flow, or double-steps, etc. We shall describe these flows in the next section. Steady flows in a two-roll mill can be of great importance simply because most other extensional flows do *not* reach a steady flow condition at the highest elongational rates.

The present study was carried out using a new experimental system that was

designed to study birefringence in time dependent strong flows, and that also allows detailed measurements, via dynamic light scattering, of the velocity gradient field as a function of time and spatial position. The latter, in our view, is *essential* for any *quantitative* interpretation of the birefringence data (that is, of the response of the polymer to the "real" strain-rate imposed by the flow), because significant departures from the equilibrium conformation will not only be accompanied by measurable amounts of birefringence, but also usually, by significant changes in the flow compared with the motion of a Newtonian fluid in the same flow device, at the same Reynolds number.[1] In spite of this, however, measurements of the velocity gradient field have *not* been made to date and will be presented elsewhere as soon as data is available. Nevertheless, important qualitative features of the measured anisotropy of this fluid have been found and these provide significant insight into the polymer dynamics and rheology of these flows. In this paper, we briefly summarize the main features of the experimental system as they are related to this particular solution (details for the apparatus can be found in reference [13] Chapters 1-3). Subsequently, the experimental data for the concentrated polystyrene solution is given and, finally, we discuss our views on the significance of these results.

5.2 A Brief Summary Description of the Experimental System

A full description of this apparatus is given in reference 13. Also, specific details of the apparatus related to the polymer solution designated as the M-1 fluid are presented in [14]. Here, we limit ourselves to a brief summary of the experimental set-up with enough detail, as it relates to the optical and rheological characteristics of this polystyrene solution, to allow the reader to understand what we have done. This experimental system is composed of three main parts: (a) the Two-Color Flow Birefringence optical arrangement used to measure the optical anisotropy of

[1] Of course, the same is true of the flows in all "extensional" rheometers, and even in time-dependent simple shear flows [7, 12].

the fluid, (b) the two-roll mill flow cell generating the strong flows, and (c) the software used to execute the different experiments under full control of a computer.

5.2.1 Two-Color Birefringence System

In order to perform birefringence measurements in time dependent flows, we have adopted the two-color flow-birefringence technique (TCFB) originally developed by Chow and Fuller [15]. The basic problem with transient birefringence measurements is that both the degree of birefringence (*i.e.*, the difference of the principal values of the refractive index tensor in the plane of the flow), and the orientation of the corresponding principal axes of the refractive index tensor are unknown and varying in time [1]. Clearly, two independent measurements are necessary to determine both the degree of optical anisotropy and the time-dependent orientation angle [16]. The two color system is designed to provide these two independent measurements simultaneously by using, for example, the two main colors of an Argon-ion laser (respectively, with wavelength of 4880 Å and 5145 Å).

The retardance of the sample is determined by measuring the light intensity that passes through crossed polarizers for both colors separately, with the relative orientation of the incident polarization of the green beam—with respect to that of the blue beam— rotated to some fixed angle. The most convenient angular separation for the polarization of the two beams is 45°, and for the experiments reported here the initial polarization of the green and the blue beams is at angles of $+22.5°$ and $-22.5°$ respectively, relative to the symmetry plane which bisects the two-roll mill. Figure 5.1 shows the relative orientation of the blue and green analyzers, as well as the principal optical axes of the solution and the symmetry axes of the flow field. The principal ideas for the two-color measurements, including the general basis for data analysis, are discussed by Chow and Fuller [15] and will not be repeated here. Our implementation of the TCFB technique is given in Chapter 2 of reference [13], emphasizing those ideas necessary for the study of non-homogeneous flows.

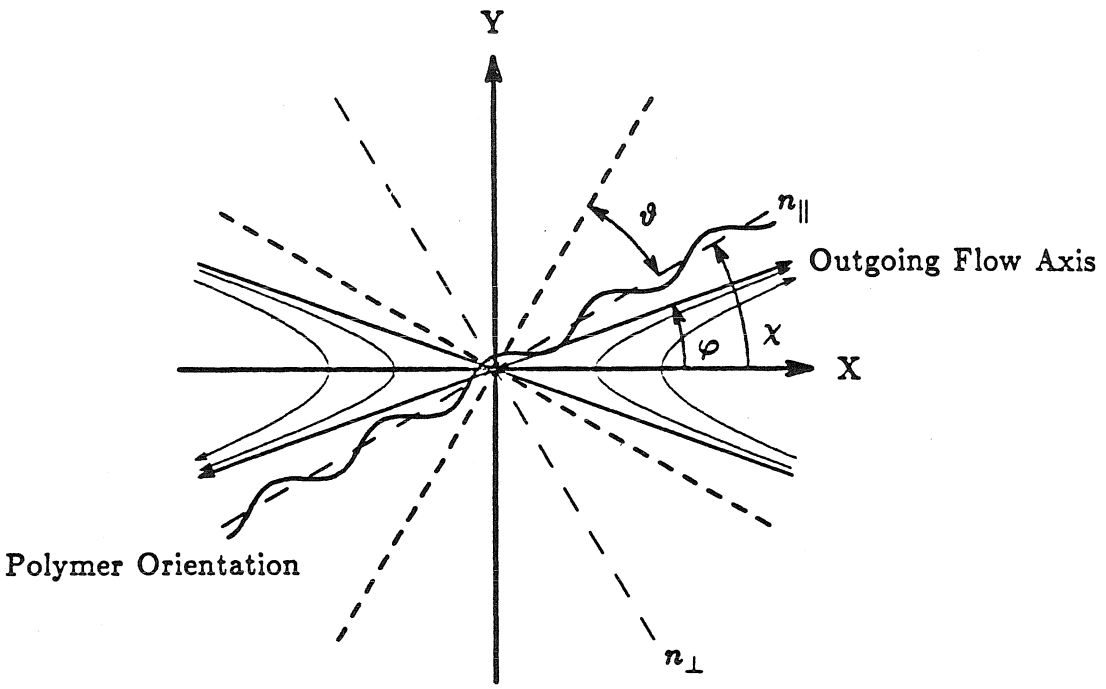

Figure 5.1: Relative orientation of the Optical system and the flow cell

However, a few details of our present system are worth stating, specifically as they relate to measurements that have been done on this polystyrene solution. First, the current system is extremely sensitive, with extinction ratios in the absence of the flow device of $\mathcal{O}(10^{-5})$, which correspond to retardations of only 0.002 radians for the full length of the flow cell. In the presence of the flow device, the residual birefringence of the glass windows is the primary limitation on sensitivity, since it can be larger than the birefringence of a slightly anisotropic fluid. The lowest detectable values for the glass birefringence depend on the minimum detectable values of the measured light intensities past the analyzers. The maximum extinction ratios detectable with our device, for both colors, are typically $\mathcal{O}(5 \times 10^4 : 1)$, which represents the maximum sensitivity of our optical arrangement. Within this range of sensitivity, the residual glass birefringence always exists, and, in fact varies (specially in its orientation angle) from day to day, due mainly to changes of

the room temperature. However, glass birefringence is a physical phenomenon to be reckoned with only if the fluid is very weakly birefringent [17], such as for some solvents used to prepared polymeric solutions (see for example Geffroy and Leal [14] for the case of a solvent made of kerosene and polybutylene with a molecular weight of only 500). For this concentrated solution of polystyrene, the solvent birefringence is two orders of magnitude smaller and glass and/or solvent birefringence were not considered significant for the studies reported here. The essential optical and rheological characteristics for the solvent used in this polystyrene solution and those of the solvent reported in reference 14 are the same.

Another important characteristic of this two color system is that the beam waists for both the green and blue beams are approximately 75 microns in diameter, and the extent of the beam waist regions is about 0.75 cm. Thus, the birefringence measurements are very localized, relative to the dimensions of the flow device. A typical beam dimension of this size is not particularly difficult to achieve for a single color birefringence system. On the other hand, for the two-color system, the optical set-up must not only provide a narrow beam, but the dimensions, shape and location of the blue and green beams must be as nearly identical as possible across the flow device. This is a difficult task when both beams are 75 microns in diameter and the above conditions are to be maintained for long periods of time. This is one of the main advantages of our apparatus [13] compared to the device originally constructed Chow and Fuller [15].

5.2.2 Two-Dimensional Strong Flows Generated by a Two-Roll Mill

All of the birefringence and light scattering studies carried out in this laboratory over a number of years have utilized either a two- or a four-roll mill to generate the flow fields [7, 18]. (streakline photography for these flow fields is shown in Figure 5.2). When properly designed, these flow devices produce a good approximation to a linear flow in the region between the rotating cylinders, with the ratio

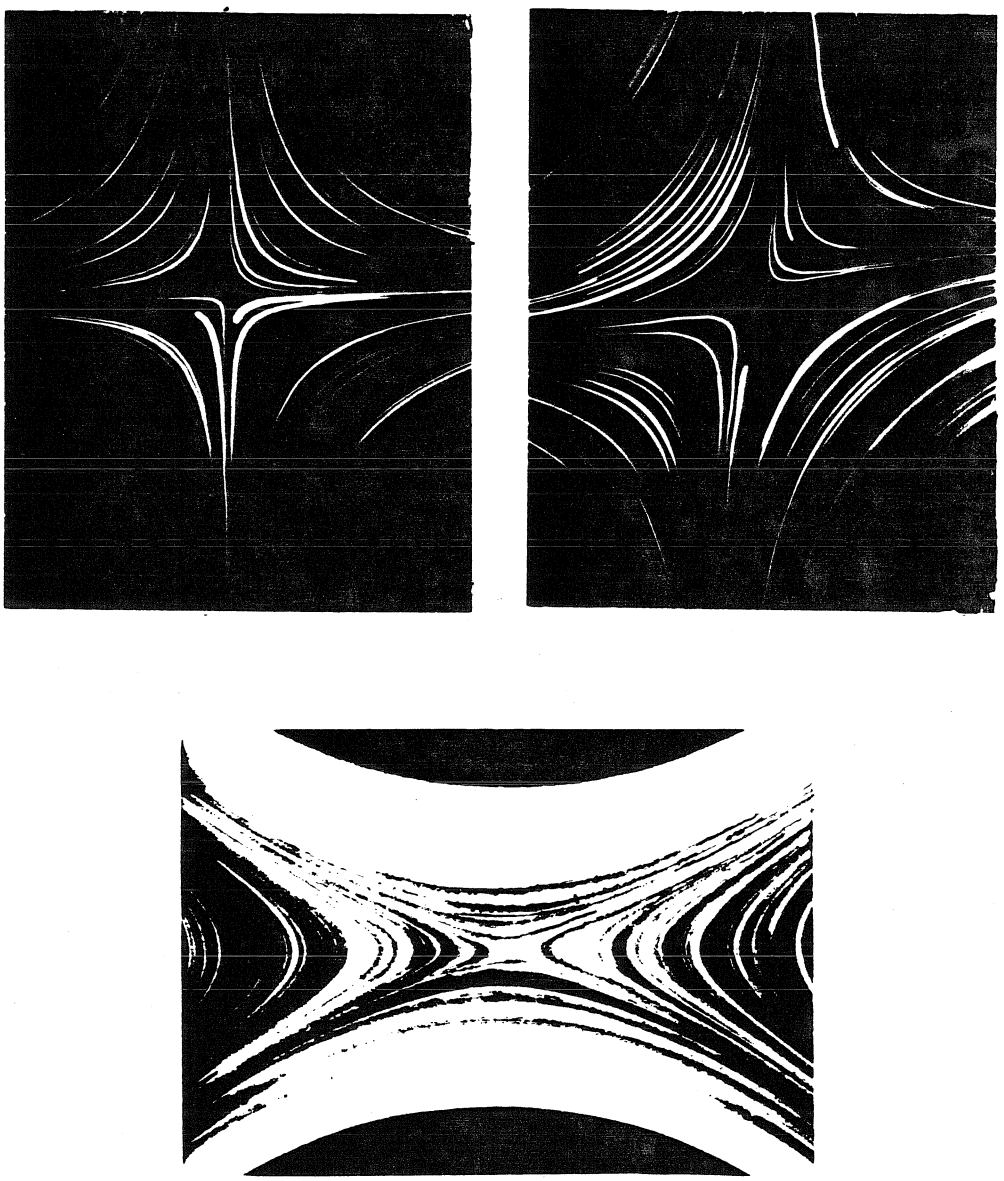

Figure 5.2: Streakline photography for the flow fields of a Four-Roll and a Two-Roll mill. The flow fields of the four roll mill correspond to $\lambda = 1$ left side and $\lambda = 0.4$ right side. The two-roll mill corresponds to a flow parameter value of $\lambda = 0.15$.

of strain-rate to vorticity and the magnitude of the velocity gradient *independently* controlled [7, 18, 19]. In the case of the two-roll mill, with cylinders *co-rotating* at the same angular velocity (and a Newtonian fluid at a very small Reynolds number), the flow type is uniquely controlled by the geometry of the flow device, i. e., by the ratio of the cylinders' radius to the gap width between the cylinders. Also, the magnitude of the velocity gradient is proportional to the angular velocity of the cylinders [7, 13, 20, 21].

It is convenient to parametrize the (approximately) linear flow that exists in the region between the cylinders by expressing the velocity field in the form

$$\mathbf{U} = \frac{\dot{\gamma}}{2}\begin{bmatrix} 0 & 1 & 0 \\ \lambda & 0 & 0 \\ 0 & 0 & 0 \end{bmatrix} \cdot \mathbf{X}, \tag{5.1}$$

where the position vector $\mathbf{X}$ is measured from the origin of a coordinate system that is centered at the geometric center of the two-roll mill, and the abscissa corresponds to the symmetry line between the rollers. The abscissa of the flow field is also equivalent to the x-axis of the coordinate system for the optical arrangement. Thus, the flow is completely characterized by the two parameters $\dot{\gamma}$ and λ, where $\dot{\gamma}$ is the magnitude of the velocity gradient (often called the shear rate), and λ determines the ratio of strain-rate to vorticity (i. e., the flow type) by the expression

$$\frac{\|E\|}{\|\Omega\|} = \frac{1+\lambda}{1-\lambda}. \tag{5.2}$$

Clearly, λ varies from -1 to $+1$, with $\lambda = +1$ representing a pure straining flow, $\lambda = 0$ a simple shear flow, and the range of possible *strong* flows (as defined earlier) corresponding to $0 < \lambda \leq 1$. The two-roll mill can generally produce flows with λ values in the range of $0 < \lambda \leq 0.25$. Another critical feature of the flow generated by a two-roll mill as indicated by equation (1) is that it contains a stagnation point at its geometric center. Thus, in contrast to many extensional flow devices, the residence time of the polymer molecules near the stagnation point are very long, and thus, they are subjected to very large total strains. Consequently, it

is possible to realize the maximum change in conformation of the macromolecules that is consistent with a particular strain-rate.

In the present study, the polystyrene solution was studied with four pairs of rollers. The dimensions of these sets of roller pairs, together with the gap width and the length-to-gap ratio are listed in Table 1. The two-roll mill used here was

Roller ID.	radius (cm)	gap (cm)	height: gap ratio	λ	$\sqrt{\lambda}\dot{\gamma}_{max}$ (sec^{-1})	$\dot{\gamma}_{max}$ (sec^{-1})
B	1.635	0.130	20:1	0.0196	109.3	780.6
D	1.510	0.380	6.7:1	0.061	58.8	239.1
F	1.278	0.844	3.1:1	0.150	32.9	84.6
H	1.075	1.250	2.0:1	0.249	21.8	43.7

Table 5.1: Characteristics of the two-roll mill, and calculated parameters of its flow field based in the creeping flow solution presented in Chapter 1 of reference 13. The minimum values for the shear rate and the magnitude of the principal eigenvalue of the velocity gradient tensor are 1/2000 of the maximum values.

designed so that both rollers are driven simultaneously by a single *stepping* motor. This type of motor has good accuracy in maintaining a constant speed, as well as a very fast acceleration. However, there is a discrete number of rotational speed that is possible to generate with such motors, and for the case of rollers B, the lowest possible shear rates are slightly high for this polystyrene solution. That is, some of the interesting behavior observed at low shear rates for other set of larger rollers is almost "skipped" in this geometry. Furthermore, for this geometry at slow shear rates, the spacing between distinct values of the shear rate is quite broad with only a "coarse sampling" of experimental points being possible to take for this polymeric fluid –these details will be discussed in length later.

The motor electronics is interfaced with a computer, so that a variety of different transient flow-histories can be produced, as well as an automated sweep through a series of steady flows with different values of $\dot{\gamma}$. In this work, data for *steady* flows and for *inception* of flow—where the fluid at rest is put abruptly into a condition

of steady[2] flow—are presented. The flow device is mounted on a support with four degrees of freedom (x, y, z, θ) in order to adjust the relative position of the two-roll mill with respect to the incident beams. The translating stages (three) for these degrees of freedom are driven by differential micrometers with a resolution of 10 microns, while the azimuthal orientation is adjusted with a micrometer providing an angular accuracy of 0.0003 radians. The re-positioning of the flow cell is always better than 25 microns and 0.001 radians, even when the flow device is dismounted for the purpose of replacing the solution.

As a general practice and whenever the flow cell is taken out and placed back into the apparatus, the relative orientation of the symmetry axes of the flow cell with respect to the bisector defined by the azimuthal orientation of the blue and green analyzers was always recalibrated. The calibration requires fine-tuning the azimuthal reference orientation of the flow cell with respect to the optical axis, and is based upon the measured orientation angle for the polymer for two sets of experiments at the stagnation point in which the direction of roller rotation was reversed.[3]

The speed of data acquisition is mainly limited by the electronics in the experimental apparatus. For steady state flows, it takes about 1 msec. to execute all the necessary irradiance readings to obtain a data-point for the extinction angle and the birefringence of the fluid sample. In order to increase the signal to noise ratio, the computer program performs several readings sequentially, at full speed, and performs the appropriate statistical analysis on the data sample. For the steady

[2]Actually, all flow conditions are achieved via an acceleration ramp for the angular velocity of the rollers that although quite high, is still finite. The motor always requires less than 1/20th of a second to reach any prescribed angular speed; mean values for the ramp-time are less than 1/100 of a second for the experiments reported here. The fastest intrinsic time-scales observed for this particular fluid sample were at least an order of magnitude longer. The acceleration ramp is one of the various parameters that the experimentalist has control of through the computer. The observed behavior was always checked for possible dependence on the ramp-time.

[3]With this fluid *i.e.*, this solution, data for the orientation angle is reproducible within $\pm 0.25°$ for the complete range of speeds of the rollers. The flow device and optical system orientation are considered to be equivalent when the absolute value of the extinction angle of the measured anisotropy coincides within 0.5°, for the clockwise and counterclockwise rotation of rollers.

state flow conditions, the average number of readings per data point was about 500. For the transient flows, ten identical readings are taken sequentially (at the fastest pace possible; 0.0002 seconds per data-point) for every point in time, and the sum of results from ten repetitions of the experiments are used for the statistical analysis.

5.2.3 The Polymer Solution Sample

Anionically polymerized polystyrene manufactured by Toyo Soda Manufacturing Ltd. of Japan with a molecular weight of 3.84×10^6 and polydispersity index of 1.04 (F-380 polystyrene standard) was dissolved in toluene (high purity solvent from American Burdick & Jackson) without further purification. Subsequently, polystyrene oligomer (obtained from Polysciences, Inc) with a molecular weight of 6000 and a broad MW distribution, was added to the dissolved polymer in order to increased the viscosity of the solution. The oligomer was allowed to dissolve in the solution at room temperature for a few days with occasional slow mixing with a magnetic stirrer. The final concentration of the high molecular weight polystyrene was 0.0484 g/ml, in a solvent made up of 33% by weight polystyrene oligomer in toluene. Finally, the complete solution was centrifuged in a Serval S-6 centrifuge at approximately 5000 rpm., for approximately 5 hours, with the top and bottom discarded.

The fluid was always transferred into, and out of, the flow cell via an air tight siphon system, where the pressure differential was maintained using compressed nitrogen gas. The use of this siphon system reduced the losses of toluene that occur in an open container. The minimal necessary pressure was always used to drive the siphon system in a way that the fluid transfer (100 ml.) was done in a couple of hours. The same polymer sample was used for all of the experiments done on all four roller systems.

5.3 Birefringence Results for the Polystyrene Solution

For a concentrated solution, birefringence measurements are directly related to changes in conformation of the polymer molecules. The complete characterization of the flow-induced anisotropy of a polymeric fluid requires determination of the birefringence Δn, as well as the orientation angle χ of the principal axes of the refractive index tensor with respect to the flow field. Two typical data sets are shown in Figure 3 and 8. In Figure 3, steady birefringence data is presented, while in Figure 8 is an example of transient data. For all steady flow data, the upper part contains Δn as a function of the principal eigenvalue of the velocity gradient tensor, *i. e.*, $\dot{\gamma}\sqrt{\lambda}$. For transient flows the birefringence is plotted as a function of time. The graph on the bottom of the figures shows the orientation of the principal axis of the refractive index tensor χ, measured relative to the bisecting symmetry axis for the two roll mill. A positive value for this angle, corresponds to the optical axis lying between the symmetry axis (x-axis) and the direction of the principal eigenvector of the velocity gradient tensor (see Figure 1). Previous studies of polymer solutions in this lab have shown that the degree of orientation (and presumably extension) of the polymer molecules is a function solely of $\dot{\gamma}\sqrt{\lambda}$ for all values of $\lambda > 0$. Thus, in the current studies we plot all results versus $\dot{\gamma}\sqrt{\lambda}$. It will be shown shortly that such a correlation exists within the linear viscoelasticity domain for the present solution.

Using the measured optical anisotropy, a number of different characteristics of the fluid can be determined. These include the necessary shear rates and/or strains in order to observe significant departures from near-equilibrium dynamics. Inception of flow provides a direct measure of the *strains* required for such departures to occur. Also, the steady and inception of steady flow birefringence can be used to evaluate the different relaxation mechanisms as proposed by the reptational models. In turn, and based on such reptational models we give a plausible qualitative

explanation for the observed birefringence for the wide variety of flow fields tested in our apparatus[4]

5.3.1 Steady Flow Birefringence

As seen in Figure 3, the birefringence is a monotonic increasing function of the magnitude of the principal eigenvalue of the velocity gradient tensor. The orientation angle χ, on the other hand, shows an initial value that is the result of the glass birefringence. This particular initial value varies from experiment to experiment and represent the limit of sensitivity for this apparatus in determining a minimum (residual) birefringence and its associated orientation. Subsequently, the maximum value is reached which corresponds to the polymeric fluid with a small anisotropy aligned along the principal axis of strain. Theoretically, it is expected the maximum orientation angle for deformation to a slightly spheroidal "shape" should be 45°. Experimentally, we have been able to measure values as high as 43° with birefringence values of only 2.5×10^{-7}. The small discrepancy, is due to comparable magnitudes of the residual glass and polymer optical anisotropy. For greater values of the principal eigenvalue of the velocity gradient tensor (equal to $\dot{\gamma}\sqrt{\lambda}$, and subsequently referred in the text and figures simply as the eigenvalue), the orientation angle decreases approaching asymptotically the outflow axis.[5] Figure 4 shows the complete range of values of $\dot{\gamma}\sqrt{\lambda}$ for the pair of rollers of smallest radius ($\lambda = 0.249$). By looking at this wider range of deformation rates, we see that the birefringence trace starts with the maximum slope and smoothly changes to a slower rate of increase at higher $\dot{\gamma}\sqrt{\lambda}$. That is, there is a fairly abrupt decrease

[4]Cessation of flow can also be used to measure the longest relaxation time for both near-equilibrium and non-equilibrium conditions [22]. We have carried out such measurement and these results will be presented elsewhere. Birefringence is also sensitive enough to detect relative changes in the molecular weight distribution for a given sample, including changes in a very small percentage of the highest molecular weight portion of the distribution [14, 23, 24].

[5]The outflow axis angle for the case of a Newtonian fluid at small Reynolds number has been calculated using the results of Chapter 1 of reference 13. For a non-Newtonian liquid such as the polymer solution been studied here, the outflow axis orientation will be dependent on the shear rate.

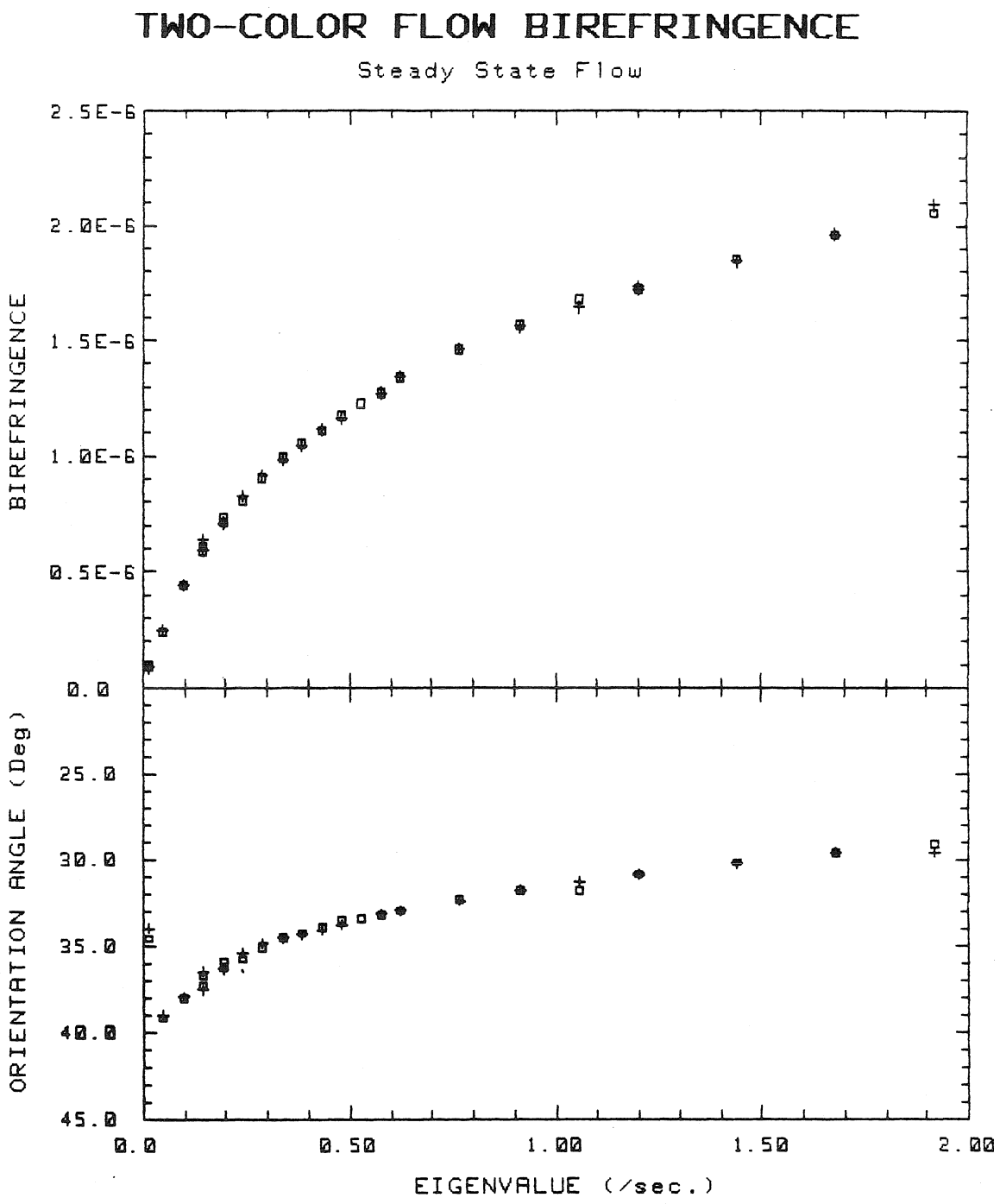

Figure 5.3: Birefringence and extinction angle as a function of $\dot{\gamma}\sqrt{\lambda}$. The flow parameter is $\lambda = 0.249$ The markers $+$, and $\square$ correspond to two different experiments.

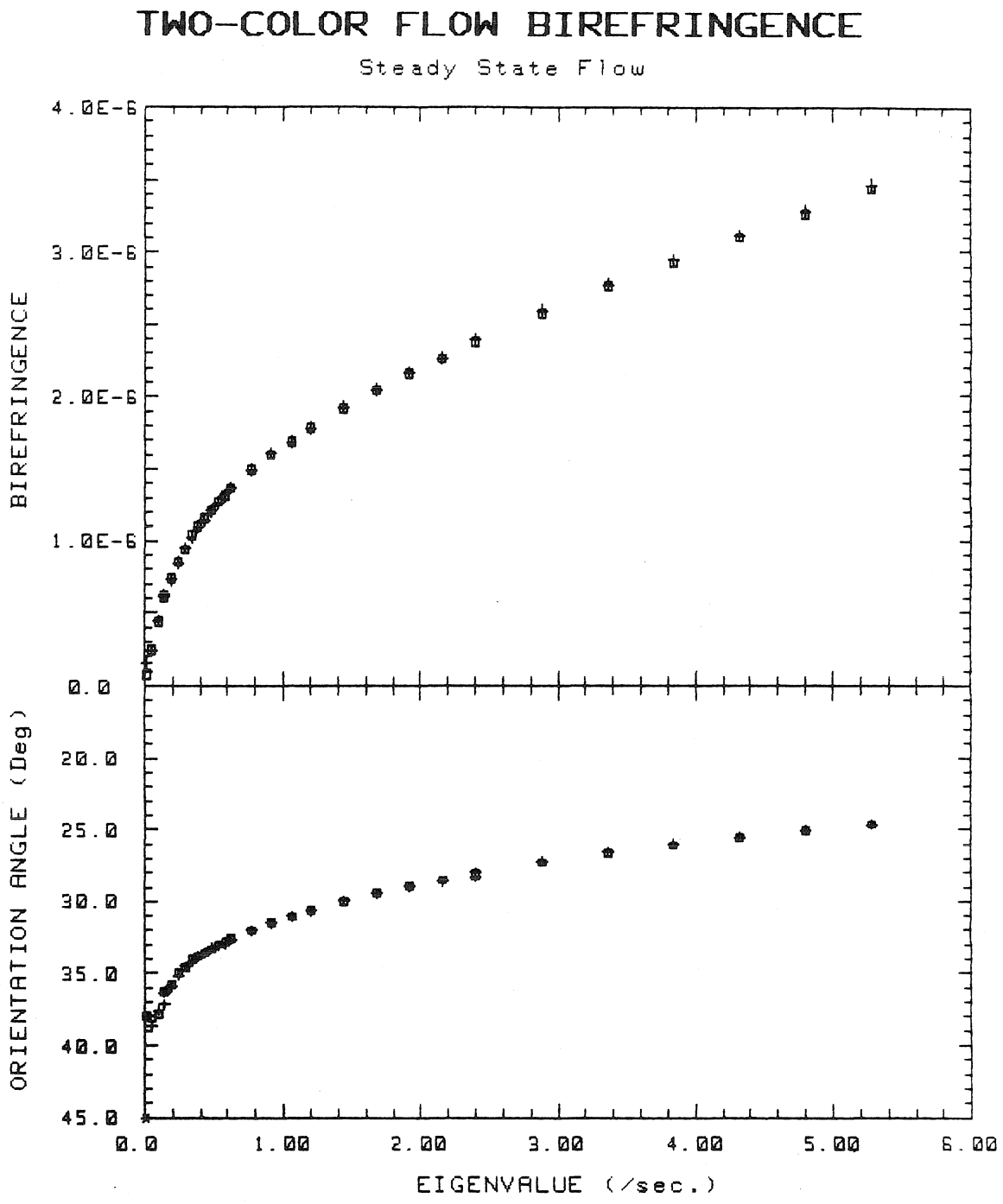

Figure 5.4: Birefringence and extinction angle as a function of $\dot{\gamma}\sqrt{\lambda}$. $\lambda = 0.249$ The markers $+$, and $\square$ correspond to two different experiments.

in the rate of increase of birefringence at about 0.4 s^{-1}. Later on, we proposed a simple method to characterize the eigenvalue where this abrupt change of the rate of increase occurs and is called the "inflection" point of the birefringence trace. However, when the observed change on the rate of deformation of the polymer molecules occurs, the orientation angle is still far from the expected orientation along the outflow axis.

In Figure 5, we show that a correlation exists for $\dot{\gamma}\sqrt{\lambda} \leq 0.4\ s^{-1}$ when the birefringence curves are plotted as a function of the principal eigenvalue, for the two flow fields with λ equal to 0.06 and 0.15. A correlation of this type was found earlier for a wider range of λ values in a four-roll mill by Fuller and Leal [8], specifically for $0.02 \leq \lambda \leq 1$. There are plaussible effects of a fluid mechanistic nature that may explain these discrepancies, and have nothing to do with the dynamics of the polymer. It is clear that for small deformations, curves for different λ's should collapse into a single one. This is not the case for $\lambda = 0.249$ as shown in Figure 6. In particular, birefringence is the result of integration of the polymer retardation along the sample cross section and therefore depends on the "thickness" of the layer of the two dimensional flow field. Flos generated by two-roll mill must include some "boundary" effects due to finite length of the flow device along the axes of the rollers. Moreover, the size of the gap between the rollers increases with increase in the flow parameter λ and consequently there will be a more pronounced boundary effect normal to the plane of the flow, for flows with the largest λ value, *i.e.*, for the flow geometries with the largest relative gap. Hence, the flow field "thickness" is smaller for larger λ, and it may be possible to obtain a good correlation if the optical path is calibrated according to the "real" thickness of the two-dimensional flow field. This correction could remove the correlation breakdown observed between rollers H and rollers F and D.

The breakdown for $\lambda = 0.02$, is probably due to a totally different effect. Theoretically a breakdown of the birefringence correlation for small λ is predicted by Leal and coworkers, [25] for a dumbbell model that includes full-conformation-

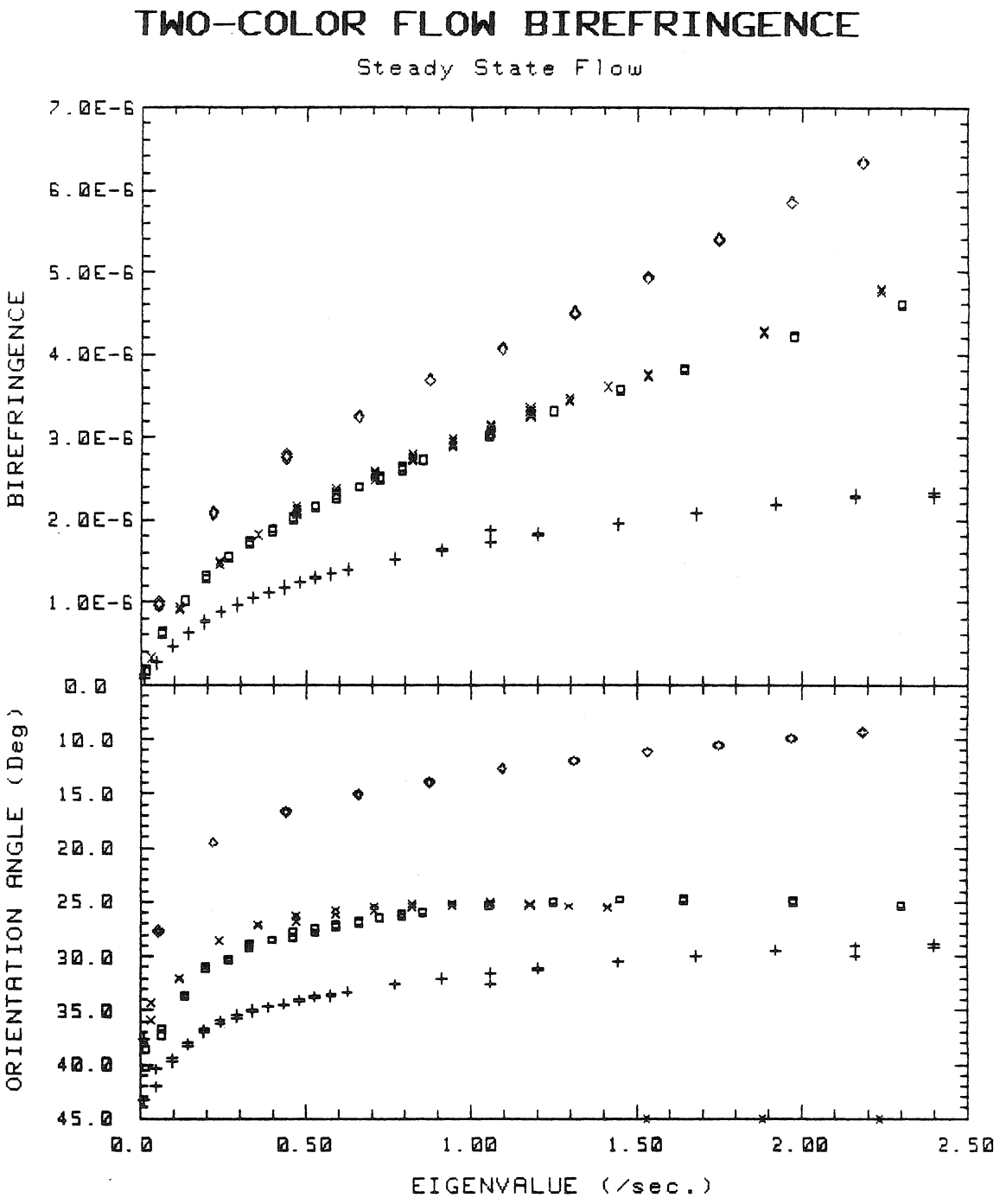

Figure 5.5: Birefringence and extinction angle as a function of $\dot{\gamma}\sqrt{\lambda}$. Different markers represent different flow geometries: $+$ for $\lambda = 0.249$, $\square$ for $\lambda = 0.151$, $\times$ for $\lambda = 0.061$, and $\diamond$ for $\lambda = 0.0196$.

dependent anisotropic bead friction and strain inefficient rotation. Specifically, for that model the breakdown of the correlation of ΔN *vs.* $\dot{\gamma}\sqrt{\lambda}$ occurs for $\lambda = 0.01$ for molecules having 100 Kuhn segments. The underlying reason for this breakdown is essentially the result of asymptotically approaching the behavior of a *weak* type of flow [2], while still using a strong flow correlation. The same type of singular behavior should be expected regardless of the solution concentration. Furthermore, the breakdown for the birefringence correlation should always occur for a non-zero positive value of λ. Taking these factors into account, we interpret the data in Figure 5 as indicating that the birefringence will correlate with $\dot{\gamma}\sqrt{\lambda}$ over the whole range of λ from 0.06 to 1.0, in an ideal two-dimensional flow provided that the magnitude of the principal eigenvector of the velocity gradient tensor is smaller than approximately 0.4 s^{-1}. This correlation defines the upper limit for the linear viscoelastic domain as we will show shortly based on data for inception of flow.

As seen in Figure 6, (which includes the birefringence data presented in Figure 5 plus a wider range of values of the principal eigenvalue) the rate of increase of birefringence—at higher shear rates—decreases for all values of λ, showing a slower but almost linear rate of increase. This linear increase in optical anisotropy of the polymeric fluid exists for eigenvalues greater than 1 s^{-1} and for λ values $0.06 \leq \lambda \leq 0.25$. For the smallest value of λ, the birefringence grows in a non-linear manner as function of the eigenvalue, distinctly to what is observed for larger λ values. There is a first section (at the smallest eigenvalues, and within the linear viscoelastic regime) where birefringence grows in an equivalent way to that observed for other λ values, that is, a fast onset that slowly changes towards a slower rate of increase. However as seen in Figure 7, at higher eigenvalues and within non-linear viscoelasticity, the birefringence appears to increase linearly, but with two distinct rates. The slower rate of increase for the smaller eigenvalues and a higher rate of increase for the largest values of the principal eigenvalue.

For eigenvalues larger than 1.0 s^{-1}, the orientation angle χ, also reaches a rate of rotation that is small but proportional to the principal eigenvalue. The be-

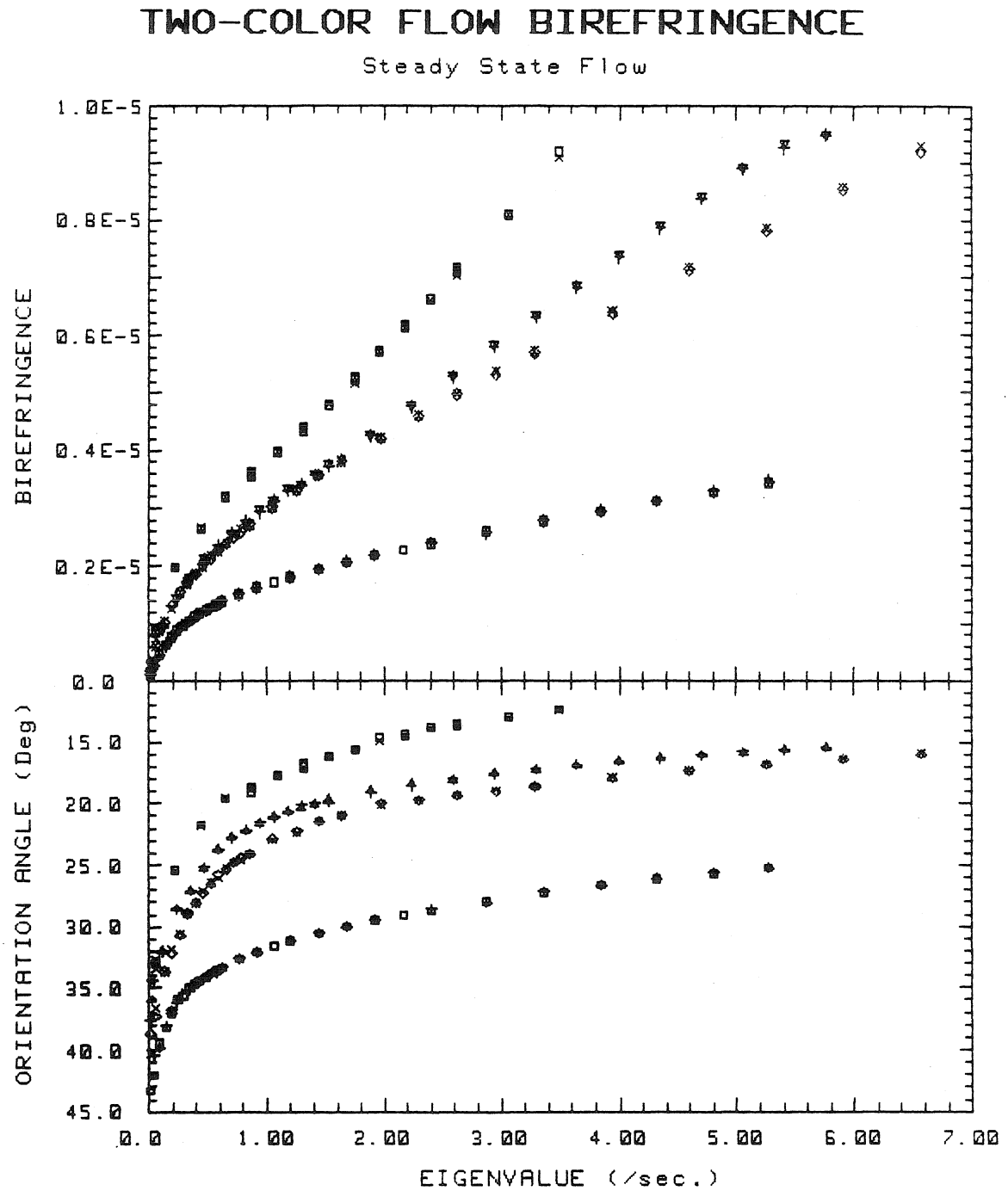

Figure 5.6: Birefringence and extinction angle as a function of $\dot{\gamma}\sqrt{\lambda}$. Different markers represent different flow geometries: $+$ for $\lambda = 0.249$, $\square$ for $\lambda = 0.151$, $\times$ for $\lambda = 0.061$, and $\diamond$ for $\lambda = 0.0196$.

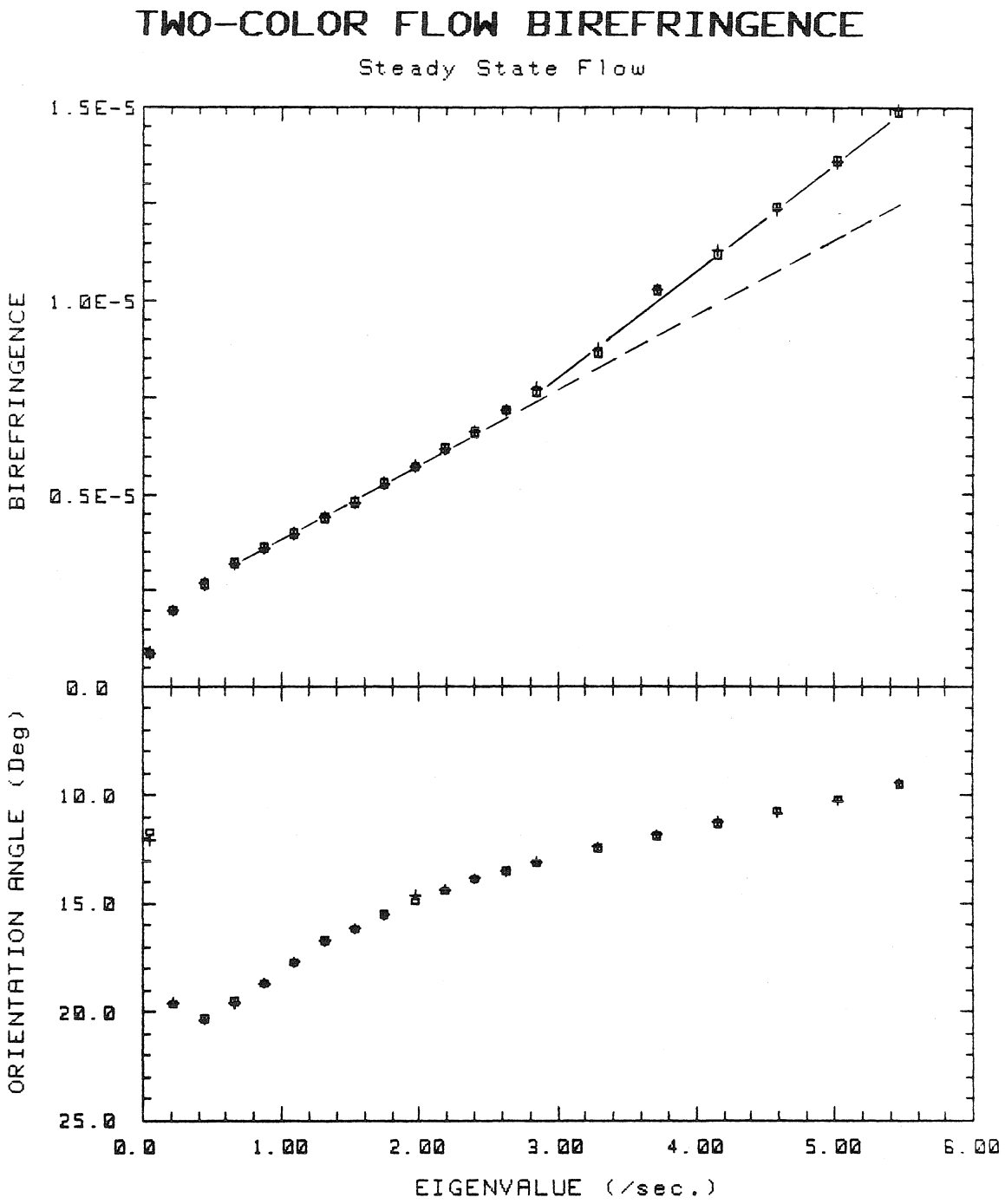

Figure 5.7: Birefringence and extinction angle as a function of $\dot{\gamma}\sqrt{\lambda}$; $\lambda = 0.0196$. For values of the birefringence larger than 0.96×10^{-5} the retardation is larger than $\pi/2$. The markers $+$, and $\square$ correspond to two different experiments.

havior of the orientation angle at large eigenvalues is representative of a polymer macromolecule that is aligned very close to the outflow axis of the flow field. Such a alignment is only possible if the polymer molecule has a conformation that resembles a highly elongated body. The observed final orientation angle decreases for smaller values of λ as the direction of the principal eigenvector of $\nabla \mathbf{U}$ rotates towards smaller χ values. Despite the good apparent alignment of the polymer molecules, it is possible to achieve even greater degrees of deformation of the polymer conformation. That is, we have observed birefringence values still linearly increasing for shear rates higher than those presented here. For the smallest λ value, we have measured birefringence levels 50% higher than those reported in Figure 6 with no apparent signs of its saturation (shown in Figure 7). A linearly increasing birefringence suggests a polymer conformation that is highly elastic and still far away from the maximum extension that can be achieved under this type of flow.

5.3.2 Inception of Steady Flow

First, we present in Figure 8 the observed transient flow birefringence for the flow geometry with the largest flow parameter. For small shear rates, the birefringence increases monotonically, until the steady state value is reached. The orientation angle at the onset of flow is dominated by the residual glass anisotropy. It is only after the anisotropic contribution of the polymer becomes dominant that the orientation angle reaches a maximum value. At this point, the polymer molecules are slightly deformed and the orientation angle of 45° corresponds to alignment along the axis of principal strain. The earliest portion of the behavior of the orientation angle, which is due mainly to the residual glass birefringence, is present in all cases for inception and cessation of flow. Since it provides little information regarding the polymeric liquids, it will be subsequently ignored in the discussion that follows. In all cases, the initial orientation of the polymer coincides with the principal strain axis of the flow.

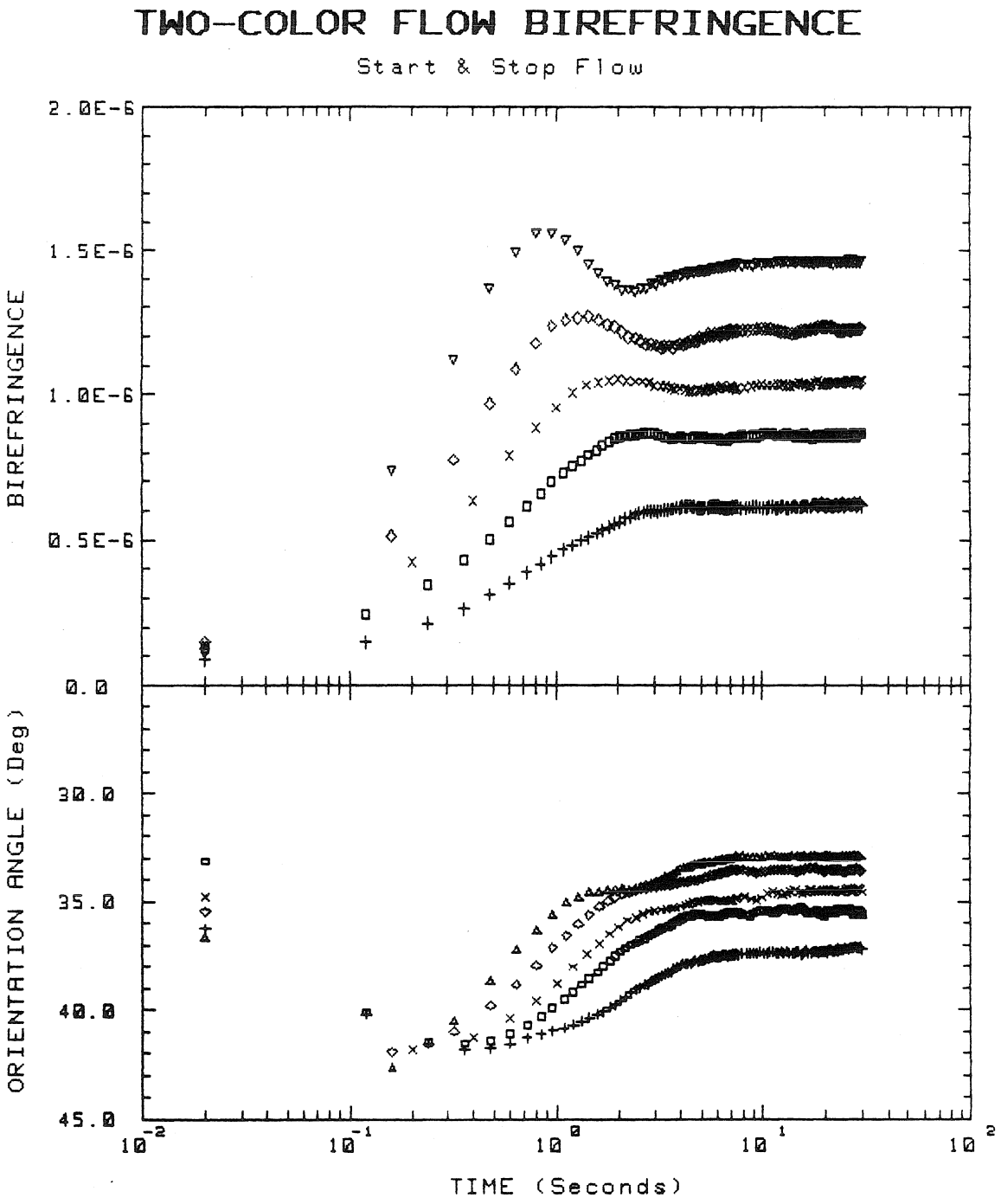

Figure 5.8: Inception of birefringence and extinction angle as a function of time for rollers H ($\lambda = 0.249$). Different markers correspond to different values of the principal eigenvalue of the velocity gradient tensor. $\dot{\gamma}\sqrt{\lambda} = 0.144\ s^{-1}$ (+), $0.24\ s^{-1}$ (□), $0.336\ s^{-1}$, (×) and $0.48\ s^{-1}$ (◇) .

For $\lambda = 0.249$, the first indication of *non-linear* viscoelastic behavior, based on start-up of flow, occurs around 0.35 s^{-1} (Figure 8). That is, the transient birefringence shows well defined *overshoots*, and *undershoots* following the maximum, for all eigenvalues greater than 0.35 s^{-1}. For this flow geometry, there is always a very large undershoot following the principal overshoot. In fact, the undershoot always coexists with the overshoot and the ratio of the relative magnitudes of the overshoot and undershoot is always less than one; we will discuss the relative values of such overshoot-undershoots shortly. Looking back on the birefringence data for steady flows in Figures 3 and 4, we can see that the birefringence and the orientation angle begin to change their respective *slopes*, towards smaller values, at approximately $\dot{\gamma}\sqrt{\lambda} \simeq 0.4\ s^{-1}$. Clearly, the change of slope in the steady flow graphs occurs at a value of $\dot{\gamma}\sqrt{\lambda}$ that coincides with the onset of *non-linear* viscoelastic behavior in the start-up data.

The temporal evolution of the orientation angle also shows *undershoots* before the final orientation is reached, although these appear at higher eigenvalues. For example, in Figure 9, the orientation shows an undershoot after 2 seconds (which corresponds to a strain of 1.44) for $\dot{\gamma}\sqrt{\lambda} = 0.72\ s^{-1}$. For $\lambda = 0.249$ and eigenvalues larger than 0.72 s^{-1} the local undershoot in the orientation angle coincides with the point at which the birefringence crosses the steady asymptotic value, between the birefringence overshoot and undershoot. The orientation angle reaches its *second* maximum (the first being that observed at the earliest times due to the artifact of glass birefringence) as the birefringence increases, after its undershoot, towards the final steady state value. The orientation continues to decrease, reaching its final value slightly after the birefringence becomes constant.

The presence of the undershoot in the birefringence, coupled with an increase in the orientation angle (*i. e.,* a rotation towards the principal axis of strain), a clear indication of segmental stretching occurring within the macromolecular "matrix" of the fluid. We believe that the stretching of polymer segment is manifested as the result of two distint effects: the first corresponds to the decrease in birefringence

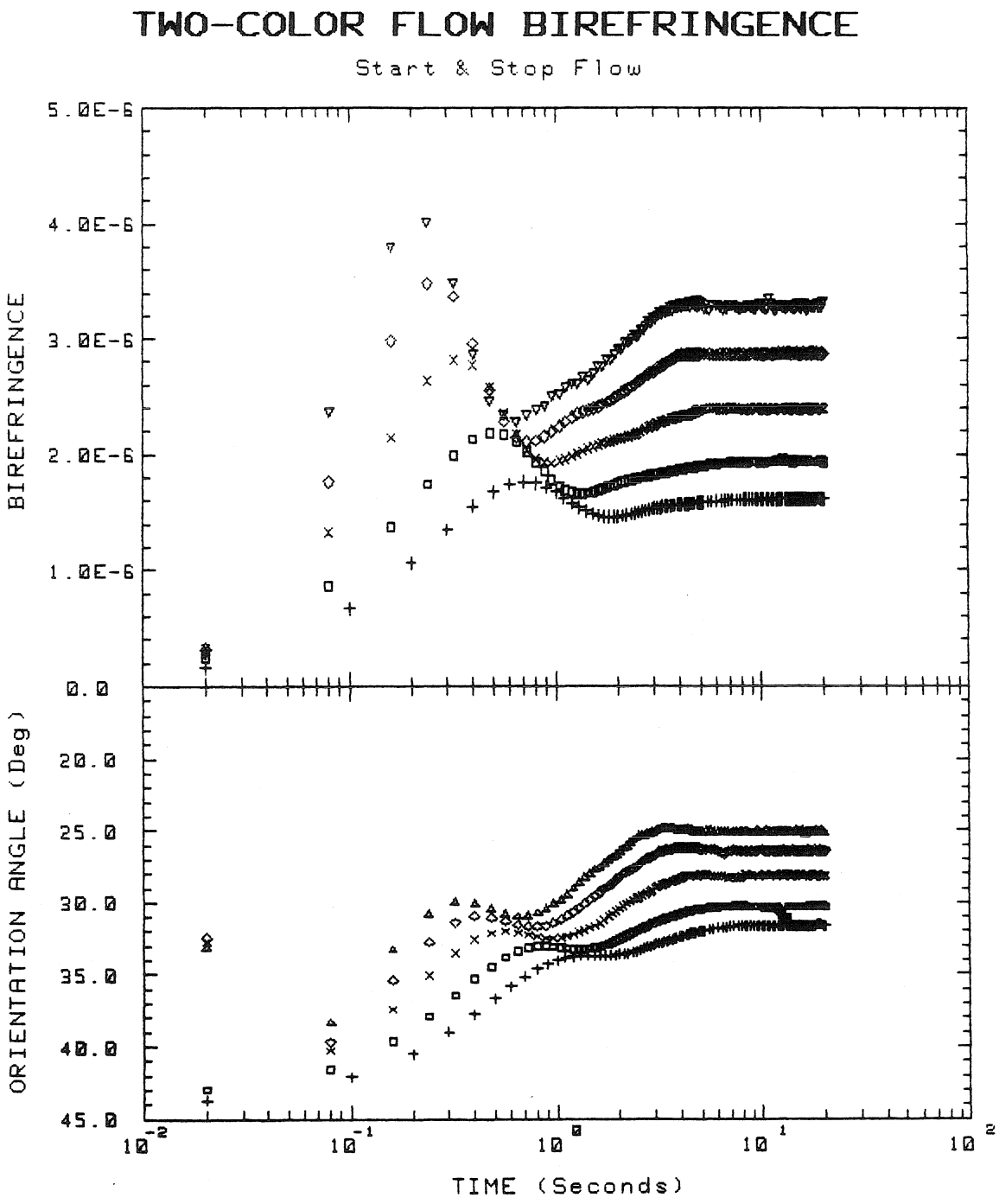

Figure 5.9: Inception of birefringence and extinction angle as a function of time for rollers H ($\lambda = 0.249$). Different markers correspond to different values of the principal eigenvalue of the velocity gradient tensor. $\dot{\gamma}\sqrt{\lambda} = 0.96\ s^{-1}$ (+), $1.44\ s^{-1}$ (□), $2.40\ s^{-1}$, (×), $3.60\ s^{-1}$ (◇), and $4.80\ s^{-1}$ (▽) .

after the overshoot and is a result of a change in the density of entanglements within the polymer network, and the second is due to the stretching of the remaining segments up to a highly elongated state. This type of behavior has *not* been reported in the published literature to knowledge of the authors. As we will show later, this behavior seems to be unique to two-roll mills of a large flow parameter value, *i.e.*, unique to flows with a significant extensional component.

For inception of flow with rollers F, which correspond to a flow parameter equal to 0.151, the birefringence trace shows the same qualitative features as for $\lambda = 0.249$. The transient behavior for $\lambda = 0.151$ is presented in Figures 10 and 11. However, there are significant quantitative differences for the two values of λ. The trace for the birefringence changes its "signature" noticeably. First, the ratio of the magnitude of the overshoot and undershoot clearly depends on λ, with the relevance of the undershoot decreasing as the vorticity of the flow increases. Secondly, after the occurrence of the birefringence undershoot, the trace is now followed by a pair of oscillations that occur just before the steady states values are reached. These oscillations have relative magnitudes of $2 - 4\%$. Thirdly, for $\lambda = 0.151$ the overshoots appear for eigenvalues larger than 0.33 s^{-1}, with overshoots followed by well defined undershoots occurring only for eigenvalues larger than 0.66 s^{-1}. Undershoots in the orientation angle are more difficult to characterize for this flow geometry, although, undershoots of the orientation angle always occur, only after the appearance of well defined undershoots for the birefringence trace.

For rollers D, and $\lambda = 0.061$ (presented in Figures 12 and 13), the birefringence for inception of flow is similar to the previous value of the flow parameter. Again, the birefringence trace shows a well defined "overshoot-undershoot" signature that, at higher shear rates, becomes even more complicated with the appearance of a more pronounced double hump just before the steady value is reached. However, the relative magnitude of the undershoot continued to decrease for this flow field, with the ratio of overshoot to undershoot now being larger than one. For eigenvalues larger than 4.72 s^{-1} the birefringence value at the overshoot corresponds to

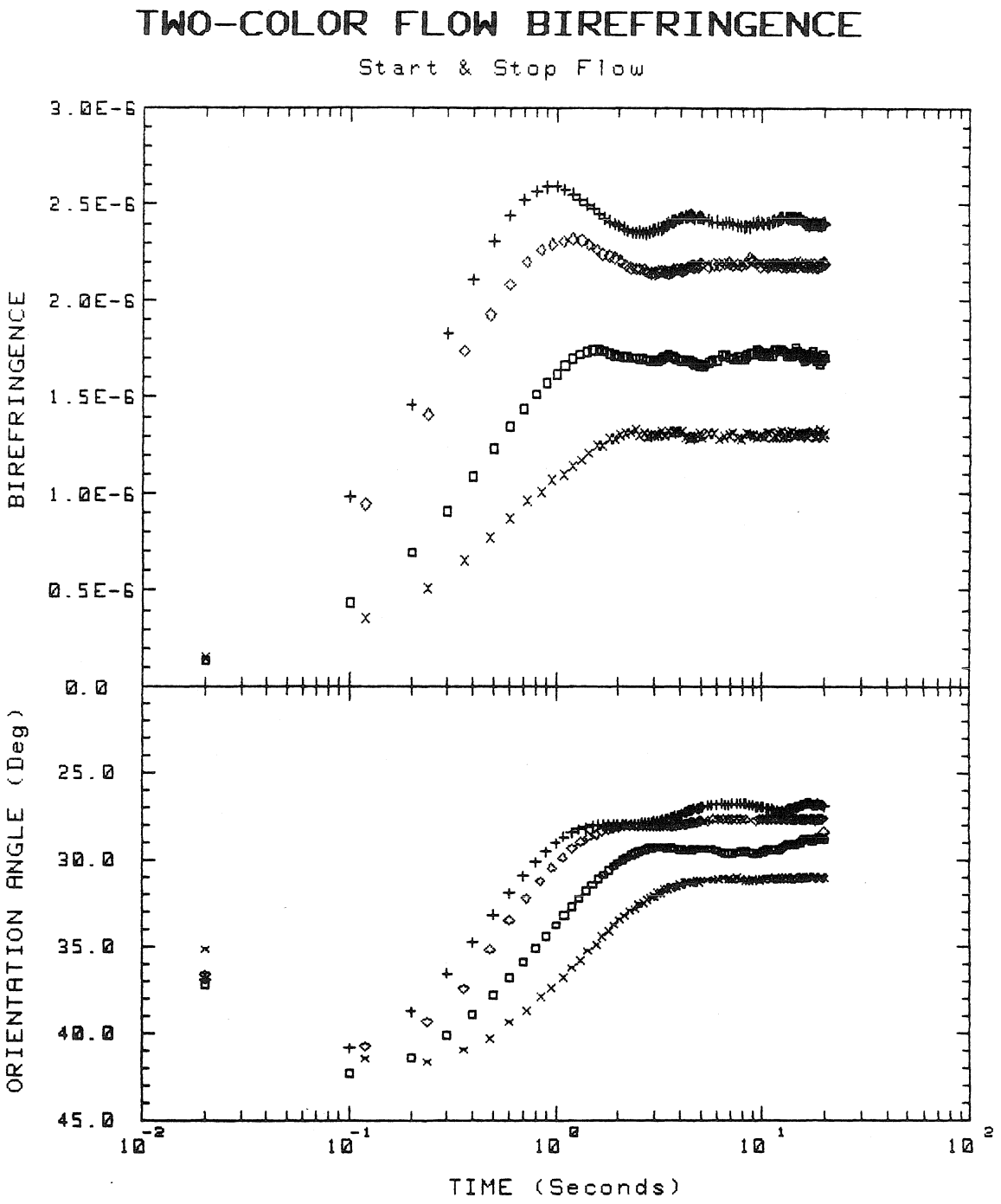

Figure 5.10: Inception of birefringence and extinction angle as a function of time for rollers F ($\lambda = 0.151$). Different markers correspond to different values of the principal eigenvalue of the velocity gradient tensor. $\dot{\gamma}\sqrt{\lambda} = 0.197\ s^{-1}$ ($\times$), $0.329\ s^{-1}$ ($\square$), $0.527\ s^{-1}$, ($\diamond$) and $0.658\ s^{-1}$ ($+$) .

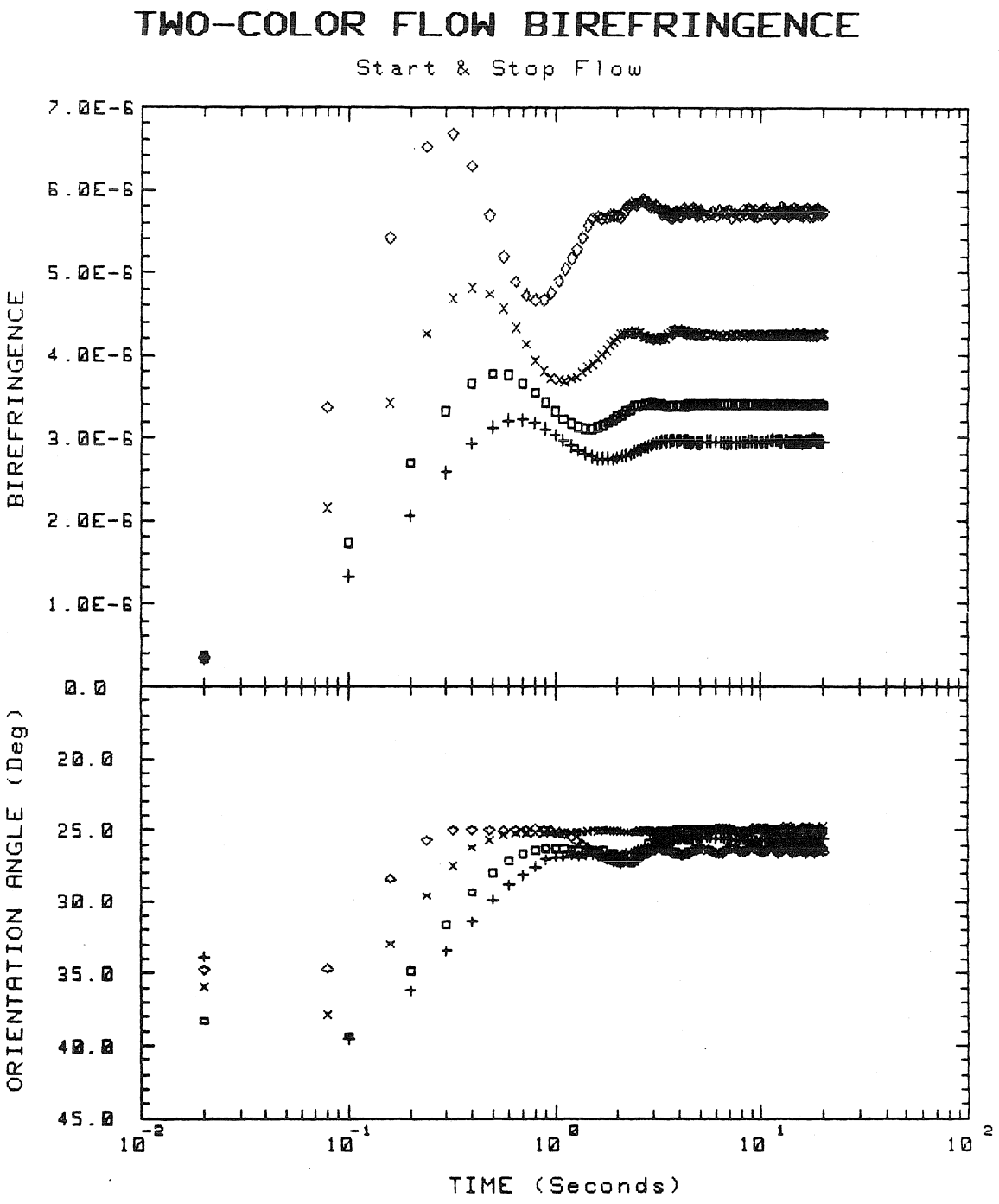

Figure 5.11: Inception of birefringence and extinction angle as a function of time for rollers F ($\lambda = 0.151$). Different markers correspond to different values of the principal eigenvalue of the velocity gradient tensor. $\dot{\gamma}\sqrt{\lambda} = 0.987\ s^{-1}$ (+), $1.32\ s^{-1}$ (□), $1.96\ s^{-1}$, (×) and $3.29\ s^{-1}$ (◇) .

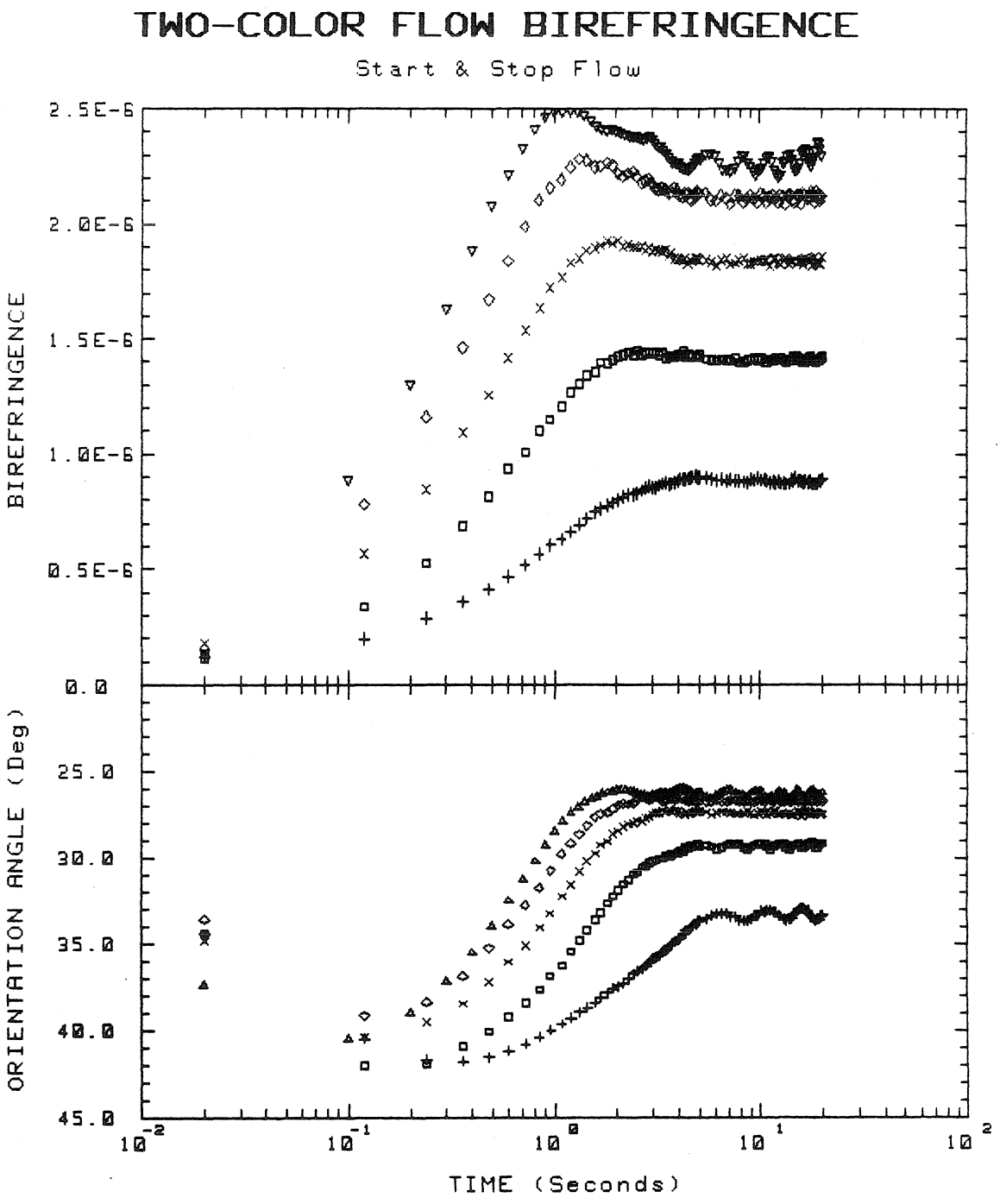

Figure 5.12: Inception of birefringence and extinction angle as a function of time for rollers D ($\lambda = 0.061$). Different markers correspond to different values of the principal eigenvalue of the velocity gradient tensor. $\dot{\gamma}\sqrt{\lambda} = 0.118\ s^{-1}$ (+), $0.236\ s^{-1}$ (□), $0.354\ s^{-1}$, (×), $0.472\ s^{-1}$, (◇) and $0.590\ s^{-1}$ (▽)
.

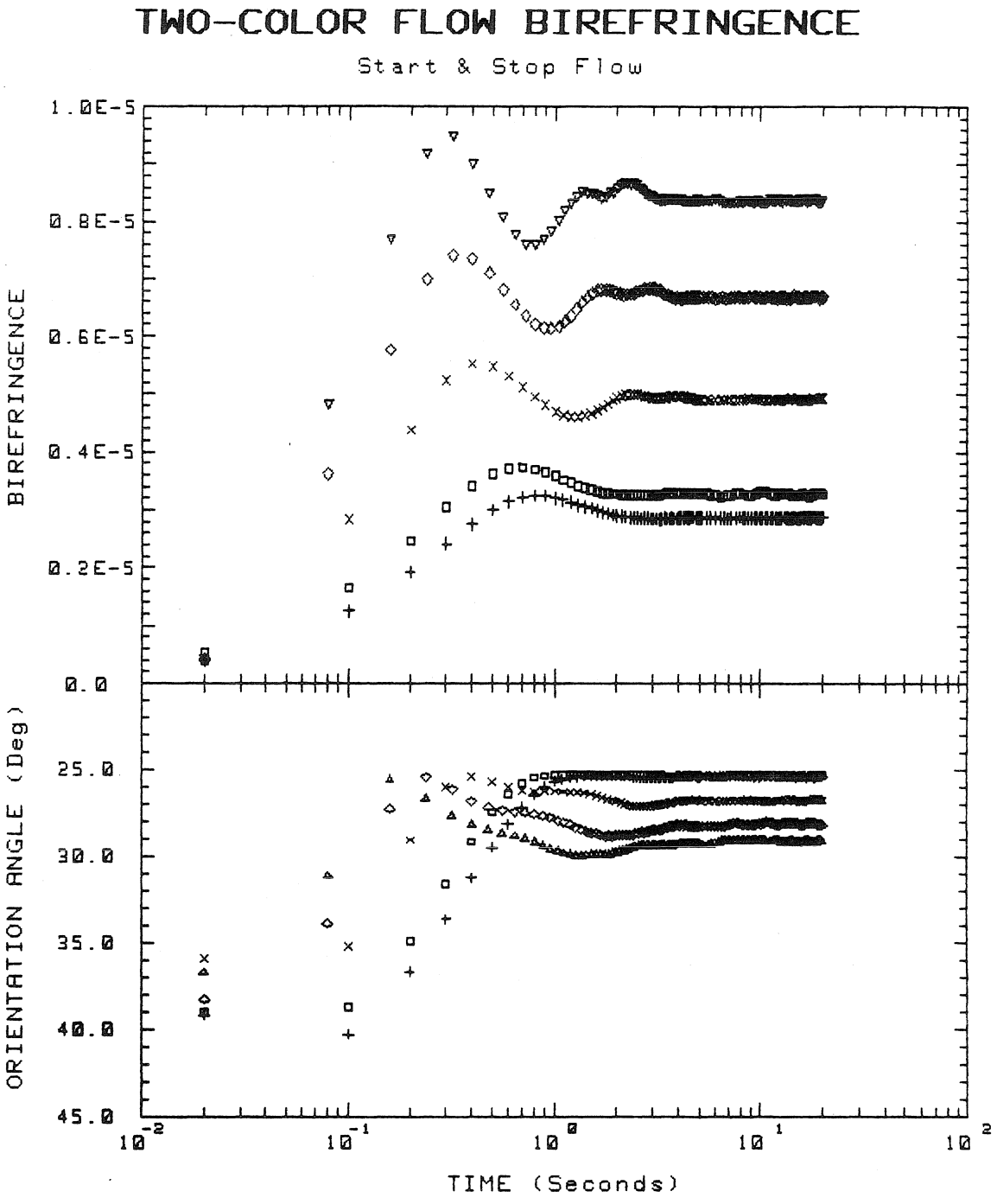

Figure 5.13: Inception of birefringence and extinction angle as a function of time for rollers D ($\lambda = 0.061$). Different markers correspond to different values of the principal eigenvalue of the velocity gradient tensor. $\dot{\gamma}\sqrt{\lambda} = 0.95\ s^{-1}$ (+), $1.18\ s^{-1}$ (□), $2.36\ s^{-1}$, (×), $3.54\ s^{-1}$, (◇) and $4.72\ s^{-1}$ (▽) .

retardation values greater than $\pi/2$. For a trace of the retardation that is oscillatory in character, and has a mean value greater than or equal to $\pi/2$, a unique determination of the birefringence trace is difficult. Thus, the transient birefringence data shown here is restricted to values of $\dot{\gamma}\sqrt{\lambda}$ where the retardance is always less than $\pi/2$ and the uniqueness of the birefringence trace is guaranteed.

Inception of flow-induced birefringence for $\lambda = 0.02$ shows some distinct characteristic not observed with the other flow geometries. For $\dot{\gamma}\sqrt{\lambda} = 0.396\ s^{-1}$ (which corresponds to the second smallest eigenvalue possible with rollers B) the birefringence data already shows an overshoot of 7.2% (see Figure 14). For higher shear rates, the birefringence overshoots become much larger until, finally, for eigenvalues $\dot{\gamma}\sqrt{\lambda} \geq 3.5\ s^{-1}$ the birefringence shows an almost imperceptible undershoot, similarly to birefringence traces observed in Couette flows [26]. The orientation angle starts with a maximum value of 37°. For the lowest eigenvalues, the temporal evolution of χ is a monotonic decrease to the steady flow value (this part of the response is within the linear viscoelastic domain). However, as has been observed with Couette devices, the orientation angle shows significant undershoots for all eigenvalues larger than $0.55\ s^{-1}$.

For the rollers with the smallest value of λ there are significant differences between the data curves for birefringence as function of the eigenvalue, and for the time evolution of birefringence and orientation angle upon inception of steady flow, compared to the same type of data for larger values of λ. There is a breakdown of the correlation of birefringence with the eigenvalue for values $\lambda \leq 0.06$, as seen in Figures 4 and 5. In addition, the transient signature of the time traces for the birefringence and orientation angle has changed significantly compared to the other geometries. Actually, There is a stronger similarity of the data for $\lambda = 0.02$ with the data reported in the literature with Couette devices [26, 27], than for the other λ values where studied here.

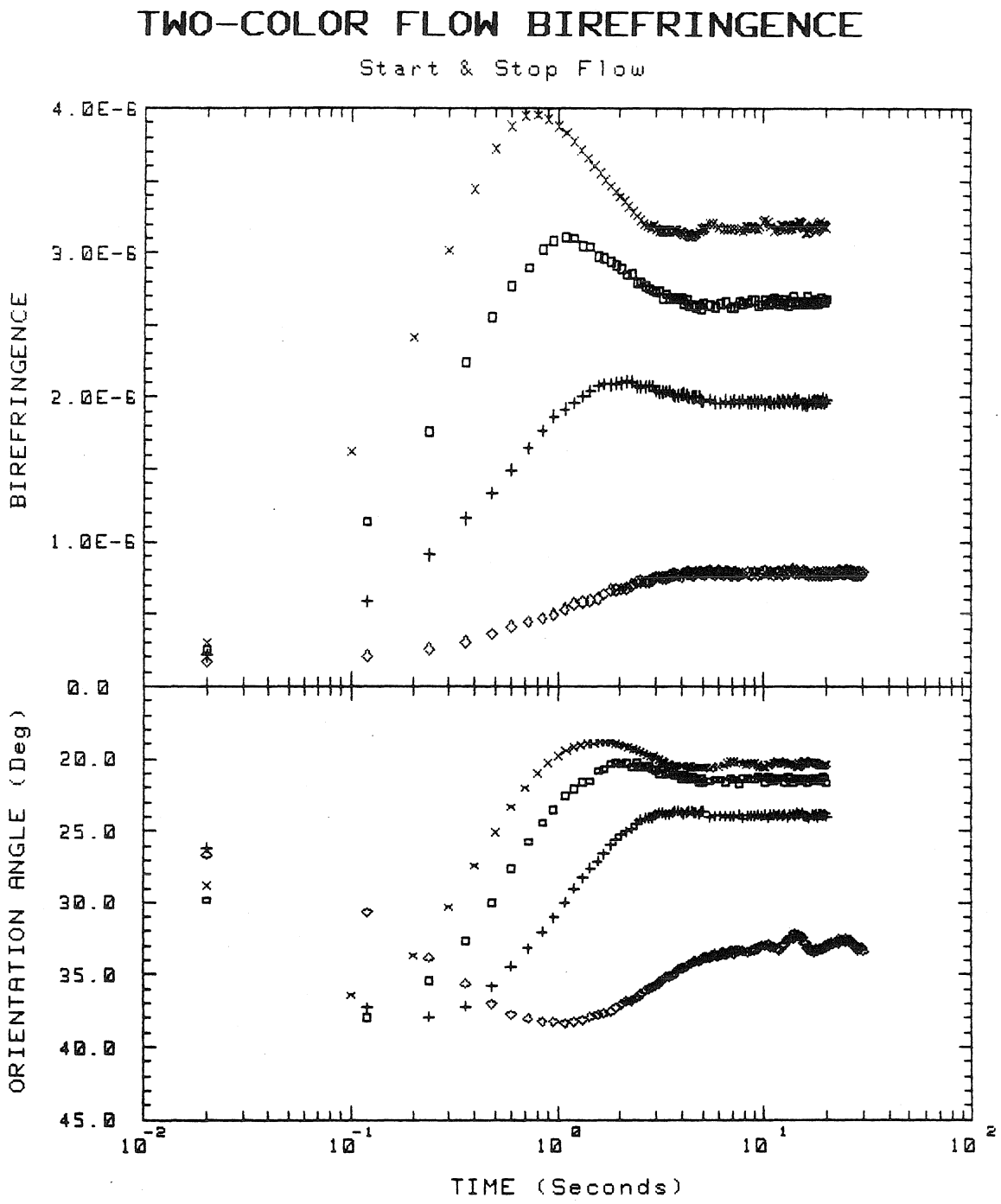

Figure 5.14: Inception of birefringence and extinction angle as a function of time for rollers B ($\lambda = 0.0196$). Different markers correspond to different values of the principal eigenvalue of the velocity gradient tensor. $\dot{\gamma}\sqrt{\lambda} = 0.099\ s^{-1}$ ($\diamond$), $0.396\ s^{-1}$ (+), $0.793\ s^{-1}$, ($\square$) and $1.19\ s^{-1}$ ($\times$) .

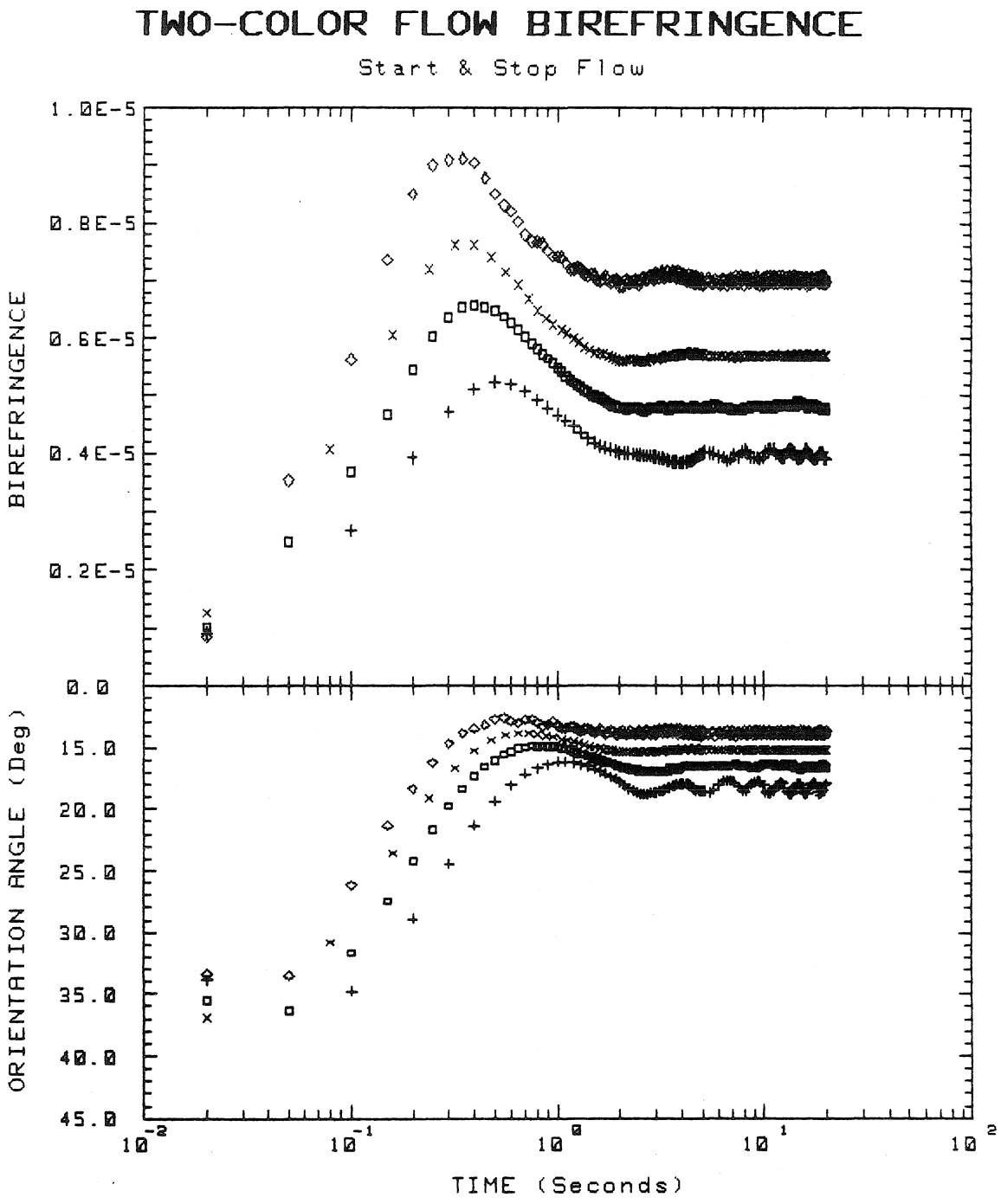

Figure 5.15: Inception of birefringence and extinction angle as a function of time for rollers B ($\lambda = 0.0196$). Different markers correspond to different values of the principal eigenvalue of the velocity gradient tensor. $\dot{\gamma}\sqrt{\lambda} = 1.98\ s^{-1}$ (+), $2.76\ s^{-1}$ (□), $3.57\ s^{-1}$, (×) and $4.76\ s^{-1}$ (◇) .

5.4 Discussion of Results

Although the polymer sample investigated here is a three component system, the use of the oligomer of styrene (referred as oligostyrene) does *not* affect the dynamics of the high molecular weight polystyrene, even at this high a concentration, except through its effects on the monomeric friction coefficient. The function of the oligomer is simply to increase the viscosity of the solvent up into the range of 1 Pa·s, with the net advantage of requiring lower shear rates to reach the same degree of conformational change in the macromolecules. The use of this type of solvent blend is especially advantageous when the high MW polymer solute has a concentration around or slightly higher than c^* since the behavior of the configurational statistics of the polymer *chain segments*[6] depends on the affinity of the solvent-polymer system, with non-Gaussian statistics more likely for a good solvent compared to a solvent at Θ-conditions[7]. In the next section we will discuss the importance of chain segment dynamics and its relationship to this work.

Whenever large deformations are induced by flows, for solutions with concentrations higher than, but close to c^*, the importance of the relaxation dynamics associated with the *chain segments* becomes more prominent, at least as suggested by recent improvements in the reptational models. These new "versions" of the reptational models, originally introduced by de Gennes [30], and Doi and Edwards [31], now include "constraint release" through "tube renewal," see, for example, references [32]-[35], and "tube relaxation" via segmental stretching when the macromolecular fluid is subjected to larger strains, see references [27] or [36]-[38]. Experimentally, it is likely that the solvent type will make a significant difference

[6]For a concentrated solution the dominant mechanism of intermolecular interaction are the entanglement "points." Chain segments are the sections of the high MW polymer between entanglements, with an average MW of M_e.

[7]Ideally, the solvent affinity should be that of the high MW polymer in the melt state. Styrene monomer, plus oligostyrene, plus the high MW polymer should be such a system as proposed by Williams and co-workers [28, 29]. However, for optical measurements, the photoreactivity of monomeric styrene excludes such a type of solvent blend for optical measurements, especially when a highly focussed laser beam is used. The use of toluene permits birefringence studies upon one sample for long periods of time without noticeable changes of its rheo-optical characteristics.

precisely upon the dominant polymer relaxation mechanisms that exist under *large* deformations. For the sample used here, the use of the oligostyrene should have a minimal effect on the storage and loss moduli for the range of frequencies in the flow and the rubber regions [39], apart from a trivial shift in the frequencies due to the change of viscosity. In particular, the oligostyrene molecules in this system act only as diluent [40] molecules.[8]

5.4.1 Linear and Non-linear Viscoelasticity

The viscoelastic properties of a material are modeled by constitutive equations which related the stress tensor and the velocity gradient tensor by means of a *non-linear* functional [31],

$$\sigma_{\alpha\beta}(t) = \mathcal{F}_{\alpha\beta}(\nabla \mathbf{U}(t')) \ , \tag{5.3}$$

where $\nabla \mathbf{U}$ is the velocity gradient prescribed by the linear relationship (5.1). However, in the special case that the velocity gradient is small, and/or slowly changing in time, equation (5.3) can be simply rewritten as a *linear* equality [31, 41]

$$\sigma_{\alpha\beta}(t) = \int_{-\infty}^{t} G(t-t')(\nabla \mathbf{U}(t') + \nabla \mathbf{U}^{\dagger}(t'))dt' \tag{5.4}$$

where $G(t-t')$ is known as the relaxation modulus [41]. Although the range of applicability of equation (5.4) is limited, it has been extensively studied and is well understood.

For the case of a highly entangled polymeric fluid, *i.e.*, one with a concentration $c \geq c^*$, the relaxation from a nonequilibrium conformation can be understood in terms of a set of relaxation mechanisms, each of which has a unique and distinct relaxation time-scale. The fastest relaxation mechanism, with characteristic time τ_a, corresponds to the so-called wriggling of the chain segments about their state

[8]The rubber-glass transition region may be affected by the use of the oligostyrene with the extent of these effects—towards slower frequencies—depending upon the polydispersity of the MW distribution of the oligostyrene sample, in relation to the lowest MW fraction between entanglements.

of equilibrium. It is independent of the MW of the polymer, and is usually very fast compared to the time-scales of typical flow experiments and is therefore of little relevance to this work. For $t > t_a$, the reptational dynamics prescribes two relaxation mechanisms: the relaxation of the contour length, with characteristic time-scale τ_R, and the reptation of the molecule away from its deformed tube, with $\tau_d \geq \tau_R$ as its characteristic time.[9] In the limit of *linear* viscoelasticity (LVE), *i.e.*, of small γ and/or $\dot{\gamma}$, the change of the contour length is an even function of the deformation, and can be neglected to first order [31]. Consequently, the contour relaxation does not contribute to the relaxation dynamics. In this case, reptation is the only relaxation mechanism for $t > t_a$. The *non-linear* viscoelastic (NLV) behavior, occurs whenever the contour length is greater than the equilibrium length and this is the case if $\dot{\gamma}\sqrt{\lambda} > \tau_d^{-1}$. At this point, the anisotropy of the fluid has two contributions: most of the chain segments are strongly aligned, and in addition some of these segments are significantly stretched. As a consequence, the dominant relaxation mechanism is no longer pure reptation but whenever $\dot{\gamma}\sqrt{\lambda} \simeq \tau_d^{-1}$, the so-called mechanism of "tube contraction" from the highly stretched state, for the polymer chain is equally important [37, 38].

The relaxation mechanisms of the polymer molecules prescribed by the reptational models can explain the inflection point for the birefringence trace in steady flows (as seen in Figures 3-7). For steady flows where $\dot{\gamma}\sqrt{\lambda} \leq \tau_d^{-1}$, and according to the reptational models, the *only* relaxation mechanism is reptation. The anisotropy of the fluid is due only to the inner fraction of the polymer chain which becomes strongly oriented and relaxes with a characteristic time proportional to τ_d. When the inverse of the disengagement time τ_d^{-1} is of the order of the eigenvalue $\dot{\gamma}\sqrt{\lambda}$, the stresses of the fluid now have two opposing contributions: one due to the orientation of the chain segments and the second one due to retraction of the some of the chain segments. Therefore, the strain rate must increase accordingly, in order

[9]The linear viscoelasticity of polydisperse polymer samples is not completely explained by assuming only a reptational model. All of the "tube renewal" reptational models tend to address this specific discrepancy see for example references [35, 27] and references therein.

to accommodate for the stresses due to the polymer orientation, and the "new" relaxation due to changes of chain length.

The observed behavior for the steady flow must also correlate with the observations of the birefringence in transient flows. For example, overshoots in the birefringence trace for inception of flow are a result of *non-linear* viscoelasticity. Hence, we can define the characteristic eigenvalue for the onset of non-linear viscoelastic behavior as the smallest eigenvalue capable of inducing overshoots in the inception of steady flow. For $\lambda = 0.249$, the non-linear viscoelasticity, based on start-up of flow, occurs around 0.35 s^{-1}. For steady flow, we can also define a characteristic eigenvalue for the "inflection" point at which the relaxation dynamics is no longer determined by pure reptation. This characteristic eigenvalue is at the intersection of two asymptotic lines, the first tangent to the birefringence trace at low $\dot{\gamma}\sqrt{\lambda}$, and the second tangent to the linear region of the birefringence trace at high eigenvalues (shown in Figure 4). For rollers H, and based on the change of slope of the birefringence trace versus the eigenvalue, the non-linear domain begins in the neighborhood of 0.41 s^{-1}.

Looking back at the onset of the non-linear domain of viscoelasticity as seen in Figures 3 and 8, the orientation angle is still far away from the final asymptotic value –which should approach the outflow axis when the molecules are highly deformed. That is, the onset of non-linear viscoelasticity (NLV) appears when the anisotropy of the fluid is still rather small and the vorticity effects are limited. The molecules tend to be aligned along the principal strain axis, where the polymer is easily deformed from its equilibrium conformation. This behavior is, in fact, found for all λ's; *i.e.*, the anisotropy of the fluid is small at the onset of NLV and the orientation of the molecules appears to be mainly along the principal strain axis.

The correlation between the onset of non-linear behavior in the transient data and the inflection point in the steady birefringence data also occurs for other values of λ. For the case of rollers F, with $\lambda = 0.151$, the change of slope for the steady state flow (see Figure 3) occurs at approximately 0.36 s^{-1} with an almost linear

increase of the birefringence beyond eigenvalues of 1.0 s^{-1}. As seen in Figure 10, the transient data becomes clearly non-linear for eigenvalues larger than 0.33 s^{-1}. These characteristic times for $\lambda = 0.15$ are slightly slower than those measured with rollers H ($\lambda = 0.25$). For $\lambda = 0.06$, the onset of non-linear viscoelasticity occurs at 0.33 s^{-1} based on the steady flow data, and for transient start-ups at 0.30 s^{-1} (see Figures 3 and 12). Finally for $\lambda = 0.02$, the onset of nonlinearity appears to occur at an even lower value of the eigenvalue. For the experiments reported with rollers B, the linear to non-linear transition occurs at a shear rate that is very close to the lower limit possible with the stepping motor used for these experiments. Therefore, at the present time, the number of experimental "points" covering the transition between the linear and the non-linear domains, is most limited and only a least upper bound for the linear viscoelastic domain can be inferred as seen in Figure 14. However, when all the data is taken together, it is clear that smaller eigenvalues are necessary for smaller values of λ.

Thus, based on the range of λ values of 0.25 to 0.06, this study suggests that the eigenvalues for the onset of NLV decreases as a function of λ (for $0 \leq \lambda \leq 1$). The eigenvalue for the onset of NLV was observed to decrease approximately by 30%. On the other hand, this decrease in the eigenvalue corresponds to an increase of the shear rate $\dot{\gamma}$ of almost three times. That is, the linear viscoelastic domain should be expected to prevail for significantly higher shear rates for flows where $\lambda \rightarrow 0$, with the highest values occurring for the case of simple shear flow. For the four sets of rollers used in this study, the determination of the "reptation" time is given in Table 5.2, together with the critical shear rate for the onset of NLV in transient flows. The reptation time corresponds to the *inverse* characteristic eigenvalues for the onset on non-linear viscoelasticity. Of course, these characteristic times depend slightly on the methodology used for its determination, *i.e.*, a slightly larger eigenvalue is obtained for the time-scale based on steady flow data, compared to the values determined by the onset of overshoots in inception of steady flow.

Finally, we consider the percentages of overshoot and undershoot as a function

of the flow parameter and eigenvalue. The relative magnitude of the undershoots *decreases* as function of λ, to the point of almost disappearing for the case of $\lambda = 0.02$. On the contrary, for the case of $\lambda = 0.249$, the undershoots are clearly larger

Rollers	λ	$\tau_c\ (s)$	$\tau^+\ (s)$	$\dot{\gamma}\ (s^{-1})$
B	0.0196	2.44	2.86	2.50
D	0.061	2.78	3.03	1.34
F	0.150	3.03	3.33	0.77
H	0.249	≈ 3.4	≈ 3.4	0.59

Table 5.2: Characteristic time-scales for the transition of linear to non-linear viscoelasticity. τ^+ corresponds to the estimated reptation time as the inverse of $\dot{\gamma}\sqrt{\lambda}$ based on inception of steady flow. τ_c is the inverse of the eigenvalue at which the birefringence changes its slope as a function of the $\dot{\gamma}\sqrt{\lambda}$. $\dot{\gamma}\ (s^{-1})$ is the shear rate needed to reach the non-linear viscoelastic domain.

Roller	λ	$\dot{\gamma}\sqrt{\lambda}$	$\%^+$	$\%^-$
B	0.0196	0.396	7.2	–
B	0.0196	1.19	25.0	–
B	0.0196	2.76	36.8	–
B	0.0196	4.76	31.1	–
B	0.0196	5.95	34.2	–
D	0.061	1.77	13.8	3.5
D	0.061	2.36	12.0	6.6
D	0.061	3.54	11.0	9.3
D	0.061	4.72	13.5	10.4
F	0.151	1.32	10.3	10.3
F	0.151	1.96	13.4	15.5
F	0.151	3.29	17.5	23.9
H	0.249	3.60	21.3	35.1
H	0.249	4.8	25.2	43.8

Table 5.3: Relative magnitudes for the overshoots ($\%^+$), and undershoots ($\%^-$) normalized by the steady state birefringence values for different magnitudes of the principal eigenvector of the velocity gradient, as well as values of the flow parameter.

than the overshoots; see Table 5.3. The above characteristic, we suggest, is a result

of the outflow axis orientation being largest, and hence, for a constant eigenvalue the rate of strain also faster for larger λ values. The effect of different flow types on the polymer conformation is therefore, to enhance the relative importance of chain stretching as compared to tube disengagement; tube stretching being minimal as $\lambda \rightarrow 0$. For the smallest λ value, the steady state value *after* the overshoot, is reached mainly by contour retraction, without significant stretching, while as $\lambda \rightarrow 1$, the steady state value is reached only after significant stretching of the polymer chains. The behavior for the smallest λ value is quite similar to the simple shear data given by Zebrowski and Fuller [26] for an equivalent solution.

5.4.2 Characteristic Strains for Inception of Flow

Characteristic strains have been shown to be another useful parameter for the determination of the transition of linear to non-linear viscoelastic behavior [27, 42, 43]. Menezes and Graessley [42] have proposed that the departure from finite linear viscoelasticity occurs approximately at a strain that is the same regardless of the molecular weight of the polymer, or whether data for shear or normal stresses is used to determine this characteristic strain. This so-called departure strain γ_d has been found to have a value of 0.9 for polybutadiene, and is equal to 1.0 for polystyrene. In contrast to γ_d, the strain at the peak of the stress overshoot in simple shear flow depends both on the shear rate and the solution, but converges to a constant value at low shear rates, with the strain at the overshoot of shear stress being $\gamma_s^+ = 2.2$, and the corresponding value for the first normal stress difference being $\gamma_N^+ = 5.1$. At higher shear rates, the strains necessary to reach the peak in the overshoot starts to grow very rapidly. For example, from the data presented by Fuller and coworkers [26], it is clear that the total strain to reach the *birefringence* overshoot can be several times larger than the values measured at low shear rates, with the initial value at low shear being close to 3.4. In Figure 16, the strain at the birefringence overshoot $\gamma^+(\dot{\gamma}, \lambda)$ found in the present experiments is shown for all four rollers.

As seen in Figure 16, the strain at the overshoot peak for small values of the shear rate is of the order of those reported by Menezes and Graessley [42] for the breakdown of the "finite" linear viscoelasticity. Based in birefringence measurements, Koyama and Ishizuka [43] have found a strain of 0.7 for the onset of NLV in *extensional* flow which corresponds very closely to the values reported here for the largest values of λ. However, for the data presented in Figure 16, it appears that the low shear rate strain γ_o^+ depends on the flow type, *i.e.* on λ, with lower γ_o^+ values occurring for larger λ's. At the higher eigenvalues, all data points deviate from the low shear values $\gamma_o^+(\lambda)$ in a similar manner to what was previously found for the case of simple shear flow [42, 27]. The pattern of departure suggests that the same macromolecular mechanism exists for the data presented in Figure 16 as originally proposed by Graessley *et al.*, where the increase in the peak strain $\gamma^+(\dot{\gamma}, \lambda)$ begins near

$$\dot{\gamma}\tau_e \simeq 1 \ , \tag{5.5}$$

where τ_e is the longest Rouse relaxation time (except for a mutiplicative factor) of the polymer molecules. The determination of this second relaxation time-scale τ_e, based on the strains at the overshoot peak is independent of the damping function and accordingly, should be insensitive even to molecular variables, such as polymer type and/or its MW. However, as seen in Figure 16, the deformation history does have an effect: the value of τ_e appears to depend on λ.

The presence of *undershoots* at high shear rates for simple shear flows ($\lambda = 0$) can also be explained by constitutive equations which explicitly take into account a parameter related to τ_e as suggested by Graessley *et al.* [42]. Our results clearly show that the relative values of overshoots and especially undershoots depend on λ. For a given eigenvalue, the presence of undershoots strongly depends on λ regardless of whether $\dot{\gamma}\tau_e \approx 1$. Therefore, although the undershoots in simple shear flows may be related to the Rouse relaxation time, the precise relationship will be rather complex since it is clear that the onset and magnitude of undershoots is strongly dependent on the relative amount of vorticity of the flow.

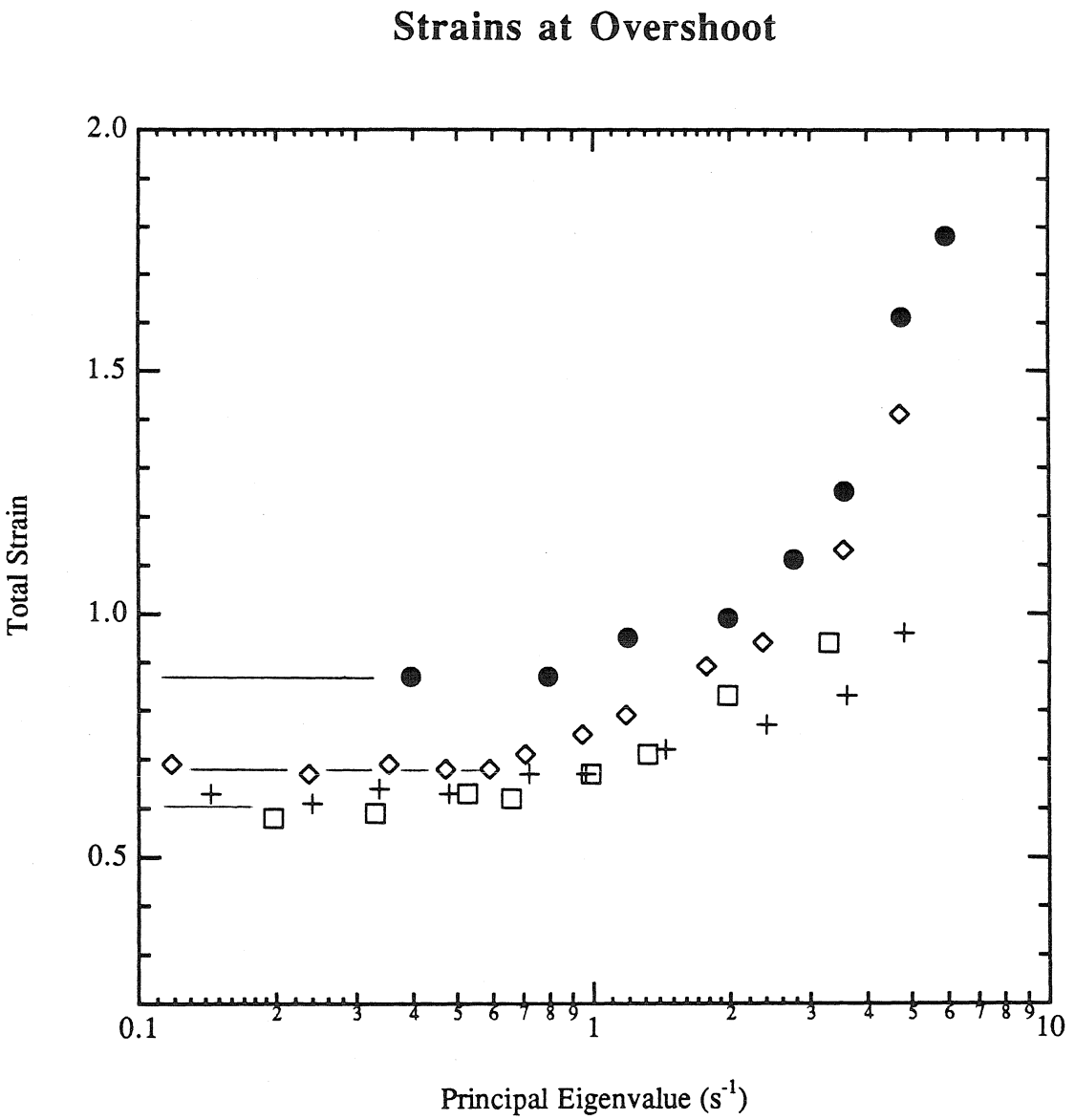

Figure 5.16: Strains at the peak of the birefringence overshoot. For rollers B (•), rollers D (▽), rollers F (□), and rollers H (+).

Based on our understanding of the effects of the two dominant relaxation processes prescribed by the reptational models, we can attempt to describe the optical anisotropy as presented in this work. For inception of slow flow with $\dot{\gamma}\sqrt{\lambda} \leq \tau_d^{-1}$ we can expect that the the polymer will get monotonically aligned, until the chain orientation is in equilibrium with the applied stresses. Macroscopically, the corresponding birefringence although small, also increases monotonically and very fast at the beginning since the polymer is in a conformation close to its equilibrium state, and the resistance to orientation is minimal. The orientation angle also rotates slowly from the principal axis of strain towards smaller angles in a similar manner to the behavior of Δn, but is still aligned mostly along the strain axis. It is now quite clear, that the level of optical anisotropy is due mainly to the reorientation of chain segments without significant stretching taking place, as determined by the small values of the birefringence. Therefore, the polymer conformation is only slightly deformed from its isotropic equilibrium state.

For inception of steady flow with $\dot{\gamma}\sqrt{\lambda} > \tau_d^{-1}$, the time evolution of the polymer conformation depends on the relative contribution of segmental orientation and stretching of segments. The total strain necessary to reach the maximum value of birefringence corresponds to γ^+. For strains less than γ^+, the conformational changes of the polymer are those observed for small eigenvalues. For $\gamma \approx \gamma^+$, the contribution to the stress of segmental stretching is as important as orientation of chain segments. That is, for longer times when $\gamma \geq \gamma^+$ the fluid is "allowed" a second relaxation mechanism that decreases the total number of entanglements on the primitive chain. The decrease in the number of entanglements is macroscopically seen on the graphs for Δn as a decrease of the fluid anisotropy beyond γ^+, with the fluid also becoming less elastic, by augmenting the mean MW between entanglements. For longer times, the effect of the flow is now to increase the anisotropy of the fluid by segmental stretching, which is most efficiently done along the principal strain axis of the flow, and then the polymer tends to aligned itself with a larger orientation angle. Thus, based on the relaxation mechanisms

prescribed by NLV as applied to flow fields generated by two-roll mill we can also explain the "local" overshoot of the orientation angle as seen for fast eigenvalues (and especially obvious in Figure 9).

The deep undershoot observed for Δn at high eigenvalues, is again a clear indication of segmental stretching, which becomes more obvious for the flow corresponding to $\lambda = 0.249$ as seen in Figures 9 and 10. Hence, after the undershoot the polymer network is at its lowest value of entanglements possible with the deformation rate. For even larger deformations, the fluid is still capable of continuing to stretch the polymer molecules to an even higher degree of deformation, and the optimum angle rotates towards the principal strain axis. This change of direction of the orientation angle corresponds to the "local" maximum before the final steady flow orientation is reached.

Acknowledgement: This research was supported by a grant from the Polymer Program in the Division of Materials Research of NSF. One of the authors (EG) thanks the Materials Research Institute from the Universidad Nacional Autónoma de México for its past support.

Bibliography

[1] H. Janeschitz-Kriegl; *Polymer Melt Rheology and Flow Birefringence*, Springer Verlag, New York, 1983.

[2] W. L. Olbricht, J. M. Rallison and L. G. Leal; *J. Non-Newtonian Fluid Mechanics*, **10**,291-318(1982).

[3] R. I. Tanner and R. R. Huigol; *Rheologica Acta*, **14**(11)959-962(1975).

[4] R. I. Tanner; *Engineering Rheology*, Section §5.4; Clarendon Press, Oxford, 1985; and references therein.

[5] G. Astarita; *J. Non-Newtonian Fluid Mech.*, **6**,69-76(1979).

[6] D. V. Khakhar and J. M. Ottino; *J. Non-Newtonian Fluid Mech.*, **21**,127-131(1986).

[7] P. N. Dunlap and L. G. Leal; *J. Non-Newtonian Fluid Mech.*, **23**,5-48(1987).

[8] G. G. Fuller and L. G. Leal; *J. Polym. Sci: Polym. Phys. Ed.*; **19**,557-587(1981).

[9] S. R. Doshi and J. M. Dealy; *J. of Rheology*, **31**(7)563-582(1987).

[10] H. Muenstedt and H. M. Laun; *Rheologica Acta*, **18**(4)492-504(1979).

[11] H. Muenstedt and H. M. Laun; *Rheologica Acta*, **20**(3)211-221(1981).

[12] J. Meissner, T. Raible and S. E. Stephenson; *J. of Rheology*, **25**(1)1-28(1981).

[13] Enrique Geffroy, Ph. D. thesis; California Institute of Technology. Pasadena, Ca., 1989.

[14] E. Geffroy and L. G. Leal; *J. Polym. Sci.: Polym. Phys. Ed.*, to appear 1990.

[15] A. W. Chow and G. G. Fuller; *J. of Rheology*, **28**(1)23-43(1984).

[16] K. Osaki, N. Bessho, T. Kojimoto and M. Kurata; *J. of Rheology*, **23**(4)457-475(1979).

[17] W. Philipoff; *Proc. of IV International Congress on Rheology*, E. H. Lee ed.; Part II, p. 343-372(1980).

[18] G. G. Fuller, J. M. Rallison, R. L. Schimdt and L. G. Leal; *J. Fluid Mechanics*, **100**(3)555-575(1980).

[19] B. J. Bentley and L. G. Leal; *J. Fluid Mechanics*, **167**,219-240(1986).

[20] F. C. Franck and M. R. Mackley; *J. Polym. Sci.: Polym. Phys. Ed.*, **14**,1121-1131(1976).

[21] T. Kasper, M. Shapira, E. P. Ascoli and L. G. Leal; In preparation.

[22] P. Attane, J. P. Pierrard and G. Turrel; *J. Non-Newtonian Fluid Mech.*, **18**,319-333(1985).

[23] J. A. Odell, A. Keller and M. J. Miles; *Polym. Comm.*, **24**(1)7-10(1983).

[24] J. A. Odell, and A. Keller; *J. Polym. Sci.: Polym. Phys.*, **24**,1889-1916(1986).

[25] N. Phan-Thien, O. Manero and L. G. Leal; *Rheologica Acta*, **23**(2)151-162(1984).

[26] B. E. Zebrowski and G. G. Fuller; *J. Pol. Sci.: Polym. Phys. Ed.*, **23**,575-589(1985).

[27] D. S. Pearson, A. D. Kiss, L. J. Fetters and M. Doi; *J. Rheology*, **33**(3)517-535(1989).

[28] C. W. Manke and M. C. Williams; *J. Non-Newtonian Fluid Mech.*, **19**,43-52(1985).

[29] J. E. McAdams and M. C. Williams; *Rheologica Acta*, **25**(2)102-109(1986).

[30] P. -G. de Gennes; *Scaling Concepts in Polymer Physics*, Cornell University Press, Ithaca, New York, 1979.

[31] M. Doi and S. F. Edwards; *The Theory of Polymer Dynamics*, Clarendon Press, Oxford, UK, 1986.

[32] M. Doud and P. G. de Gennes; *J. Pol. Sci.: Polym. Phys. Ed.*, **17**,1971(1979).

[33] J. P. Monfort, G. Marin and P. Monge; *Macromolecules*, **17**(8)1551-1560(1984).

[34] W. W. Graessley; *Adv. Polym. Sci.*, **47**,67-117(1982).

[35] H. Watanabe and M. Tirrell; *Macromolecules*, **22**(2)927-939(1989).

[36] J. L. Viovy, L. Monnerie and J. F. Tassin; *J. Pol. Sci.: Polym. Phys. Ed.*, **21**,2427-2444(1983).

[37] G. Marrucci and N. Grizzuti; *Gazzetta Chim. Italiana*, **118**,179-185(1988).

[38] G. Marrucci and N. Grizzuti; *Xth International Congress on Rheology*, P. H. T. Uhlherr ed., **1**,43-47(1988).

[39] A. Schausberger, H. Knoglinger and H. Janeschitz-Kriegl; *Rheologica Acta*, **26**(5)468-473(1987).

[40] Y. H. Lin; *Macromolecules*, **20**(4)885-893(1989).

[41] J. D. Ferry; *Viscoelastic Properties of polymers*, (3rd Edition), John Wiley & Sons, New York (1980).

[42] E. V. Menezes and W. W. Graessley; *J. Polym. Sci.: Polym. Phys.*, **20**,1817-1833(1982).

[43] K. Koyama and O. Ishizuka; *J. Polym. Sci.: Polym. Phys.*, **27**,297-306(1989).